FOURIER TRANSFORM TECHNIQUES IN ELECTRON SPIN ECHO MODULATION

A THESIS
SUBMITTED TO THE
UNIVERSITY OF HYDERABAD
IN PARTIAL FULFILMENT OF THE REQUIREMENTS
FOR THE DEGREE OF
DOCTOR OF PHILOSOPHY

BY
Y. V. S. RAMA KRISHNA

SCHOOL OF PHYSICS
UNIVERSITY OF HYDERABAD
HYDERABAD, INDIA

JUNE, 1982

This is to state that I, YALLAPRAGADA VENKATA
SIVA RAMA KRISHNA have carried out the research embodied
in the present thesis for the full period prescribed
under Ph.D. Ordinances of the University under the
supervision of Dr. P.A. Narayana and Dr. V.S.S. Sastry.

I declare to the best of my knowledge that no
part of this thesis was earlier submitted for the
award of research degree of any University.

Date: 30ᵗʰ June 1982

[Y.V.S. RAMA KRISHNA]
Enrolment No. AP 13

(Signature of the Supervisor)

DEAN
School of Physics
University of Hyderabad
Hyderabad - 500 134

ACKNOWLEDGEMENTS

[Y.V.S. RAMA KRISHNA]

TO MY PARENTS .....

CONTENTS

CHAPTER I
INTRODUCTION

It is well known that electron paramagnetic resonance (EPR) is a very useful technique for investigating the properties of paramagnetic complexes.[1] As the name implies, it is a resonance phenomenon where the frequency of the applied radiation matches with the Zeeman splitting. This is schematically represented in Fig. 1, which shows the energy level diagram of an unpaired electron in a static magnetic field. If the unpaired electron spin interacts with a magnetic nucleus of spin I, the transition shown in Fig. 1 is split into (2I+1) transitions and this is referred to as the hyperfine splitting. Thus instead of a single EPR line (2I+1) components are observed in the presence of hyperfine coupling. The separation between these components is related to the hyperfine coupling between the unpaired electron and the nucleus. The hyperfine coupling between the unpaired electron and the nucleus belonging to the same ion or atom is typically of the order of a few tens of gauss, while the hyperfine coupling with the surrounding nuclei referred to as superhyperfine (SHF) interaction, ranges typically from a few tenths of a gauss to a few gauss. The analysis of the superhyperfine structure yeilds a very detailed information about the geometrical and electronic structure of paramagnetic complexes. However, there are a number of situations where the SHF structure is not resolved because it is small compared to the EPR line-width and in fact it contributes to the observed linewidth giving rise to an inhomogeneously broadened line. Thus the

Fig. 1

Energy level diagram for an $S = \frac{1}{2}$ system in a
magnetic field H. The frequency of the applied
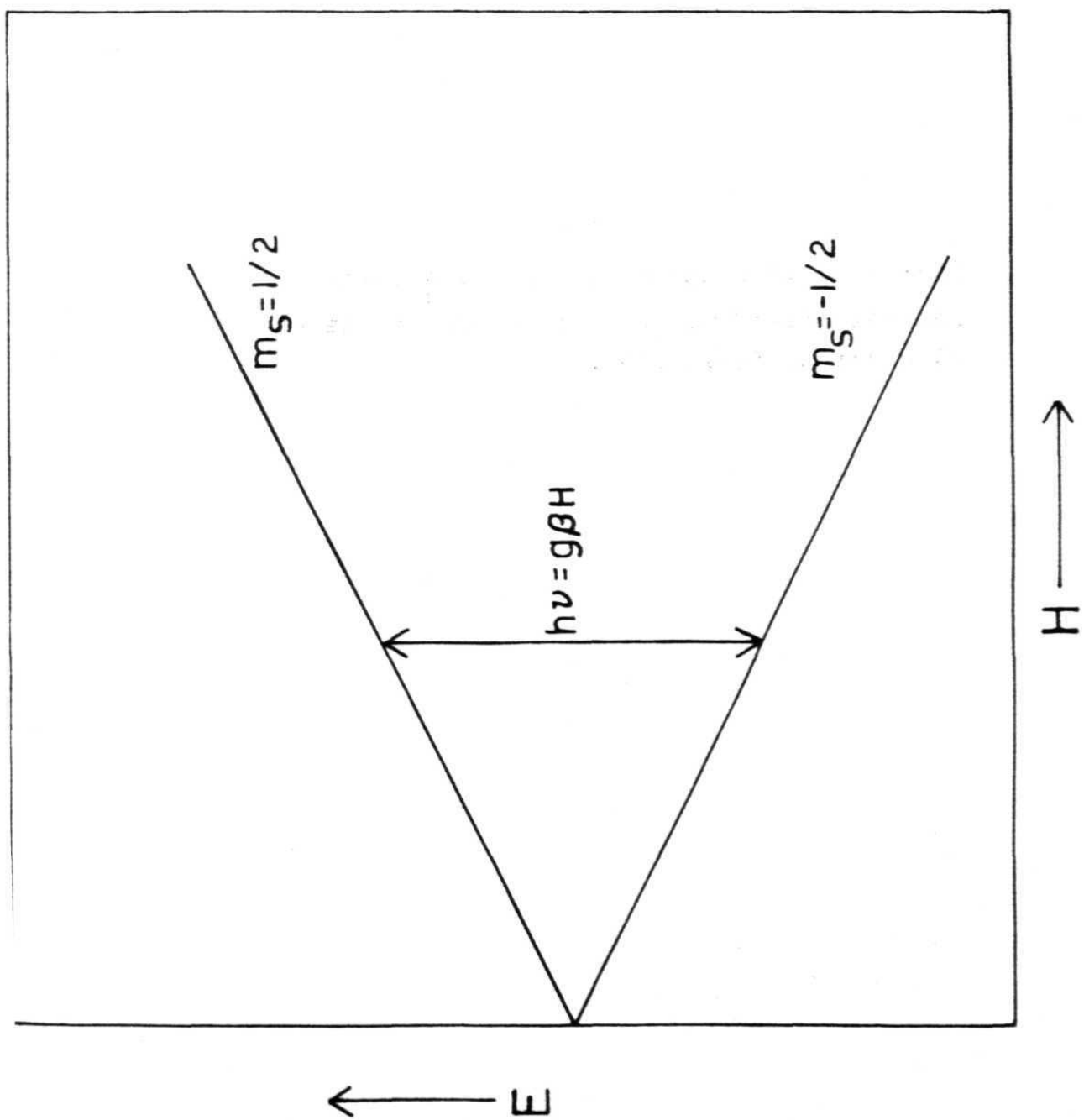alternating field is ν .

Fig. 2

Inhomogeneous broadening of an EPR line. Each of
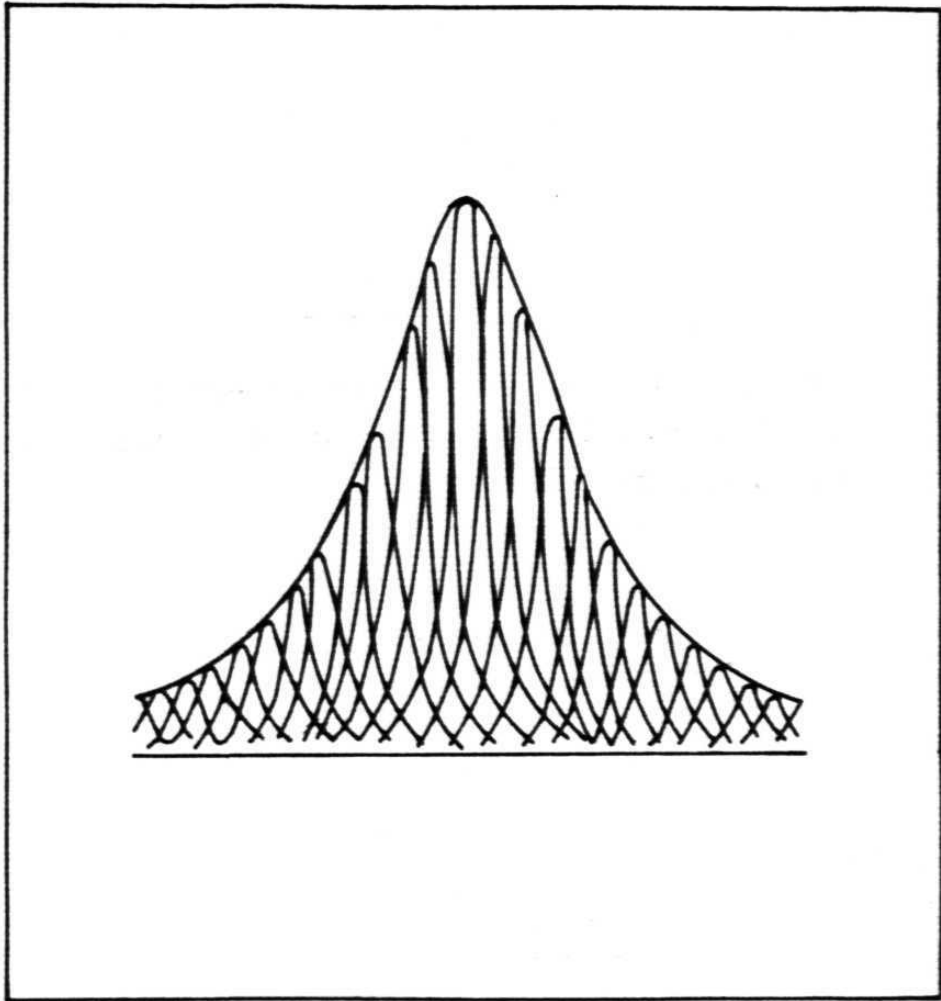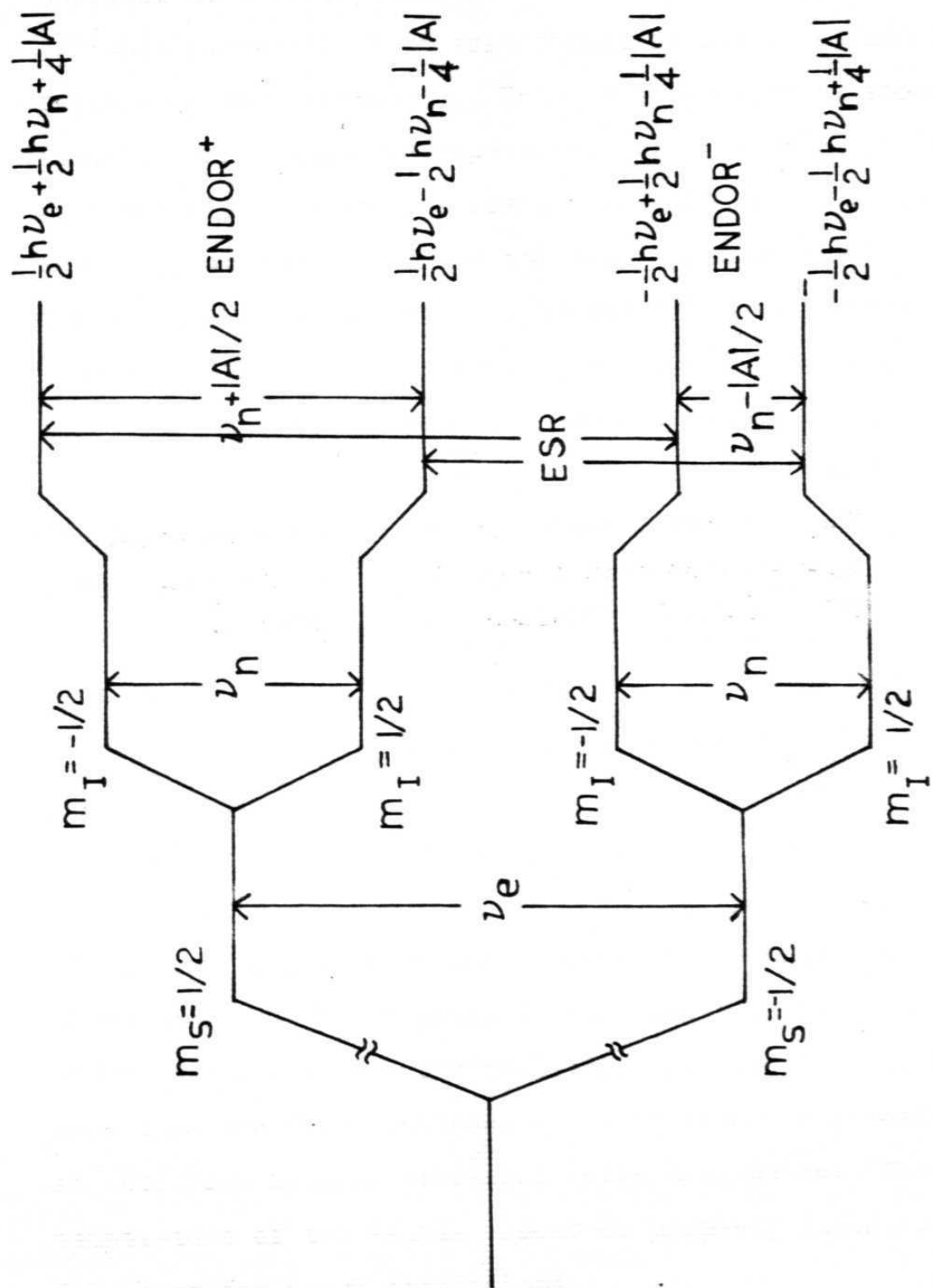the individual lines represents a 'spin packet' or
an isochromat.

Fig. 3

Energy level diagram for an $S = \frac{1}{2}$ system coupled
to a nucleus with $I = \frac{1}{2}$ such that $\nu_n > |A|$. The
ESR and ENDOR transitions are indicated.

observed line essentially is an envelope of a distribution
of 'spin packets'. Each spin packet is characterized by a
distinct Larmor frequency. This is schematically shown in
Fig. 2. Thus in an EPR experiment the resolution is limited
by the inhomogeneous linewidth. Feher has invented an
ingeneous scheme to improve the resolution obtainable in an
EPR spectrum and it is called Electron Nuclear Double
Resonance (ENDOR) technique[2]. The way ENDOR is observed
can be understood by referring to Fig. 3, where the energy
level diagram for an $S = \frac{1}{2}$ and an $I = \frac{1}{2}$ system with a weak
hyperfine coupling is shown. The EPR transitions are
saturated, and an r.f. field is applied to the system.
Whenever the r.f. field is in resonance with the hyperfine
splitting, the EPR line is partially desaturated and a change
in the EPR line is detected. This is referred to as the
ENDOR spectrum. For example, it can be seen from Fig. 3 that
two ENDOR lines are expected for an $S = \frac{1}{2}$, $I = \frac{1}{2}$ system and
are separated by A, where A is the hyperfine coupling
constant. Thus in an ENDOR experiment the high resolution
of nuclear magnetic resonance (NMR) and the high sensitivity
of EPR are simultaneously realized. It should be mentioned
here that the ENDOR enhancement is observed as a result of
an interplay between different relaxation paths. Thus the
temperature of the sample should be properly adjusted for
detecting the ENDOR transitions.

In general, in single crystals the additional resolution
offered by ENDOR is realized. However, there are a number

of problems associated with ENDOR technique[3]: 1) it is **very**
difficult to observe ENDOR for nuclei with low magnetic
moment because of sensitivity considerations; 2) it is
difficult to signal-average to improve the signal to noise
ratio in the case of ENDOR. Also, there are a number of
very important systems which are either very difficult or
impossible to obtain in the form of single crystals. These
include such biologically important systems like hemoglobin,
and bacteriochlorophyll and technologically important
materials like polyacetylene, and a number of low temperature
glasses, etc. These are available only in the form of
randomly oriented samples and the EPR lines are generally
very broad. The randomly oriented samples exhibit a broad
line called 'Matrix ENDOR' [5-7] line. It is in principle
possible to analyse the matrix ENDOR line to obtain the
hyperfine parameters. However, the analysis of the matrix
ENDOR line could be quite tedious and requires a knowledge
of the electronic and nuclear relaxation times[5,6]. One
exception to this arises when the samples exhibit a signi-
ficant g-anisotropy[7]. It is then possible to set the static
magnetic field corresponding to one of the canonical
orientations and obtain almost a single crystal like spectrum.
It is thus necessary to develop a different technique to
obtain a high resolution electron spin resonance spectrum
which is applicable to polycrystalline and other randomly
oriented systems.

In the last few years it has been shown that electron spin echo envelope modulation (ESEEM) spectroscopy offers a number of advantages over other conventional electron magnetic resonance techniques and is particularly well suited for investigating randomly oriented samples[8,9]. The theory of ESEEM is presented elsewhere in this thesis. The salient features of ESEEM are described below.

Electron spin echo is a response of the spin system to the application of two or more resonant microwave pulses. The most popular types of pulse sequences employed are two pulse and three pulse sequences. The time relation between the microwave pulses and the formation of echo are shown in Fig. 4. In a two pulse echo, the amplitude of the echo is recorded as a function of the time separation between the two pulses. In a stimulated or three pulse echo experiment, the time separation between either pulses I and II or pulses II and III is varied keeping the other pulse separation fixed. As a result of various relaxation mechanisms operative in the system, the amplitude of the echo falls off as the separation between pulses is increased[10]. In many cases this electron spin echo envelope (electron spin echo amplitude plotted as a function of time separation between the pulses) does not fall off monotonically but exhibits periodic intensity variations[11-13]. This is called the 'nuclear modulation effect' and arises due to the hyperfine interaction between the unpaired electron and

Fig. 4

The time relationships between the pulses for the
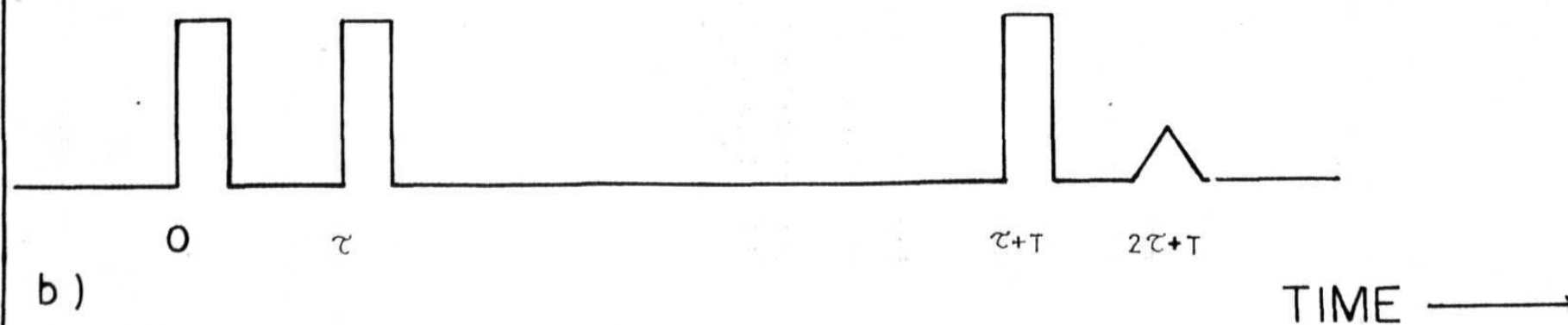generation of

(a) a two-pulse or Hahn echo ($90^{\circ}-\tau-180^{\circ}$)
(b) a three-pulse or stimulated echo
    ($90^{\circ}-\tau-90^{\circ}-\tau+T-90^{\circ}$).
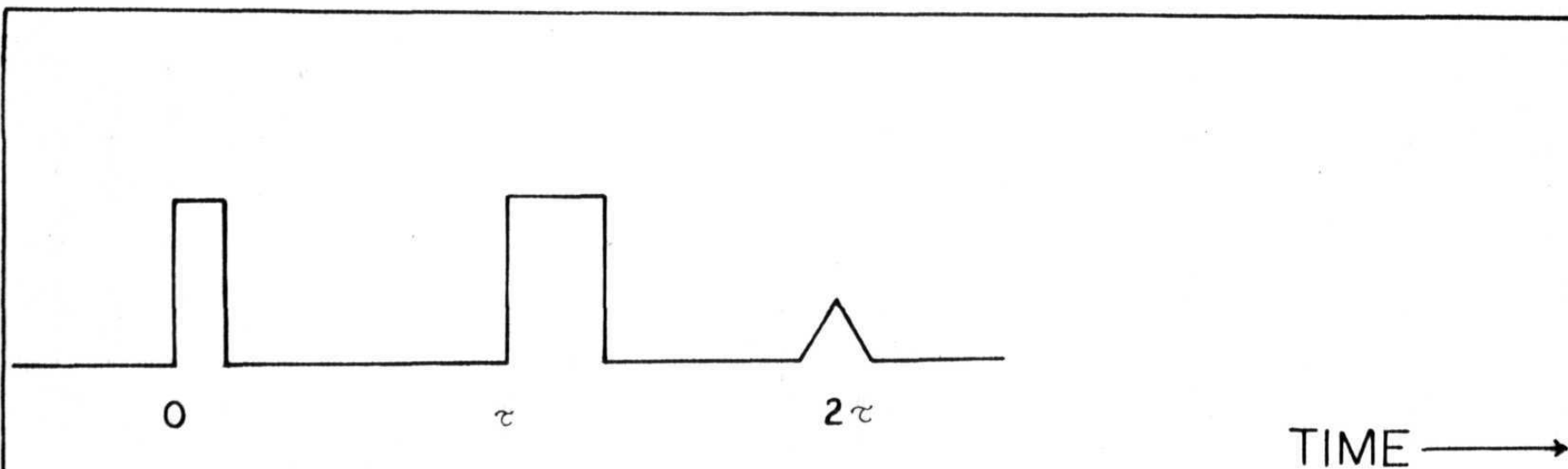
a) TWO PULSE ECHO

b) THREE PULSE ECHO

the surrounding magnetic nuclei. The condition for observing
the nuclear modulation is that the r.f. power should be large
enough to excite all the so called 'allowed' and 'forbidden'
transitions. Also the pulses should be narrow enough to
excite all the frequency components of interest.

An analysis of the nuclear modulation yields infor-
mation about the superhyperfine frequencies and the number
of interacting nuclei. One way to obtain this information
is to carry out the analysis in the time domain[8]. Generally,
the modulation is calculated for a set of parameters viz.,
the electron nuclear distance (r), the isotropic hyperfine
coupling (a), the quadrupole coupling (Q) and the number
of interacting nuclei (n). These parameters are varied
until the calculated modulation agrees well with the
observed modulation. The uniqueness of the set of para-
meters which gives a good fit with the experimental
modulation has been demonstrated in literature[8]. This
analysis, at least for simple systems is not as formidable
as it appears. Often clues could be obtained about the
values of various parameters from the presence of 'phase
reversal' in the three-pulse ESEEM[14] and from the second
moment analysis[15]. Using the time domain analysis,
structural information has been obtained for a number of
systems. In particular the time domain analysis of ESEEM
has yielded definitive answers to some problems for the

first time. The first problem deals with the solvation
structure of trapped electrons in aqueous glass. This is the
simplest radiolysis product. There has been some controversy
about the number and orientation of water molecules surrounding
the trapped electron[16-18]. The ESEEM studies clearly showed
that the trapped electron is surrounded by six water molecules
with the OH bond dipole pointing towards the electron[19]. The
second problem is about the localization of excess electrons
in non-polar glasses. A microdipole model for these excess
electrons has been proposed which seemed to have explained
some of the experimental features[20]. However, ESEEM results
clearly indicated that the microdipole model could not
explain the local structure of the excess electrons in these
systems. This has led to a new theoretical model for these
systems where hydrogen-hydrogen repulsion has been shown to
play a very important role[22]. The third problem for which a
unique answer has been obtained from the ESEEM studies is the
coordination of Cu^{2+} in stellacyanin, a blue copper protein[23].
EPR studies[24] could not provide any definite information
regarding the ligands at the Cu^{2+} site in such blue-copper
proteins. Some indirect physical and chemical evidences[25]
have shown that a cysteinyl sulphur is one of the ligands.
A limited amount of information, however, has been obtained
by ENDOR studies by Rist et al.[26] which indicated that a
nitrogen is ligated to copper. But for the first time ESEEM
studies[23] have demonstrated that an imidazole, presumably

from a histidine residue, is bound to the copper of stellacyanin.

The time domain analysis is well suited when the modulation is relatively simple. However, if the modulation is complex, it is more difficult to carry out the time domain analysis. This is the case when the unpaired electron interacts simultaneously with a number of different nuclei[41] or if the principal axes of the hyperfine tensor and the quadrupole tensor are noncollinear[27]. It is therefore necessary to apply alternate techniques to analyse the ESEEM data. Since the modulation contains, in principle, all the information about the superhyperfine frequencies, one obvious way to analyse the modulation data is to transform the recorded time domain data to frequency domain[28]. This is accomplished by Fourier transform techniques. This technique has been found to be very successful in the case of NMR[29-31]. However, there are a number of problems associated with the Fourier transform technique when applied to electron paramagnetic resonance. These problems essentially arise due to intrinsically short relaxation times encountered in EPR. In the case of NMR the free induction decay (FID) is Fourier transformed. However, in the case of EPR the Fourier transform of FID yields very little information due to the rapid decay of FID. For instance an EPR line with 0.1 mT linewidth gives rise to a free induction signal which decays with a time constant of 100 nsec. Since the resolution

obtained in the frequency spectrum is proportional to the total amount of time over which the data is recorded, it is clear that the Fourier transform of the FID in EPR yields very poor resolution. In practice the situation is even worse because the instrumental dead time prevents even this meagre data to be recorded completely. The second problem arises due to the large linewidths encountered in the case of EPR. In the case of NMR typical linewidths do not exceed a few KHz and thus it is possible to excite all the transitions. However, EPR lines are typically 10 to 100 MHz wide. Thus with the available power it is not possible to excite all the transitions. Therefore the Fourier transform of the FID depends on the irradiating power and essentially yields the shape of the irradiating microwave pulses. These problems can be to some extent overcome by Fourier trans- forming the spin echo envelope instead of the FID. The reason for this is that the spin echo envelope decays with a time constant dictated by the inverse of the spin packet linewidth. The spin packet linewidth is much smaller compared to the observed inhomogeneous linewidth and therefore the spin echo signal decays more slowly compared to the FID.

Eventhough the Fourier transform spectrum of the echo envelope offers a number of distinct advantages, there are a number of problems, both experimental and theoretical, associated with it. These problems have to be solved first

before the full potentialities of this method can be
exploited. The need for obtaining better resolution and
consequently higher bandwidth in the FT spectrum nece-
ssitates the application of narrow and high power microwave
pulses. This is important because the echo envelope decays
in a few microseconds in typical randomly oriented samples.
Typically 1 KW microwave pulses are employed with pulse
widths of 20 nsec. These narrow and high power microwave
pulses introduce problems in recording the data. For
instance, the echo signal generally cannot be detected
until the effects of the high power microwave pulses, which
are typically 140 dB above the noise level, have completely
disappeared. This gives rise to instrumental dead time.
Thus no echo can be detected during this time. However,
for Fourier transformation it is assumed that the recording
of the envelope begins at zero time and continues upto
time $\tau = \infty$. In practice it is possible only to record
the echo envelope from time $\tau = \tau_i$ to time upto which the
signal merges with the noise corresponding to a time $\tau = \tau_f$.
The loss of data beyond τ_f does not pose any serious
problems. However, the loss of data in the region $0 < \tau_i$ is
more serious and introduces artifacts in the transformed
spectrum. The truncation of data corresponds to a multi-
plication of the data with a rectangular window function.
Fourier transformation of such a function gives rise to
sidelobes and distorts the FT spectrum[31]. The problem can

be to some extent eliminated by tapering the data with a suitable window function[32], or by extrapolating the recorded envelope modulation back to zero time[33]. But there are no critical and systematic studies comparing these two methods to preprocess the data to minimize the effects of truncation. The second problem that arises is associated with the decay of the electron spin echo signal. Upon Fourier transformation this gives rise to a large dc component which overwhelms the entire spectrum. However, very little is known about the form of the decay function. Generally, this function is approximated to a polynomial and divided out from the modulation data before Fourier transformation[28].

Apart from the problems mentioned above there are also difficulties associated with the so called interference effects and suppression effects. The interference effect arises because in a typical three-pulse experiment besides the main stimulated echo, two-pulse echoes are also observed due to the combination of various pulses. On the other hand the suppression effect arises because the amplitude of the Fourier peaks strongly depend on τ and T. Because of this dependence it is possible that some of the frequency components are completely absent in the three-pulse ESEEM[32].

Thus there seems to be a need to critically evaluate the FT method in the analysis of ESEEM before it could be established as viable and perhaps a unique technique. In

Next this analysis has been extended to the ESEEM data from the polycrystalline samples of Ag^o in D_2O[36] and glassy samples of Ag^o in CH_3OD and CD_3OH[37]. The ESEEM of these systems has already been analysed in the time domain. It is therefore possible to compare the results obtained using the time domain and FT analysis of the data. It is further possible to investigate the effects of apodization and extrapolation on the FT spectrum.

Finally, the FT technique is applied to study the derivatives of hemoglobin, viz., $HbCN^-$, HbN_3^-, HbNO and HbNO+IHP (Inositol hexaphosphate). Hemoglobin (Hb) is one of the most important biological molecules. The properties of hemoglobin depend upon the detailed electronic structure at the active site, the heme, and also on the conformation of the protein. HbNO is particularly interesting because of its similarity in the electronic structure with oxyhemoglobin and could be switched to the deoxy conformation on binding by inositol hexaphosphate[38-40]. These conformational changes reflect in the electronic properties of the heme and the FT ESEEM is employed to investigate these effects.

It is hoped that the present studies would help in pointing out the relative merits of the FT ESEEM method over other high resolution techniques and bring out some of the problems associated with it into a slightly sharper focus.

References

1. A. Abragam and B. Bleaney, 'Electron Paramagnetic Resonance of Transition Ions', Clarendon Press, Oxford, 1970.

2. G. Feher, Physica, XXIV, S80, 1958.

3. L. Kevan and L.D. Kispert, 'Electron Spin Double Resonance Spectroscopy', John Wiley and Sons, New York, 1976.

4. L. Kevan and P.A. Narayana, in 'Multiple Electron Resonance Spectroscopy', Ch. 6, p229, ed., M.M. Dorio and J.H. Freed, Plenum, 1979.

5. P.A. Narayana, M.K. Bowman, D. Becker, L. Kevan and R.N. Schwartz, J. Chem. Phys. 67, 1990 (1977).

6. L. Kevan, P.A. Narayana, K. Toriyama and M. Iwasaki, J. Chem. Phys. 70, 5006 (1979).

7. G.H. Rist and J.S. Hyde, J. Chem. Phys. 52, 4633 (1970).

8. L. Kevan, in 'Time Domain Electron Spin Resonance', (L. Kevan and R.N. Schwartz, Ed.) Wiley Interscience, New York, 1979.

9. P.A. Narayana and L. Kevan, J. Mag. Res. 46, 84 (1982).

10. W.B. Mims, in 'Electron Paramagnetic Resonance', Ch.4, p263, ed. S. Geschwind, Plenum Press, New York, 1972.

11. W.B. Mims, K. Nassau and J.D. McGee, Phys. Rev. 123, 2059 (1961).

12. J.A. Cowen and D.E. Kaplan, Phys. Rev. 124, 1098 (1961).

13. L.G. Rowan, E.L. Hahn and W.B. Mims, Phys. Rev. 137, A61, 1965.

14. P.A. Narayana and L. Kevan, J. Mag. Res. 23, 385 (1970).

15. S. Schlick, P.A. Narayana and L. Kevan, J. Chem. Phys. 64, 3153 (1976).

16. M. Natori, J. Phys. Soc. Jpn. 27, 1309 (1969).

17. T.H. Dunning, R.M. Pitzer and S. Aung, J. Chem. Phys. 57, 5044 (1972).

18. K. Fueki, D.F. Feng and L. Kevan, J. Amer. Chem. Soc. 95, 1398 (1973).

19. P.A. Narayana, M.K. Bowman, L. Kevan, V.F. Yudanov and Yu.D. Tsvetkov, J. Chem. Phys. 63, 3365 (1975).

20. D.F. Feng, H. Yoshida and L. Kevan, J. Chem. Phys. 61, 4440 (1974).

21. P.A. Narayana and L. Kevan, J. Chem. Phys. 65, 3379 (1976).

22. T. Kimura, K. Fueki, P.A. Narayana and L. Kevan, Can. J. Chem. 55, 1940 (1977).

23. W.B. Mims and J. Peisach, Biochemistry, 15, 3863 (1976).

24. A. Finaggi-Agro, G. Rotilio, L. Avigliano, P. Guerrieri, V. Boffi and B. Mondovi, Biochemistry 9, 2009 (1970).

25. J. Peisach and W.E. Blumberg, Arch. Biochem. Biophys. 162, 502 (1975).

26. G.H. Rist, J.S. Hyde and T. Vanngard, Proc. Nat. Acad. Sci. (U.S.) 67, 79 (1970).

27. W.B. Mims and J. Peisach, J. Chem. Phys. 69, 4921-4930, 1979.

28. W.E. Blumberg, W.B. Mims and D. Zuckerman, Rev. Sci. Instrum. 44, 546, 1973.

29. H.D.W. Hill and R. Freeman, 'Introduction to Fourier Transform NMR'. Varian Associates-Palo Alto, California, 1970.

30. T.C. Farrar and E.D. Becker, 'Pulse and Fourier Transform NMR', Academic Press, New York, 1971.

31. D. Shaw, 'Fourier Transform NMR Spectroscopy', Elsevier, Amsterdam, 1976.

32. R.P.J. Merks and R. deBeer, J. Mag. Res. 37, 305 (1980).

33. T. Shimizu, W.B. Mims, J. Peisach and J.L. Davis, J. Chem. Phys. 70, 2249 (1979).

34. S.H. Hagen and N.J. Trappeniers, Physica 47, 165 (1970).

35. F. Boettcher and J.M. Spaeth, Phys. Stat. Sol. (b), 61, 465 (1974).

36. T. Ichikawa, L. Kevan and P.A. Narayana, J. Chem. Phys. 71, 3792 (1979).

37. T. Ichikawa, L. Kevan and P.A. Narayana, J. Phys. Chem. 83, 3378 (1979).

38. H. Kon, J. Biol. Chem. 243, 4350 (1968).

39. H. Kon, Biochemistry, 8, 4757 (1969).

40. D.C. Doetschman, Chem. Phys. 48, 307 (1980).

41. J. Peisach, W.B. Mims and J.L. Davis, J. Biol. Chem. 254, 12379 (1979).

CHAPTER II

THEORY

Electron spin echoes are a response of the spin system to the application of a series of resonant microwave pulses. The most popular types of pulse sequences employed involve two and three pulses. The echoes observed in the former case are called Hahn echoes or two-pulse echoes and those observed in the latter case are called three-pulse echoes or stimulated echoes. The amplitude of the echoes plotted as a function of time separation between the pulses is referred to as echo envelope. The echo envelope amplitude does not stay constant but rather falls off due to the presence of various relaxation mechanisms operative within the spin system. Therefore an analysis of the echo envelope decay yields information about relaxation times. It has been quite frequently observed that an echo envelope does not decay monotonically but exhibits a periodic intensity variation[1-3]. This is referred to as the nuclear modulation effect and arises due to the hyperfine coupling of the unpaired electron spin with the surrounding nuclei. The nuclear modulation contains information about the super-hyperfine frequencies, and Fourier transformation of it gives the superhyperfine spectrum. This chapter deals with the necessary theoretical background to understand the echo formation, nuclear modulation effect and Fourier transformation of the ESEEM.

Classical Description: The echo formation can be understood either in terms of classical description of precessing magnetization or quantum mechanical description employing the density matrix formalism. The classical description is presented first in this section because it provides a physical insight into the processes responsible for the echo formation.[4]

It is assumed that the observed resonance line is inhomogeneously broadened, i.e., it consists of a distribution of spectral components or spin packets. The observed line is an envelope of these spin packets or isochromats. These spin packets are all independent of each other and their only common interaction is with the microwave magnetic field H_1. The dynamics of this system can most readily be described in a coordinate system which rotates about the static magnetic field. The static magnetic field H_0 defines the z-direction and the coordinate system rotates at a frequency ω_0 corresponding to the frequency of the applied microwave field. In this rotating coordinate system the driving microwave field is represented by a vector H_1 which is taken as defining the y-direction. The rotating coordinate system also reduces the apparent magnetic field to a value $H_{o,j}$ for the j_{th} spin packet where

$$\gamma_j H_{o,j} = \gamma_j H_o - \omega_o \, , \text{ where } \gamma_j = g_j \beta / \hbar \quad \text{is the}$$

Fig. 1

Magnetic fields in a coordinate system rotating
at the microwave frequency ω_o. H_1 is the microwave
field vector which is stationary in this coordinate
system. $H_{o,j}$ is defined as $\gamma_j \, H_{o,j} = \gamma_j \, H_o - \omega_o$.
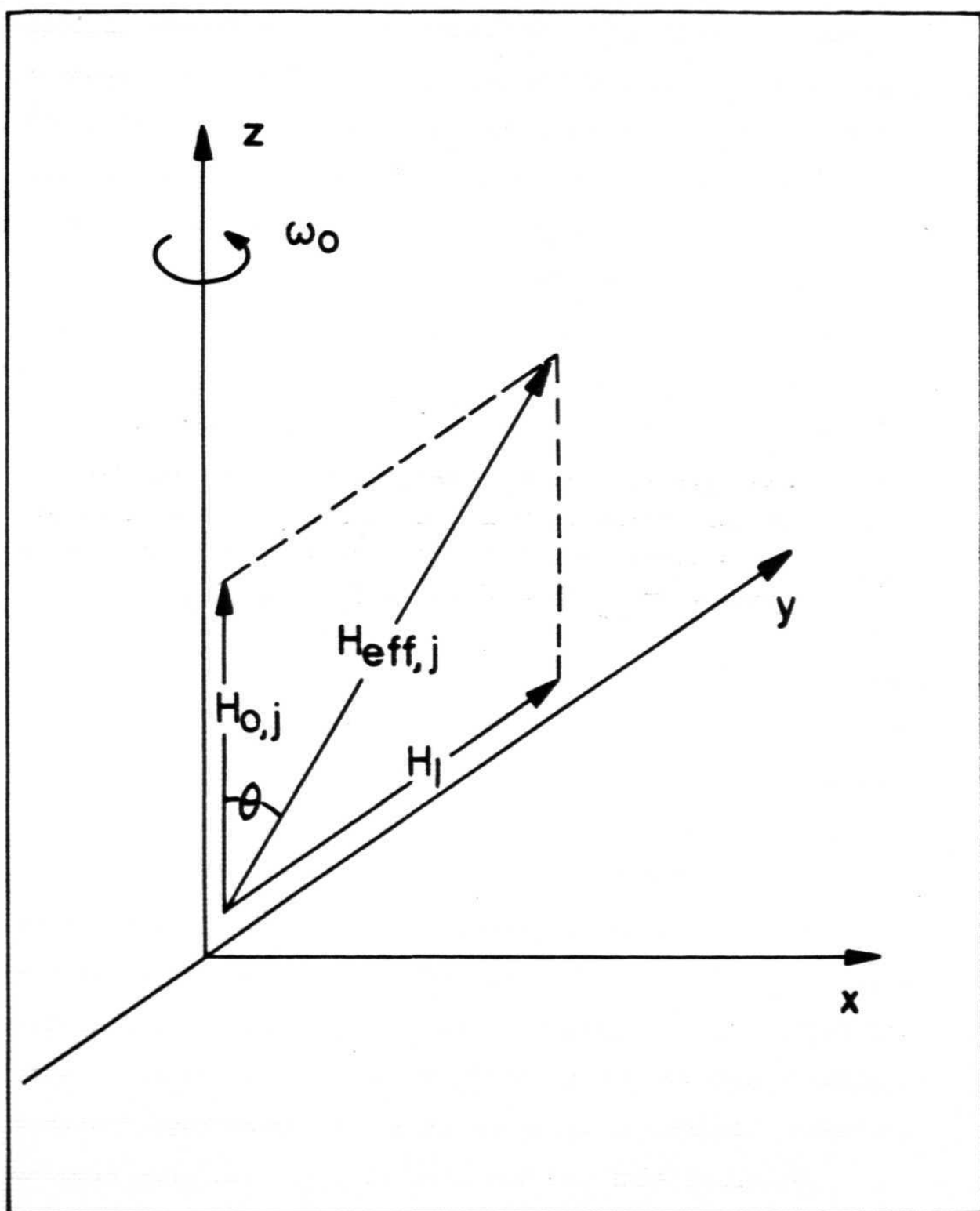
appropriate gyromagnetic ratio. The situation is shown
schematically in Fig. 1. In the absence of microwave magnetic
field the precession takes place about the z-axis with an
angular velocity $\omega_j = \gamma H_{o,j}$ where it is assumed that to a
first approximation all the spin packets have the same
gyromagnetic ratio. However, in the presence of the microwave
magnetic field each spin packet precesses with an angular
velocity $\omega_{ij} = \gamma H_{eff,j}$ about a field $H_{eff,j} = (H_1^2 + H_{o,j}^2)^{1/2}$
and is oriented at an angle of $\theta_j = $ arc tan $H_1/H_{o,j}$ with
respect to the z-axis. Since each spin packet is characte-
rized by a different $H_{eff,j}$ each will have its own dynamical
history. The overall magnetization at any time in the echo
cycle of events is obtained by summing the magnetic moments
of individual spin packets. If the applied field H_1 is large
compared to the linewidth all the spin packets precess about
H_1 with a uniform angular velocity $\omega = \gamma H_1$. Initially we
consider a two pulse sequence and assume a $\pi/2-\pi$ pulse
sequence where the angle θ of a pulse is defined by the
relation $\theta = \gamma H_1 t_p$, where t_p is the pulse width. The angle
θ actually corresponds to the angle through which the magne-
tization is rotated by the applied pulse. It is easier to
understand the events taking place by considering a $\pi/2-\pi$
sequence eventhough it is by no means essential. However,
maximum echo intensity is obtained for this sequence.

Fig. 2

Motion of the magnetization M during a two-pulse
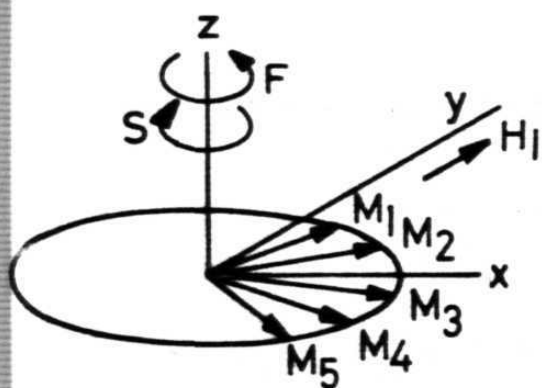spin echo cycle of events.

   a) Before the 90° pulse.
   b) After the 90° pulse.
   c) Dephasing of the individual spin packets
      between the two pulses.
   d) The effect of the 180° pulse. S and F denote
      the directions of slower and faster spin
      packets.
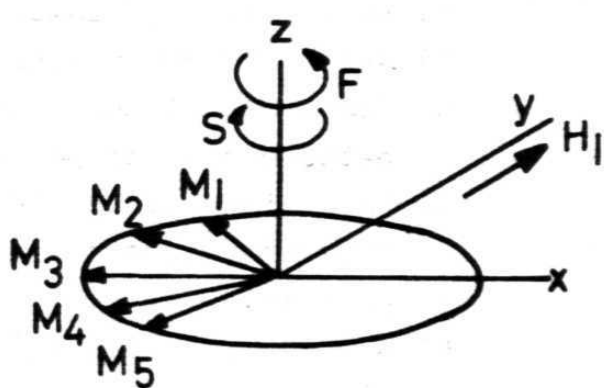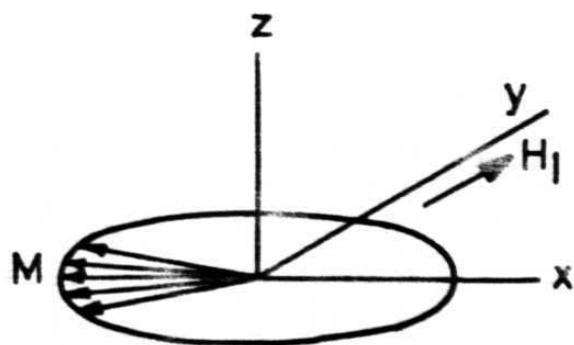   e) Rephasing of the spins to generate an echo.
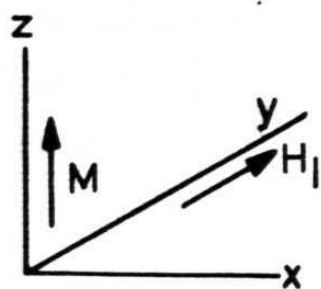
(a)
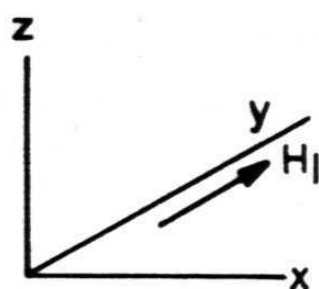
(b)

(c)

(d)

(e)

The sequence of events resulting in an echo formation
can be described by referring to Fig. 2. In the equilibrium
situation the total magnetic moment along the z-axis is
given by

$$M = \sum_j M_{o,j}, \text{ where j refers to the } j^{th} \text{ spin packet.}$$

The first $\pi/2$ microwave pulse which is assumed to be applied
along the positive y-direction rotates M and brings it into
alignment with the positive x-axis. As soon as the microwave
field is removed the spin packets start precessing at
different rates because their Larmor frequencies differ.
At any time t after the application of the first pulse,
the resultant magnetic moment in the xy-plane is given by

$$M_{x+iy}(t_{pI}+t) = \sum_j M_{o,j} \exp(i\omega_j t) \qquad [1]$$

where t_{pI} is the pulse width.

In the laboratory system of coordinates this corresponds to
a moment precessing at a frequency ω_o and gives rise to a
free induction signal. This signal decays with time due to
the dephasing of the individual magnetic moments in the
xy plane. The application of the second π-pulse results in
the rotation of a magnetization by 180° in the xy-plane.

Therefore those moments M_j whose phases have advanced the farthest during the interval following pulse I now find themselves retarded in relation to the rest and those that have lagged behind are now advanced. If τ is the time separation between pulses I and II, the resulting magnetic moment in the xy-plane immediately following the second pulse is given by

$$M_{x+iy}(t_{pI}+\tau+t_{pII}) = - \sum_j M_{o,j} \exp(i\omega_j\tau) \qquad [2]$$

The spin packets start rephasing themselves after the application of the second pulse. The resultant magnetization at a time $\tau + t$ after the application of the second pulse is

$$M_{x+iy}(t_{pI}+t_{pII}+2\tau+t) = - \sum_j M_{o,j} \exp(i\omega_j t) \qquad [3]$$

This expression is similar to given by Eq. (1) and t can take both negative and positive values. Thus Eq. (3) results in an echo signal which consists of two free induction signals back to back peaking at a time τ after the second pulse.

The three pulse echo formation can also be described in a similar way. Here one applies three $\pi/2$ microwave pulses. It should be pointed out again that it is not necessary to employ only $\pi/2$ pulses, even though such a

Fig. 3

Diagram showing the origin of Electron Spin Echo
Envelope Modulation.

a) $H_{n(1)}(t)$ is a time dependent magnetic field
   produced by I at the site of S.

b) The effect of a sudden reversal of the electron
   spin. This produces branching of the precessing
   nuclei some of which precess with frequencies
   $\gamma H_{n(1)}(t)$ and some with $\gamma H_{n(2)}(t)$. Interference
   between these produces modulation beats in the
   electron precession at the nuclear precession
   frequency.
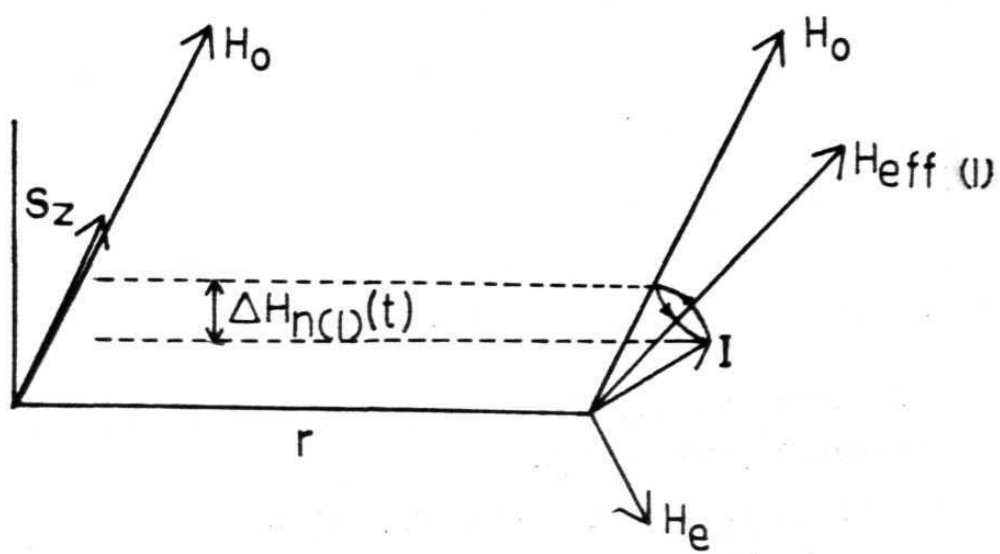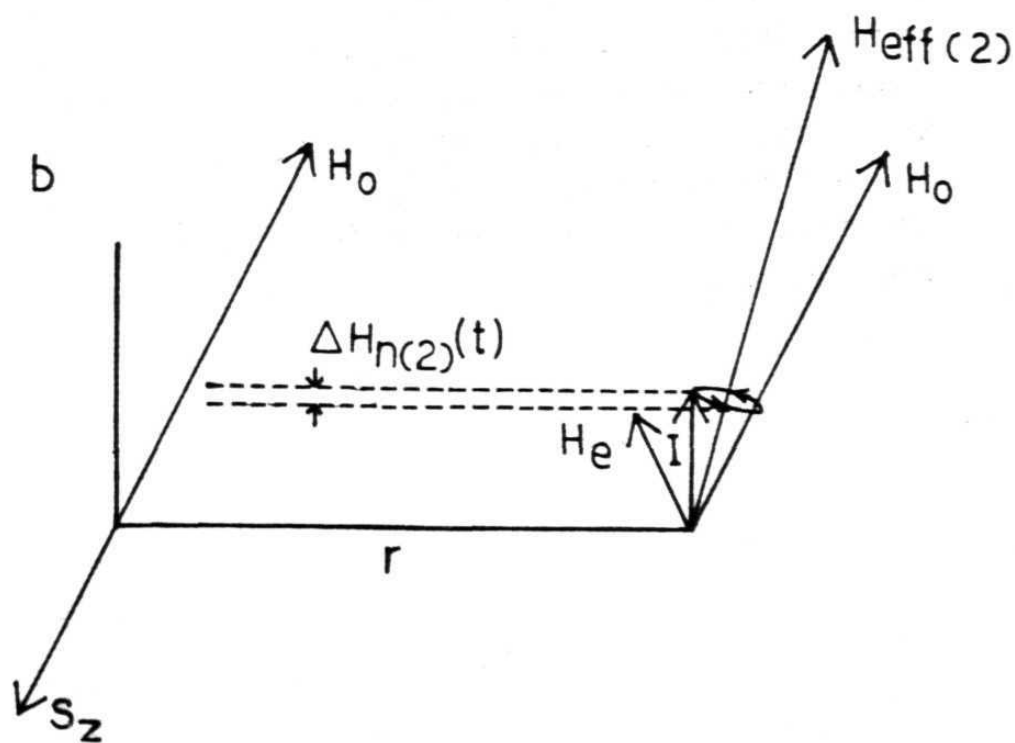
sequence results in maximum echo intensity. Following the arguments given above, it can be shown that the magnetization after the application of three pulses is given by

$$M_{x+iy}(t_{pI}+t_{pII}+t_{pIII}+T+2\tau+t) = -\frac{1}{2} \sum_j M_{o,j} \; \exp \; (i\omega_j t) \quad [4]$$

where the various times are defined in Fig. 4 of Chapter I. Since in the three-pulse case the third pulse essentially holds the magnetization in the z-direction the echo envelope decays much more slowly than the two pulse echo envelope.

As mentioned earlier the echo envelope shows periodic variation in intensity called the nuclear modulation effect due to hyperfine interactions with the surrounding nuclei.[1-3] The presence of such a modulation can be classically understood by referring to Fig. 3. We shall consider an electron spin system with an isotropic g characterised by spin angular momentum vector S in an external magnetic field H_o. Defining the z-direction as that of H_o, the z-component S_z is aligned along H_o as shown in Fig. 3a. Typically H_o is ~ 0.3 T. A nearby nucleus with spin I located at a distance r from S is subject to H_o and the dipolar magnetic field from the electron spin H_e. Since $H_e = \mu_e/er^3$ where μ_e is the electron magnetic moment, H_e is a significant fraction of H_o for r = 0.2 to 0.5 nm. For example $H_e = 0.0343T$ for r = 0.3 nm. The H_o and H_e fields combine vectorially to produce an effective field H_{eff} about

which the nuclear spin vector I precesses. The precession cone is shown in Fig. 3a. The nuclei also produce a dipolar field H_n back at the electron, but H_n is typically much smaller than H_o and the precession of S around H_o is little perturbed. For example $H_n \sim \mu_n/r^3$, where μ_n is nuclear Bohr magneton and is smaller by a factor of 658 than H_e for protons. Thus H_n is less than 0.1 mT for r>0.25 nm. However, precession of I about H_{eff} causes a time dependent variation in H_n at S. This is represented as $\Delta H_{n(1)}(t)$ in Fig. 3a, where the magnitude of $\Delta H_{n(1)}(t)$ reflects the changing magnitude of the I_z component and depends on the orientation of H_{eff}. Thus $\Delta H_{n(1)}(t)$ modulates the electron Larmor frequency by its frequency which is the nuclear Larmor frequency $\omega_{n(1)}$.

When the electron spins are flipped by a resonant microwave pulse, the direction of S_z instantaneously changes to $-S_z$ as shown in Fig. 3b. This instantaneously reverses the direction of H_e at the nuclei and alters the direction of H_{eff}. If this microwave pulse occurs in a time short compared to the nuclear Larmor period (~ 80 ns for protons and ~ 500 ns for deuterons in a field of 0.3 tesla) all the nuclei can not adiabatically follow the new $H_{eff(2)}$ direction. Those nuclei that can not follow continue to precess around $H_{eff(1)}$ as in Fig. 3a and to produce $H_{n(1)}(t)$ at a frequency $\omega_{n(1)}$. Those nuclei that are near H_o in the precession path in Fig. 3a are able to adiabatically

follow the new $H_{eff(2)}$ field and begin to precess about $H_{eff(2)}$ to produce $\triangle H_{n(2)}(t)$ at frequency $\omega_{n(2)}$. The net result of the microwave pulse is to produce a branching of the precessing nuclei into two sets which in turn produce two different nuclear modulation fields at the electrons. The electron Larmor frequency is thus modulated by magnitudes $\gamma_e|\triangle H_{n(1)}|$ and $\gamma_e|\triangle H_{n(2)}|$ at frequencies $\omega_{n(1)} = \gamma_n|H_{eff(1)}|$ and $\omega_{n(2)} = \gamma_n|H_{eff(2)}|$ where γ_e and γ_n are the electron and nuclear magnetogyric ratios. Interference between these two nuclear frequencies produces beats in the electron free precession signal at the nuclear frequencies.

The modulation of the electron Larmor frequency by the nuclear frequencies also appears after a second resonant microwave pulse is applied to produce an electron spin echo. The echo measures the magnitude of the electron magnetization which is proportional to S_z and is modulated by the nuclear fields. A quantitative calculation shows that the two pulse echo is modulated by $\omega_{n(1)}$, $\omega_{n(1)}+\omega_{n(2)}$ and $\omega_{n(1)}-\omega_{n(2)}$. These nuclear frequencies serve to identify the interacting nuclei. From Fig. 3 one can directly see that the amplitude of the echo modulation $\triangle H_n(t)$ depends on the tilt of the nuclear precession cone with respect to H_o, hence on the magnitude of H_{eff} and therefore on the number of equivalent nuclei at r. Thus we see qualitatively that an analysis of the echo modulation pattern should give information on the

identity, number and distance of weakly interacting nuclei. A quantitative understanding of nuclear modulation requires a quantum mechanical treatment.

Quantum Mechanical Treatment:

The nuclear modulation effect in the electron spin echo envelope due to the hyperfine interaction with the surrounding nuclei was first theoretically treated by Rowan, Hahn and Mims[5] for an $S = \frac{1}{2}$, $I = \frac{1}{2}$ spin system for a case where all the hyperfine components are excited. Later Zhidomirov and Salikhov[6] treated an $S = \frac{1}{2}$, $I = \frac{1}{2}$ system where the transitions are only partially excited. Mims has proposed a general scheme to calculate the envelope modulation for $S = \frac{1}{2}$, $I = \frac{1}{2}$ and $S = \frac{1}{2}$, $I = 1$ systems including quadrupolar interaction[6,7]. Dikanov, Shubin and Parmon[8] have recently extended these calculations to systems with $S = \frac{1}{2}$ and any arbitrary value of I. In the following treatment we shall closely adhere to the procedure developed by Mims[7,8] and Dikanov, Shubin and Parmon[9].

Before discussing the envelope modulation calculation, we shall briefly discuss the type of Hamiltonian employed in these calculations. The Hamiltonian in the presence of a magnetic field H_o for a spin system characterized by an electron spin S and a nuclear spin I in a crystalline

lattice has the form

$$\mathcal{H}_T = \beta\vec{H}_o \cdot \tilde{g} \cdot \vec{S} + \beta_n g_n \vec{H}_o \cdot \vec{I} + a\vec{I} \cdot \tilde{g} \cdot \vec{S} + (\beta\beta_n g_n P/r^5)$$

$$[3(\vec{r} \cdot \tilde{g} \cdot \vec{S})(\vec{r} \cdot \vec{I}) - r^2 \vec{I} \cdot \tilde{g} \cdot \vec{S}] \qquad [5]$$

where β and β_n are the electron and nuclear Bohr magnetons respectively; g_n is the nuclear g-factor, $\tilde{g}$ is the electron g-tensor which depends on the orientation of the magnetic field $\vec{H}_o$ with respect to the symmetry axis; and $\vec{r}$ is the position vector of the nuclear spin with respect to the electron spin. The first two terms in the above Hamiltonian represent the electron and nuclear Zeeman terms respectively, the third term represents the isotropic hyperfine coupling and the last term represents direct dipole-dipole and pseudodipole anisotropic hyperfine interactions. The parameters a and P are experimentally determined. The above Hamiltonian completely neglects the coupling of the unpaired electron with its own nucleus. This Hamiltonian can be put in a simpler form by letting the field H_o and the symmetry axis of the complex lie in the xz-plane. Following a series of rotational transformations,[10] the transformed Hamiltonian for the echo calculation can be written as

$$\mathcal{H}_o = \hbar\omega_e S_z - \hbar\omega_n I_z + \hbar A S_z I_z + \hbar B S_z I_x \qquad [6]$$

where $\hbar\omega_e = g\beta H_o$ and an isotropic g-value is assumed. In the above expression

$$A = \frac{gg_n\beta\beta_n}{\hbar r^3} - 2\pi a; \quad \text{and}$$

$$B = \frac{3gg_n\beta\beta_n}{\hbar r^3} \cos\theta \sin\theta$$

It is the term $\hbar B\, S_z I_x$ which is responsible for the branching of the transitions (both allowed and the so-called forbidden transitions) needed for observing the modulation.

The eigenvalues of $\mathcal{H}$ are easily obtained in a representation in which S_z and I_z are diagonal. Since $\mathcal{H}$ is already diagonal with respect of S_z, we can consider each electron Zeeman level $S_z = m_s$ separately. The Hamiltonian then is written as

$$\mathcal{H}_o = \hbar\omega_e m_s + \hbar(Am_s - \omega_n)I_z + Bm_s I_x$$

$$= R(\phi)[\hbar\omega_e m_s + \hbar K I_z]R(-\phi), \qquad [7]$$

$$K = [(Am_s - \omega_n)^2 + B^2 m_s^2]^{1/2}$$

where $R(\phi) = \exp(-i\phi I_y)$ performs a unitary rotation about the I_y axis. A new Hamiltonian is obtained

$$\mathcal{H}_{new} = R(\phi)\mathcal{H}R(-\phi)$$

$$= \hbar\omega_e m_s + \hbar\omega I_z$$

Fig. 4

Energy level diagram for dipolar coupling of an electron with $S = \frac{1}{2}$ with a nucleus of $I = \frac{1}{2}$. The eigenstates are denoted by $|E_{m_I}(m_S)\rangle$ where $+$ and $-$ correspond to m_I, m_S values of $+1/2$ and $-1/2$.
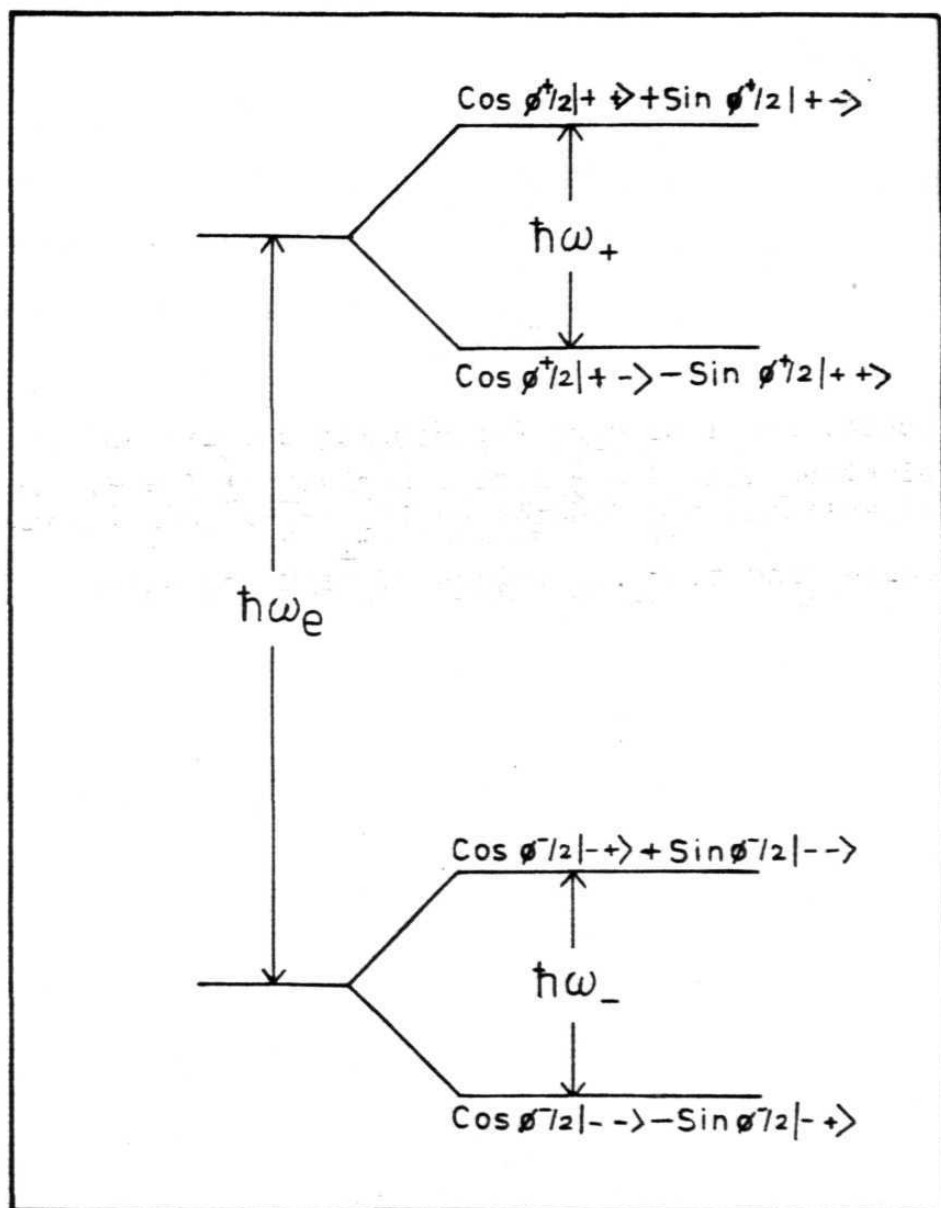
where $\omega = [(Am_s - \omega_n)^2 + B^2 m_s^2]^{1/2}$

and $\tan \phi = \dfrac{BM_s}{Am_s - \omega_n}$

For $m_s = \pm \frac{1}{2}$, ω_+ (or ω_α) and ω_- (or ω_β) correspond to the hyperfine frequencies for the two possible orientations $m_s = \pm \frac{1}{2}$ for the electron spin. The eigenvectors of $\mathcal{H}_{new}$ are $\exp(i\phi I_y)|m_s, m_I\rangle$ [8]

An energy level diagram for the case $S = \frac{1}{2}$, and $I = \frac{1}{2}$ is shown in Fig. 4.

The evolution of the spin system can now be considered during the successive steps of nutation and the free precession. If P is the density matrix[11] describing the systems and $\mathcal{H}$ is the Hamiltonian of the system, the equation of motion is given by

$$\frac{dP}{dt} = i/\hbar | [P, \mathcal{H}]$$ [9]

This equation is readily integrated for a spin system for which the Hamiltonian $\mathcal{H} = \mathcal{H}_o$ does not explicitly depend on time. If P (0) denotes the equilibrium density matrix, it is related to the density matrix P (t) at time t by the

relation

$$P(t) = \exp(-i\mathcal{H}_0 t/\hbar) \, P(0) \, \exp(i\mathcal{H}_0 t/\hbar) \qquad [10]$$

It is best to solve the problem in a coordinate system which rotates about the external magnetic field at a frequency ω corresponding to the applied microwave frequency. The Hamiltonian in such a coordinate system can be written as

$$\mathcal{H}_r = \exp(-i\omega S_z t) \, \mathcal{H}_0 \, \exp(+i\omega S_z t)$$

$$= \mathcal{H}_0 - \hbar\omega S_z \qquad [11]$$

during the periods of free precession.

Under the action of the applied microwave field, the Hamiltonian contains an additional time dependent term describing the interaction of the spin system with the applied microwave field. Assuming that the field H_1 is applied along the y-direction, we have

$$\mathcal{H}_r = \mathcal{H}_0 - \hbar\omega S_z + \hbar\omega_1 S_y \qquad [12]$$

where $\hbar\omega_1 = \frac{1}{2} g \beta H_1$

In the two pulse and the three pulse cases, the exponential operators corresponding to the periods of

nutation and free precession are

$$R_{ip} = \exp(-i\mathcal{H}_r t_{ip}/\hbar) \qquad i = 1,2,3 \qquad [13]$$

$$R_t = \exp(-i\mathcal{H}_o t/\hbar) \qquad t = \tau, T \qquad [14]$$

where t_{ip} is the pulse width of the ith pulse and τ and T
are the time intervals between the first and second, and
second and third pulses respectively.

It follows from Eq. [10] that the final density
matrices after the transformation are given by

$$P(j) = R_j P_o R_j^{-1} \qquad [15]$$

where j = 2 corresponds to the two pulse echo case and
j = 3 corresponds to the three pulse echo case. In the
above equations the rotation operators R_2 and R_3 are
related to the nutation and free precession operators by

$$R_2 = R_\tau R_{2p} R_\tau R_{1p}$$

and

$$R_3 = R_\tau R_{3p} R_T R_{2p} R_\tau R_{1p} \qquad [16]$$

The normalized echo signal amplitude at times 2τ and $2\tau + T$ corresponding to two pulse and three pulse echoes respectively is

$$V(t) = \frac{Tr\ (P(j)S_y)}{Tr\ (P(o)S_y)} \qquad [17]$$

where Tr refers to the trace of the matrix. In order to evaluate Eqs. [16] and [17], generally two approximations are made. The first approximation is the so called high temperature approximation. In this approximation, the equilibrium density matrix is written as

$$P(o) = \sum_{j=1}^{N} \mathcal{H}_{oj}/kT\ Tr(1)$$

$$= \hbar\omega\ [\sum_{j=1}^{N} S_{zj}/kT\ Tr(1)] \qquad [18]$$

where the sum is taken over N electrons cm^{-3} and the electron Zeeman term dominates the contribution to $P(o)$. The second approximation is about the amplitude of the irradiating microwave field H_1. It is assumed that H_1 greatly exceeds the linewidth. Therefore during the application of microwave pulses we can approximately write

$$\mathcal{H}_r \sim \hbar\ \omega_1 S_y \qquad [19]$$

In order to evaluate the above expressions, the states given in Eq. [8] are used. Since the operator $\exp(i\phi I_y)$ mixes states with equal electron spin projection only, it can be written in the matrix form

$$\begin{bmatrix} M_\alpha & 0 \\ 0 & M_\beta \end{bmatrix} \qquad [20]$$

where M_α and M_β are sub-matrices with a dimension $(2I+1)$, describing the rotation of I through the angles $\phi_{\alpha,\beta}$ about the y-axis for $m_s = \alpha, \beta$. For instance, the operator S_y can be expressed as

$$S_y = \exp(i\phi I_y) S_y \exp(-i\phi I_y)$$

$$= \frac{i}{2} \begin{bmatrix} 0 & -M_\alpha M_\beta \\ M_\beta M_\alpha^+ & 0 \end{bmatrix}$$

$$= \frac{i}{2} \begin{bmatrix} 0 & -M \\ M^+ & 0 \end{bmatrix} \qquad [21]$$

The nutation (R_{ip}) and the free precession (R_t) operators also can be described in a similar way to obtain the final density matrix.

Substituting these matrices into Eq. [17] and averaging over the Zeeman frequency difference of the paramagnetic centres, we have for electronic spin $S = \frac{1}{2}$.

$$V_I(\tau) = \frac{1}{2I+1} \text{Re Tr}[e^{-i\omega_\beta \tau} M^+ e^{-i\omega_\alpha \tau} M \, e^{i\omega_\beta \tau} M^+ e^{i\omega_\alpha \tau} M] \quad [22]$$

for the two pulse echo signal.

For the three pulse echo case the expression for the modulation becomes

$$V_I(\tau,T) = \frac{1}{2(2I+1)} \text{ReTr}[\, e^{-i\omega_\alpha(\tau+T)} M e^{-i\omega_\beta} M^+ e^{i\omega_\alpha(\tau+T)} M$$

$$e^{i\omega_\beta \tau} M^+ + e^{i\omega_\beta(\tau+T)} M^+ e^{-i\omega_\alpha \tau} M e^{i\omega_\beta(\tau+T)} M^+ e^{i\omega_\alpha \tau} M] \quad [23]$$

Here $e^{\pm i\omega_\alpha t}$ and $e^{\pm i\omega_\beta t}(t=\tau, \tau+T)$ are diagonal matrices, the elements of which are $\exp(\pm i\, E_{mI}(\alpha)t/\hbar)$ and $\exp(\pm i\, E_{mI}(\beta)t/\hbar)$. For a nuclear spin $I = \frac{1}{2}$, we have

$$M = M_\alpha M_\beta^+ = \begin{bmatrix} \cos \dfrac{\phi_\alpha - \phi_\beta}{2} & \sin \dfrac{\phi_\alpha - \phi_\beta}{2} \\ -\sin \dfrac{\phi_\alpha - \phi_\beta}{2} & \cos \dfrac{\phi_\alpha - \phi_\beta}{2} \end{bmatrix} \quad [24]$$

By substituting this matrix into Eq. [22], the expression for the two pulse echo envelope can be written as

$$V_{1/2}(\tau) = 1 - 2k \sin^2 \frac{\omega_\alpha \tau}{2} \sin^2 \frac{\omega_\beta \tau}{2} \qquad [25]$$

where $\qquad k = (\omega_I \beta / \omega_\alpha \omega_\beta)^2 \qquad [26]$

and for the three pulse echo the expression becomes

$$V_{1/2}(\tau, T) = \frac{1}{2}[V_{1/2}\alpha(\tau, T) + V_{1/2}\beta(\tau, T)$$

$$V_{1/2}(\alpha, \beta)(\tau, T) = 1 - 2k \sin^2 \frac{\omega_{\alpha, \beta}(\tau + T)}{2} \sin^2 \frac{\omega_{\beta, \alpha}\tau}{2} \qquad [27]$$

Following Dikanov, Shubin and Parmon,[9] one can obtain an analytic relation for the echo signal amplitude V_I for an arbitrary spin I expressed in terms of the signal amplitude $V_{1/2}$. The expressions for the modulation amplitudes become

$$V_{1/2}(\tau) = \cos(\xi/2)$$

$$V_I(\tau) = \frac{1}{2I+1} \frac{\sin(I+1/2)\xi}{\sin(\xi/2)} \qquad [28]$$

where $V_{1/2}(\tau)$ is the amplitude of modulation for a spin 1/2 nucleus and $V_I(\tau)$ is the amplitude of modulation for a nucleus whose spin is I. 'ξ' is a parameter which relates the modulation with the elements of the continuous group SU(2). $V_I(\tau)$ can be simply computed in terms of $V_{1/2}(\tau)$. Moreover inasmuch as

$$\frac{\sin (I+\frac{1}{2})\xi}{\sin (\xi/2)} = \sum_{m=-I}^{I} \cos m\xi \qquad [29]$$

and $\cos m\xi$ can be presented as an expansion in $\cos (\xi/2)$ powers, it follows from Eq. [27] to [29] that $V_I(\tau)$ can be written as a polynomial of degree 2I in $V_{1/2}(\tau)$.

The expressions for the three pulse echo can be obtained in an analogous way and are given by

$$V_I(\tau,T) = \frac{1}{2}[(V_I^{(\alpha)}(\tau,T) + V_I^{(\beta)}(\tau,T)]$$

$$V_I^{(\alpha,\beta)}(\tau,T) = \frac{1}{2I+1} \frac{\sin(I+1/2)\xi_{\alpha,\beta}}{\sin(\xi_{\alpha,\beta}/2)} \qquad [30]$$

$$V_{1/2}^{(\alpha,\beta)}(\tau,T) = \cos (\xi_{\alpha,\beta}/2)$$

If the unpaired spin interacts simultaneously with nuclei with an arbitrary spin I (j = 1,.........n) the total

modulation can be expressed as

$$V(\tau) \;=\; \prod_{j=1}^{n} V_{Ij}(\tau)$$

$$V(\tau,T) = \frac{1}{2}[\prod_{k=1}^{n} V_{Ij}^{(\alpha)}(\tau,T) + \prod_{j=1}^{n} V_{Ij}^{(\beta)}(\tau,T)] \quad [31]$$

For the case of $I = 1$, the expressions for the echo modulations are given by

$$V_{mod}(\tau) = 1 - \frac{16}{3}k \; \sin^2\frac{\omega_\alpha\tau}{2}\sin^2\frac{\omega_\beta\tau}{2}+\frac{16}{3}k^2 \; \sin^4(\omega_\alpha\tau/2)\sin^4(\omega_\beta\tau/2) \quad [32]$$

in the case of two pulse echo, and

$$V_{mod}(\tau,T) = 1 - \frac{8}{3}k[\sin^2(\omega_\alpha\tau/2)\sin^2\omega_\beta(\tau+T)/2$$

$$+ \; \sin^2\omega_\alpha(\tau+T/2)\sin^2(\omega_\beta\tau/2)]$$

$$+ \; \frac{8}{3}k^2 \; \sin^4(\omega_\alpha\tau/2)\sin^2\omega_\beta(\tau+T)/2$$

$$+ \; \sin^4\omega_\alpha(\tau+T)/2 \; \sin^2(\omega_\beta\tau/2)] \quad [33]$$

for the three pulse case.

In deriving the above equations the effects of quadrupole coupling have been **ignored.** If the quadrupole coupling is small, the effect of such a coupling can be incorporated in the expressions for $V_{mod}(\tau)$ as small frequency shifts given by Δ. In such a case, the expressions for the normalized echo envelopes are[7,8]

$$
\begin{aligned}
V_{mod}(\tau) = \;& (1-\tfrac{4}{3}k+\tfrac{3}{4}k^2)+(\tfrac{2k}{3}-\tfrac{1}{2}k^2)(\cos\omega_{ab}\tau+\cos\omega_{bc}\tau+\cos\omega_{de}\tau+\cos\omega_{ef}\tau) \\
& -[\tfrac{1}{6}k-\tfrac{1}{6}k^2+\tfrac{1}{6}k(1-k^2)^{1/2}][\cos(\omega_{ab}+\omega_{de})\tau+\cos(\omega_{ab}-\omega_{de})\tau \\
& +\cos(\omega_{bc}+\omega_{ef})\tau+\cos(\omega_{bc}-\omega_{ef})\tau]-[\tfrac{1}{6}k-\tfrac{1}{6}k^2-\tfrac{1}{6}k(1-k^2)^{1/2}] \\
& [\cos(\omega_{bc}+\omega_{de})\tau+\cos(\omega_{bc}-\omega_{de})\tau+\cos(\omega_{ab}+\omega_{ef})\tau \\
& +\cos(\omega_{ab}-\omega_{ef})\tau]+\tfrac{1}{4}k^2(\cos\omega_{ac}\tau+\cos\omega_{df}\tau) \\
& +\tfrac{1}{24}k^2[\cos(\omega_{ac}+\omega_{df})\tau+\cos(\omega_{ac}-\omega_{df})\tau] \\
& -\tfrac{1}{12}k^2[\cos(\omega_{de}+\omega_{ac})\tau+\cos(\omega_{de}-\omega_{ac})\tau \\
& +\cos(\omega_{df}+\omega_{ab})\tau+\cos(\omega_{df}-\omega_{ab})\tau+\cos(\omega_{df}+\omega_{bc})\tau \\
& +\cos(\omega_{ef}+\omega_{ac})\tau+\cos(\omega_{ef}-\omega_{ac})\tau] \qquad\qquad [34]
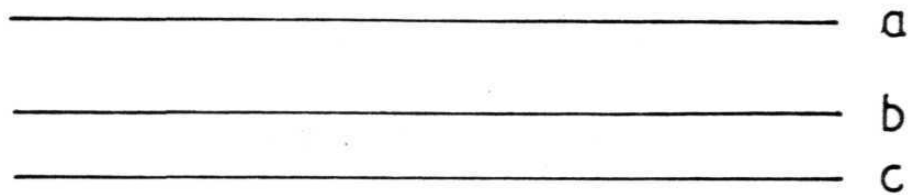\end{aligned}
$$

and

$$V_{mod}(\tau,T) = (1-\tfrac{4}{3}k+\tfrac{3}{4}k^2)+(\tfrac{1}{3}k-\tfrac{1}{4}k^2)[\cos\omega_{ab}\tau+\cos\omega_{bc}\tau+\cos\omega_{de}\tau$$

$$+\cos\omega_{ef}\tau+\cos\omega_{ab}(\tau+T)+\cos\omega_{bc}(\tau+T)\cos\omega_{de}(\tau+T)$$

$$+\cos\omega_{ef}(\tau+T)-[\tfrac{1}{6}k-\tfrac{1}{6}k^2+\tfrac{1}{6}k(1-k^2)^{1/2}][\cos\omega_{ab}\tau\cos\omega_{de}(\tau+T)$$

$$+\cos\omega_{bc}\tau\cos\omega_{ef}(\tau+T)$$

$$+\cos\omega_{de}\tau\cos\omega_{ab}(\tau+T)\cos\omega_{ef}\tau\cos\omega_{bc}(\tau+T)$$

$$-[\tfrac{1}{6}k-\tfrac{1}{6}k^2-\tfrac{1}{6}k(1-k^2)^{1/2}][\cos\omega_{ab}\tau\cos\omega_{ef}(\tau+T)$$

$$+\cos\omega_{bc}\tau\cos\omega_{de}(\tau+T)+\cos\omega_{de}\tau\cos\omega_{bc}(\tau+T)$$

$$+\cos\omega_{ef}\tau\cos\omega_{ab}(\tau+T)]+\tfrac{1}{8}k^2[\cos\omega_{ac}\tau+\cos\omega_{df}\tau$$

$$+\cos\omega_{ab}(\tau+T)+\cos\omega_{df}(\tau+T)]+\tfrac{1}{24}k^2[\cos\omega_{ac}\tau\cos\omega_{df}(\tau+T)$$

$$+\cos\omega_{df}\tau\cos\omega_{ac}(\tau+T)]-\tfrac{1}{12}k^2[\cos\omega_{ab}\tau\cos\omega_{df}(\tau+T)$$

$$+\cos\omega_{df}\tau\cos\omega_{ab}(\tau+T)+\cos\omega_{df}(\tau+T)\cos\omega_{bc}\tau$$

$$+\cos\omega_{df}\tau\cos\omega_{bc}(\tau+T)+\cos\omega_{de}\tau\cos\omega_{ac}(\tau+T)$$

$$+\cos\omega_{ac}\tau\cos\omega_{de}(\tau+T)+\cos\omega_{ef}\tau\cos\omega_{ac}(\tau+T)$$

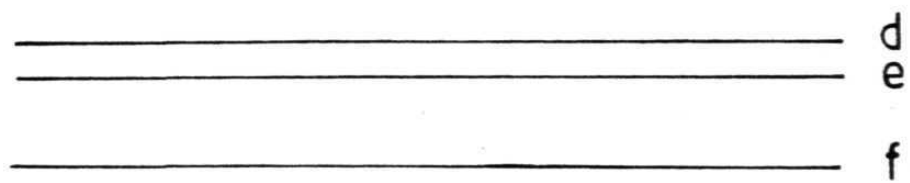$$+\cos\omega_{ac}\tau\cos\omega_{ef}(\tau+T)] \qquad\qquad [35a]$$

Fig. 5

Energy level diagram for an $S = \frac{1}{2}$ system coupled
to an $I = 1$ nucleus. The levels have been corrected
for quadrupole coupling to first order.

where $V_{mod}(\tau)$ and $V_{mod}(\tau+T)$ represent the modulation amplitudes for the two pulse and three pulse envelopes respectively.

Here $\qquad \omega_{ab} = \omega_{\alpha} + \Delta$

$$\omega_{ac} = \omega_{\alpha} + \Delta$$

$$\omega_{ed} = \omega_{\beta} + \Delta \qquad\qquad [35b]$$

$$\omega_{df} = \omega_{\beta} + \Delta$$

where Δ is the appropriate quadrupolar correction. The energy level scheme corrected for first order quadrupolar coupling is shown in Fig. 5.

Thus $V_{mod}(\tau)$ or $V_{mod}(\tau,T)$ contain all the information about the superhyperfine frequencies associated with the magnetic nuclei surrounding the paramagnetic site.

Fourier Transformation: Our interest is to obtain the frequency spectrum directly. It is therefore necessary to Fourier transform the modulation. Fourier transform[12] of a function $f(t)$ of time is defined as

$$f(\omega) = \int_{-\infty}^{+\infty} f(t) \exp(-i\omega t)dt \qquad\qquad [36]$$

Here ω is the angular frequency ($\omega = 2\pi\nu$). It can be shown that the inverse relation is also true:

$$f(t) \;=\; \frac{1}{2\pi} \int_{-\infty}^{\infty} f(\omega) \exp (i\omega t) \, d\omega \qquad [37]$$

The imaginary function in the Eqs. [36] and [37] includes both the sine and cosine contributions. We can also define the sine and cosine Fourier transforms as

$$s(\omega) \;=\; 2 \int_{0}^{\infty} f(t) \sin (\omega t) \, dt \qquad [38]$$

and

$$c(\omega) \;=\; 2 \int_{0}^{\infty} f(t) \cos (\omega t) \, dt \qquad [39]$$

and the power transform $P(\omega) = S(\omega)^2 + C(\omega)^2 \qquad [40]$

In this section we discuss Fourier transformation of three pulse echo envelope only. Similar arguments hold good for the two pulse case also.

The envelope modulation function given by Eq. [33], can be rewritten as

$$V_{mod}(\tau, \tau') \;=\; 1 - \frac{2}{3}k[(1-\cos\omega_\alpha\tau)(1-\cos\omega_\beta\tau')$$

$$+ (1-\cos\omega_\beta\tau)(1-\cos\omega_\alpha\tau')] \qquad [41]$$

where $\tau' = \tau + T$. As already discussed, if the modulation
has contributions from n nuclei then we may write

$$[V_{mod}(\tau, \tau')]_n = \prod_{i=1}^{n}[V_{mod,i}(\tau, \tau')] \qquad [42]$$

substituting Eq. [32] in Eq. [33], we have

$$V_{mod}(\tau, \tau')]_n = 1 - \sum_{i=1}^{n}\frac{2}{3}k_i[(1 - \cos\omega_\alpha^i\tau)(1 - \cos\omega_\beta^i\tau')$$

$$+ (1 - \cos\omega_\beta^i\tau)(1 - \cos\omega_\alpha^i\tau')] \qquad [43]$$

The cosine terms involving higher powers of 'k' have been
neglected because for weak interactions we can assume that
k<<1. Experimentally the envelope amplitude can be recorded
by varying T for a fixed value of τ or by varying τ for a
constant value of T. Usually $V_{mod}(\tau, \tau')$ is recorded by
varying T for a fixed because in general the echo decays
faster with τ than with T. For constant τ the stimulated
echo envelope modulation function given by Eq. [43] can be
expressed as

$$V_{mod,\tau}(\tau') = 1 - \sum_{r=1}^{2n} a_r(1 - \cos\omega\tau') \qquad [44]$$

where the constants a_r depend on τ.

In the above equation the relaxation effects have so far been ignored. In general, one could divide the relaxation causing the decay of echo envelope into two categories[13]. The first mechanism causes the decay of the modulation amplitude due to the randomization of the precessional phases of the nuclear moments. If this randomization is fast and the modulation is deep it may completely determine the decay of the stimulated echo[14]. The decay of the modulation is associated with a broadening of the nuclear resonance lines, which may be homogeneous or inhomogeneous in character. The homogeneous broadening of the nuclear resonance lines can be accounted for by multiplying each cosine term in Eq. [44] by a decay function $F_r(\tau')$. Thus the modulation can now be written as

$$V_{mod,\tau}(\tau') = 1 - \sum_{r=1}^{2n} a_r [1 - F_r(\tau') \cos\omega_r \tau'] \qquad [45]$$

in this form, Eq. [45] does not take into account any inhomogeneous broadening. Second, all the remaining mechanisms that cause the stimulated echo to decay will be represented by the decay function $F_o(\tau')$, which may be considered as the normalized echo amplitude that would be observed in the absence of the envelope modulation effect. Thus in the presence of envelope modulation, the normalized echo amplitude is

$$V(\tau') = F_o(\tau') \left\{ 1 - \sum_{r=1}^{2n} a_r [1 - F_r(\tau') \cos\omega_r \tau'] \right\} \qquad [46]$$

This result is essentially equivalent to that obtained by Blumberg et al[15].

$$V_{mod,\tau}(T) = \sum_{r=0}^{n} a_r F_r(T) \cos\omega_r(T+\tau) \qquad [47]$$

In the absence of the decay function, $F_o(\tau')$, the Fourier transform of Eq.[44] yields 2n superhyperfine lines and a δ-function at the origin in the frequency domain. Each of these superhyperfine lines is centered at frequency ω_r with amplitude a_r and a shape given by the Fourier transform of $F_r(\tau')$. The presence of $F_o(\tau')$ has the effect of broadening these superhyperfine lines and the δ-function at the origin in the frequency domain. This results in a loss of resolution in the frequency spectrum. It is therefore essential to divide the data by the decay function to improve the resolution.

In the absence of modulation (i.e., $a_r = 0$) the decay function is given by $Fo(\tau')$. In the presence of modulation we can write Eq. [40] as

$$V(\tau') = F_o'(\tau')[1 + \sum_{r=1}^{2n} a_r' F(\tau')\cos\omega_r(\tau')]$$

where

$$F_o'(\tau') = F_o(\tau')(1 - \sum_{r=1}^{2n} a_r) \qquad [48]$$

$$a_r' = a_r(1 - \sum_{r=1}^{2n} a_r)^{-1}$$

and $F_o'(\tau')$ is now the decay function. Following Blumberg et al.[15], this decay function was fitted to a fifth degree polynomial as given in Eq. [49] over the experimentally observed range. Division of Eq. [48] by

$$F_o'(\tau') = \sum_{i=1}^{5} b_i (\tau')^i \qquad [49]$$

and subtraction of unity gives the modulation function which was Fourier transformed.

Eqs. [47] and [48] are valid for oriented single crystals. But the same formalism can be applied to polycrystalline samples with the assumption that the decay function $Fo'(\tau')$ does not strongly depend on the orientation of the electron-nuclear vector with respect to static magnetic field[16]. In a single crystal the above procedure totally removes the large dc component while in polycrystalline systems the dc component is only approximately removed from the Fourier-transformed spectrum.

A serious problem arises in Fourier transforming the recorded modulation because of the truncation of the recorded envelope. Ideally the envelope should be recorded from $\tau' = 0$ to ∞. However, because of instrumental limitations and the computer memory requirements the envelope is generally recorded in the range $\tau_i' \leqslant \tau \leqslant \tau_f'$. The loss of

data beyond τ_f' is of little concern because by this time the signal would have merged into the noise. However, the loss of data in the region $0< \tau_i'$ is more serious and introduces artifacts into the transformed spectrum[17]. The truncation of the envelope in the time domain is equivalent to a multiplication by a rectangular window function

$$h(\tau) = 1 \qquad\qquad \tau_i' \leqslant \tau \leqslant \tau_f'$$

$$h(\tau) = 0 \qquad\qquad \text{otherwise}$$

Such a truncation in the time domain is equivalent to convolution in the frequency domain by FT $\{h(t)\}$, which is the well known $\sin \omega t/\omega t$ function. In general a line shape will result that has negative side lobes, an undesirable feature in a multiline spectrum. To illustrate this, the influence of truncation on a Lorentizian lineshape is shown in Fig. 6. This lineshape originates from an exponential decay function $F(t) = \exp(-t/T_2)$. In Fig. 6 the original and truncated decay functions are shown together with the real part (cosine) and modulus ($\sqrt{P(\omega)}$) of their Fourier transform. In this example, we chose $\tau_i' = T_2/2$. As can be seen from this figure, the modulus spectrum can be used to circumvent the side lobes problem. There are, however, some disadvantages with the modulus spectrum. First, the lines are broader than those in a cosine spectrum, originating from the long tails of the imaginary part of the transform. Second, the

Fig. 6

Effect of Fourier transformation of a Lorentzian Line.
On the left the time domain plot and on the right the
modulus and Cosine Fourier transforms are shown. The
modulus Fourier transform is always positive and
definite.

a) An exponential decay (e^{-t/T_2}) and its Fourier
   transformed spectra.

b) The decay truncated before $t < T_2/2$. The Cosine
   Fourier transform shows prominent sidelobes.

c) The time domain data of (b) treated with a
   window. The amplitudes of the sidelobes as
   well as the main line are reduced.
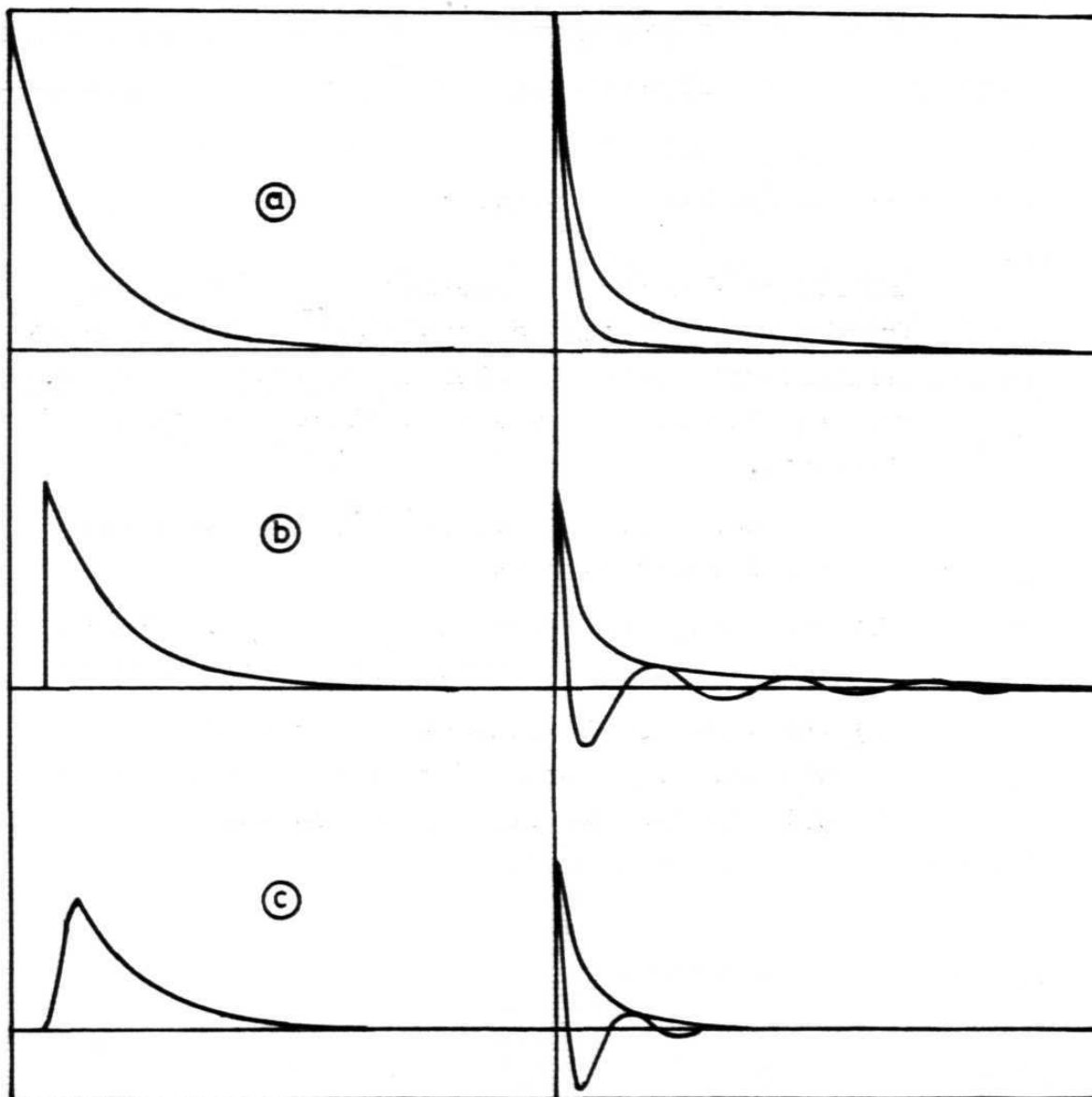
← Time →   ← Frequency →

nonlinearity of the modulus spectrum will cause problems for
spectra with regions of overlap of different lines. This
nonlinearity will also manifest itself when a background is
present in the spectrum. A background may be caused by the
fact that the first data sample which is numerically equal
to the sum of the data points in the cosine spectrum is not
taken at $\tau' = 0$, but at $\tau' = \tau_i'$. Both disadvantages may
be eliminated to a certain extent by the so called apodization
of the spectrum. The apodization involves multiplying the
time domain data by a window function which varies smoothly.
In the present studies we have used the window function
suggested by Bingham et al.[18]

$$
\begin{aligned}
h(\tau') \; &= \; 1 && for \quad \tau_i'+\alpha(\tau_f'-\tau_i') \leqslant \tau' \leqslant \tau_f'-\alpha(\tau_f'-\tau_i') \\[2ex]
&= \; \frac{1}{2}\left[1 - \cos\frac{\pi}{\alpha}\left(\frac{\tau'-\tau_i'}{\tau_f'-\tau_i'}\right)\right] && for \quad \tau_i' \leqslant \tau' \leqslant \tau_i'+\alpha(\tau_f'-\tau_i') \\[2ex]
&= \; \frac{1}{2}\left[1 - \cos\frac{\pi}{\alpha}\left(\frac{\tau'-\tau_f'}{\tau_f'-\tau_i'}\right)\right] && for \quad \tau_f'-\alpha(\tau_f'-\tau_i') \leqslant \tau' \leqslant \tau_f' \\[2ex]
&= \; 0 && otherwise \qquad\qquad [50]
\end{aligned}
$$

where the window parameter α takes the values $0 \leqslant \alpha \leqslant 0.5$.
Instead of having a discontinuity at $\tau' = \tau_i'$ the window
function $h(\tau)$ rises smoothly to unity according to a half
cosine bell. The multiplication of the data by this time

Fig. 7

A plot of the window function given by Bingham et al.[18]
[Eq.(50)] for τ_i = 0.8 µsecs and τ_f = 8 µsecs for
different values of α.
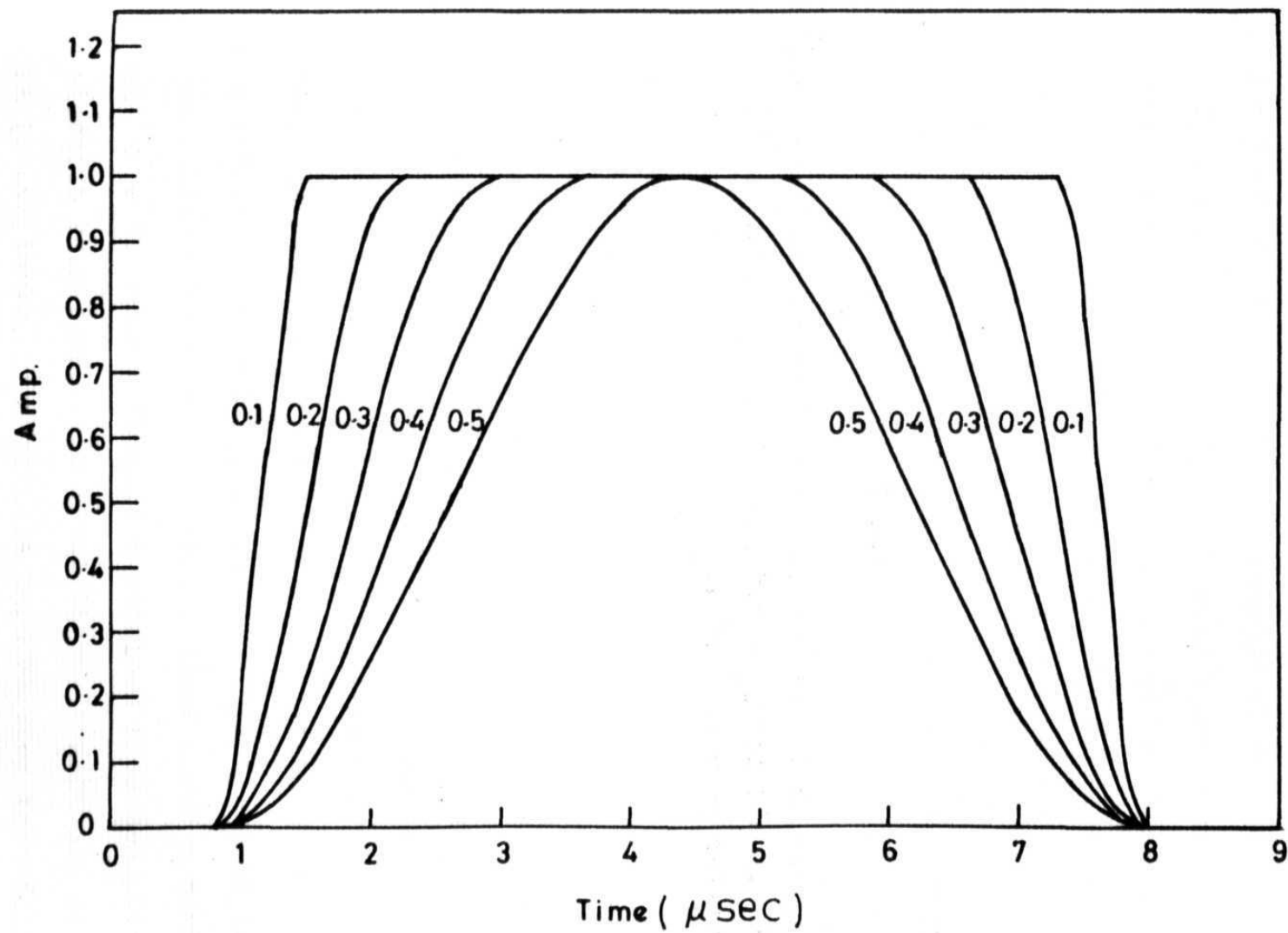
BINGHAM et al.[18] (WINDOW FUNCTION)

window is sometimes referred to as tapering the data. The width of the cosine bell is determined by the parameter α. $\alpha = 0$ corresponds to the rectangular window and for $\alpha = 0.5$ the window is identical to the well known Hanning window[19]. Increasing α reduces the amplitudes of the side libes of FT $\{ h(t) \}$ relative to the amplitude of the main lobe at the expense of the amplitude and narrowness of the main lobe. The truncated exponential function in Fig. 6 was tapered with $\alpha(\tau_f' - \tau_i') = T_2/2$. A reduction of the side lobes of the real part of the line shape function and shortening of the tails of the modulus line shape function are the results. For non-Lorenzian lines similar results are expected. A plot of the window function with $\tau_i' = 0.8$ μs and $\tau_f = 8$ μs, for different values of α is shown in the Fig. 7.

Another way of solving the problem of truncation of the time domain data is to extrapolate the data to time $\tau' = 0$.[20,21] As can be seen from the expression for the modulation function $V(\tau')$, the envelope modulation function contains several cosine cycles. The cosine nature of these cycles shows that they all reach their maximum values at time $\tau' = 0$. The data is extrapolated by continuing the oscillations to time $\tau' = 0$ and taking care that these oscillations reach a maximum at $\tau' = 0$. Also information obtained from two-pulse electron spin echoes and simulations is made use of whenever it is available. The data is then Fourier transformed by dividing it out with the decay function.

One problem associated with the Fourier transformation discussed above arises due to the so called blind spots in the spectrum[22]. From Eq. (41) it can be seen that the echo amplitude depends on both τ and τ'. In principle the Fourier spectrum can be obtained by Fourier transforming the echo envelope either as a function of τ, keeping T fixed or as a function of T keeping τ fixed. As the echo decays slower as a function of T than as a function of τ, a better spectral resolution is obtained by varying T for a fixed value of τ. The fact that in this spectrum the time parameter τ is kept fixed at some chosen value constitutes a problem as the Fourier peak intensities strongly depend on τ. In the worst case it is even possible that some peaks in the spectrum disappear completely. This phenomenon is called 'suppression effect' ang gives rise to blind spots in the FT spectrum. The suppression effect can be circumvented by measuring the echo envelope as a function of T for various values of τ.

There is another complication which arises in recording the data. This arises due to the so called 'interference' effect. This could be understood by referring to Fig. 8. As mentioned earlier the three pulse echo envelope is recorded by applying three microwave pulses at t = 0, τ and τ'. Spin echoes are formed at t = 2τ (Hahn echo) and at t = $\tau + \tau'$ (stimulated echo) and additional echoes

Fig. 8

Pulse sequence and the echoes generated in a three
pulse echo experiment. The echoes at 2τ, $2\tau'-\tau$ and
$2\tau'$ are generated by combinations between pulses
I and II, II and III, I and III respectively.

INTERFERENCE EFFECT
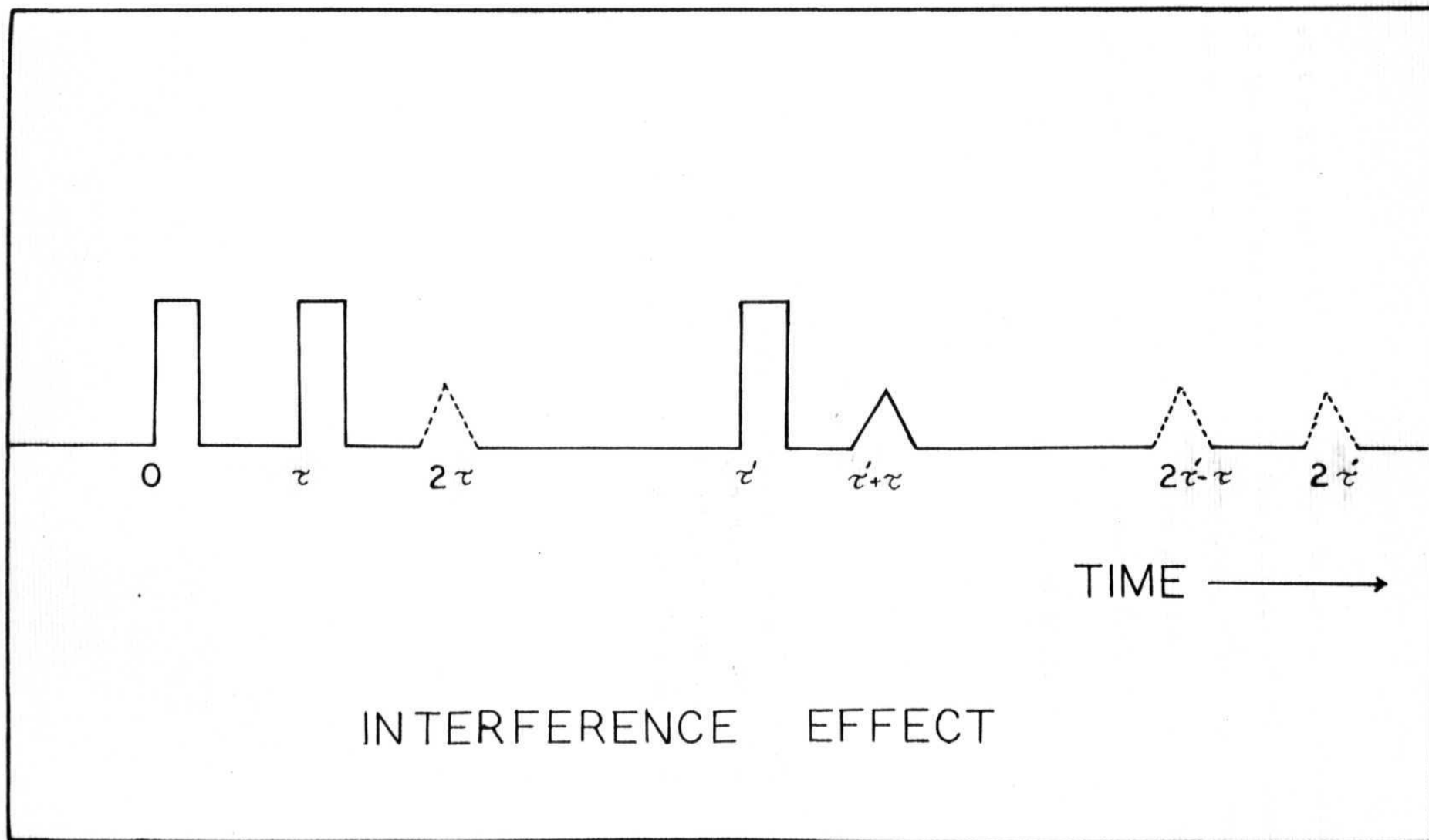
at $t = 2\tau'$ and $2\tau' - \tau$. In order to avoid the interference of the additional echoes with the stimulated echo, recording of the data has to start after $\tau' \geqslant 3\tau$. This again results in the loss of initial data. This problem can be eliminated by removing these interfering glitches manually.

The theory developed here will be applied to various problems in the following chapters.

References

1. W.B. Mims, K. Nassau and J.D. McGee, Phys. Rev. 123, 2059 (1961).

2. W.B. Mims in 'Electron Paramagnetic Resonance', S. Geschwind Ed., Ch. 4, p 263, Plenem Press, New York 1972 .

3. L. Kevan in 'Time Domain Electron Spin Resonance', L. Kevan and R.N. Schwartz ed., Wiley Interscience, New York, 1979

4. E.L. Hahn, Phys. Rev. 80, 580 (1950).

5. L.G. Rowan, E.L. Hahn and W.B. Mims, Phys. Rev. A137, 61, (1965).

6. G.M. Zhidomorov and K.M. Salikhov, Teor, Eksp. Khim. 4, 514 (1968) (Theor. Exp. Chem. 4, 332 (1968).

7. W.B. Mims, Phys. Rev. B5, 2409 (1972).

8. W.B. Mims, Phys. Rev. B6, 3543, (1972).

9. S.A. Dikanov, A.A. Shubin and V.N. Parmon, J. Mag. Res. 42, 474 (1981).

10. W. Low, 'Paramagnetic Resonance in Solids', Academic Press, New York, 1960.

11. C.P. Stichter, 'Principles of Magnetic Resonance', 2nd Ed., Springer-Verlag, New York, p150 1978 .

12. T.C. Farrar and E.D. Becker, 'Pulse and Fourier Transform NMR', Academic Press, New York, 1971.

13. R.P.J. Merks and R. de Beer, J. Mag. Res. 37, 305 (1980).

14. J.P. Hurrell and E.R. Davies, Solid State Commun. 9, 461 (1971).

15. W.E. Blumberg, W.B. Mims and D. Zuckerman, Rev. Sci. Instrum. 44, 5460 (1973).

16. P.A. Narayana and L. Kevan, J. Mag. Res. 46, 84 (1982).

17. D. Shaw, 'Fourier Transform NMR Spectroscopy', Elsevier Amsterdam, 1976.

18. C. Bingham, M.D. Godfrey and J.W. Tukey, IEEE Trans. Audio Electroacoustics, AU15, 56 (1959).

19. R.B. Blackman and J.W. Tukey, 'The Measurement of Power Spectra', Dover, New York, 1959.

20. T. Shimizu, W.B. Mims, J. Peisach and J.L. Davis, J. Chem. Phys. 70, 2249 (1979).

21. J. Peisach, W.B. Mims and J.L. Davis, J. Biol. Chem. 254, 12379 (1979).

22. R.P.J. Merks and R. de Beer, J. Phys. Chem. 83, 3319 (1979).

CHAPTER III

ENVELOPE MODULATION STUDIES OF AMMONIUM HALIDE SINGLE CRYSTALS

INTRODUCTION:

The electron spin echo modulation contains, in principle, all the information about the hyperfine interactions with the surrounding nuclei. However as the complexity of the modulation increases, it becomes increasingly difficult to analyse the envelope modulation in the time domain. An alternative way to analyze the modulation pattern is to transform the time domain data into frequency domain by Fourier transformation. Such studies have been carried out by a number of groups[1-5]. The most systematic studies were carried out by Merks and de Beer on $Cu^{2+}:Cs_2ZnCl_4$ single crystal system[5]. These studies clearly demonstrated that the FT ESEEM could be an alternative to the ENDOR technique and in fact it could be superior to ENDOR in a number of respects like excellent base line stability, ability to observe very small splittings and noise immunity from the microphonics.

The system chosen by Merks and de Beer exhibits a very long phase memory time and this results in a good resolution in the FT spectrum. Our main interest is in the application of this technique to randomly oriented samples which generally exhibit short phase memory times. In order to assess the applicability of their technique to randomly oriented samples it is necessary to study the FT ESEEM of single crystal systems which exhibit short phase memory

times. One such system is Cu^{2+} doped ammonium halide single crystals. Specifically we report in this Chapter the studies on Cu^{2+} doped NH_4Cl, ND_4Cl and NH_4Br single crystals. Apart from short phase memory times, the choice of the systems was dictated by a number of other considerations: 1) the frequency spectrum is very rich because all the nuclei present in the system such as ^{14}N, ^{35}Cl and ^2D are all magnetic, 2) the nuclei N, Cl (Br), and D exhibit large quadrupole couplings and therefore it is possible to investigate the effects of quadrupole couplings on the FT spectrum and this is particularly important because many of these nuclei are present in a number of biologically important molecules, 3) the axial ligands can be easily changed by controlling the pH value[6] of the growth solution. In crystals grown from an acidic medium, the axial ligands are two water molecules and in the crystals grown from basic medium the ligands are two ammonia molecules[6]. Thus it is possible to study the effects of axial ligands on the Fourier spectrum. This is a very important consideration in studying ligand binding to iron in hemoglobin and myoglobin molecules[7]. The FT spectrum from these crystals was Fourier transformed in two different ways as discussed in the last chapter. 1) The recorded data was apodized by multiplying it with a smoothly varying window function suggested by Bingham et al. for different window parameters, and 2) the data was extrapolated to $\tau' = 0$[2]. The large

dc component in the FT spectrum was eliminated by dividing
the data by a decay function obtained by using a sixth
degree polynomial. The frequency components in the FT
spectrum were identified with specific nuclei around the
paramagnetic centre and were compared with the ENDOR data
available[8].

Theory:

The ESEEM spectra of these were recorded with the
magnetic field parallel to one of the cube edges of the
crystals. At room temperature the local symmetry of the
copper complex is tetragonal. At 4.2 K there is a slight
orthorhombic distortion of the crystalline field[9]. In the
following discussion such an orthorhombic distortion was
neglected and the complex was treated as tetragonal. The
spin Hamiltonian for such a system can be written as

$$\mathcal{H} = g_n\beta_n \, H \, I_z + AI_zS_z + B \, I_xS_z$$

$$+ Q_{zz} \left[I_z - \frac{1}{3} I(I+1) \right] \qquad [1]$$

where Q_{zz} is the principal component of the quadrupole
tensor along the z direction. The other symbols have their
usual meaning. The spin Hamiltonian could be written
in this form because the ENDOR studies indicate that the

quadrupolar and the hyperfine tensors have almost collinear principal axes[8]. The small noncollinearity is neglected. In the above equation the first term represents the nuclear Zeeman interaction, and the second, the isotropic hyperfine interaction. The z-axis defines the quantization axis of the electron spin. The angle θ is the angle between the line joining the electron and the nucleus and the quantizing axis of S_z. The expressions for A and B are given by

$$A = \frac{1}{h} gg_n\beta\beta_n\ r^{-3}\ (3\cos^2\theta-1) + a$$

[2]

$$B = \frac{1}{h} gg_n\beta\beta_n\ r^{-3}\ (3\cos\theta\sin\theta)$$

The first term in the expression for A arises due to dipolar interaction and the second arises from the contact coupling. Here r is the electron-nuclear distance.

In this Hamiltonian the hyperfine coupling of the electron spin with a ^{63}Cu or ^{65}Cu ($I = 3/2$) nucleus is neglected. Coupling with the Cu nucleus mixes the $m_s = \pm\frac{1}{2}$ electron spin states and modifies the magnetic moment seen by the nearby nucleus. This effect is negligible here and the terms describing this interaction are not included in the above Hamiltonian. Since the geometry of the complex is known along with the g-values, the dipolar term in the electron-nuclear interactions could be calculated.

The calculated values for the dipolar interaction for different nuclei are tabulated in Table 1. It is seen that the dipolar coupling is negligible for nuclei other than those directly liganded to Cu^{2+}. Also these dipolar couplings to these nuclei are negligibly small compared to the nuclear Zeeman or contact couplings. Therefore in calculating the energies the dipolar couplings are neglected. The Hamiltonian therefore is diagonal and the superhyperfine frequencies for the coupling between an $S = \frac{1}{2}$ and $I = \frac{1}{2}$ ($Q_{zz} = 0$) nucleus are given by

$$h\nu_{ENDOR} = |g_n\beta_n H \pm \frac{1}{2}|a||$$

for $I = 1$ there are four transition energies possible, given by

$$h\nu_{ENDOR} = |g_n\beta_n H \pm \frac{1}{2}|a| \pm |Q_{zz}||$$

and for $I = 3/2$

$$h\nu_{ENDOR} = |g_n\beta_n H \pm \frac{1}{2}|a| \pm 2|Q_{zz}||$$

$$= |g_n\beta_n H \pm \frac{1}{2}|a||$$

Fig. 1

Energies of the $I = 1$ superhyperfine levels as
a function of the resultant field seen by the
nucleus. The frequencies f_1 and f_2 are
$|H_o - \frac{1}{2}| a| h/g_n \beta_n|$ and $|H_o + \frac{1}{2}| a| h/g_n \beta_n|$ respectively,
where H_o is the applied field and $|a|$ is the
contact coupling constant. If $H_o \approx \frac{1}{2}| a| h/g_n \beta_n$,
then $f_1 = \nu_+$, the largest of the zero field
quadrupole frequency, ν_- and ν_o being the other
two.
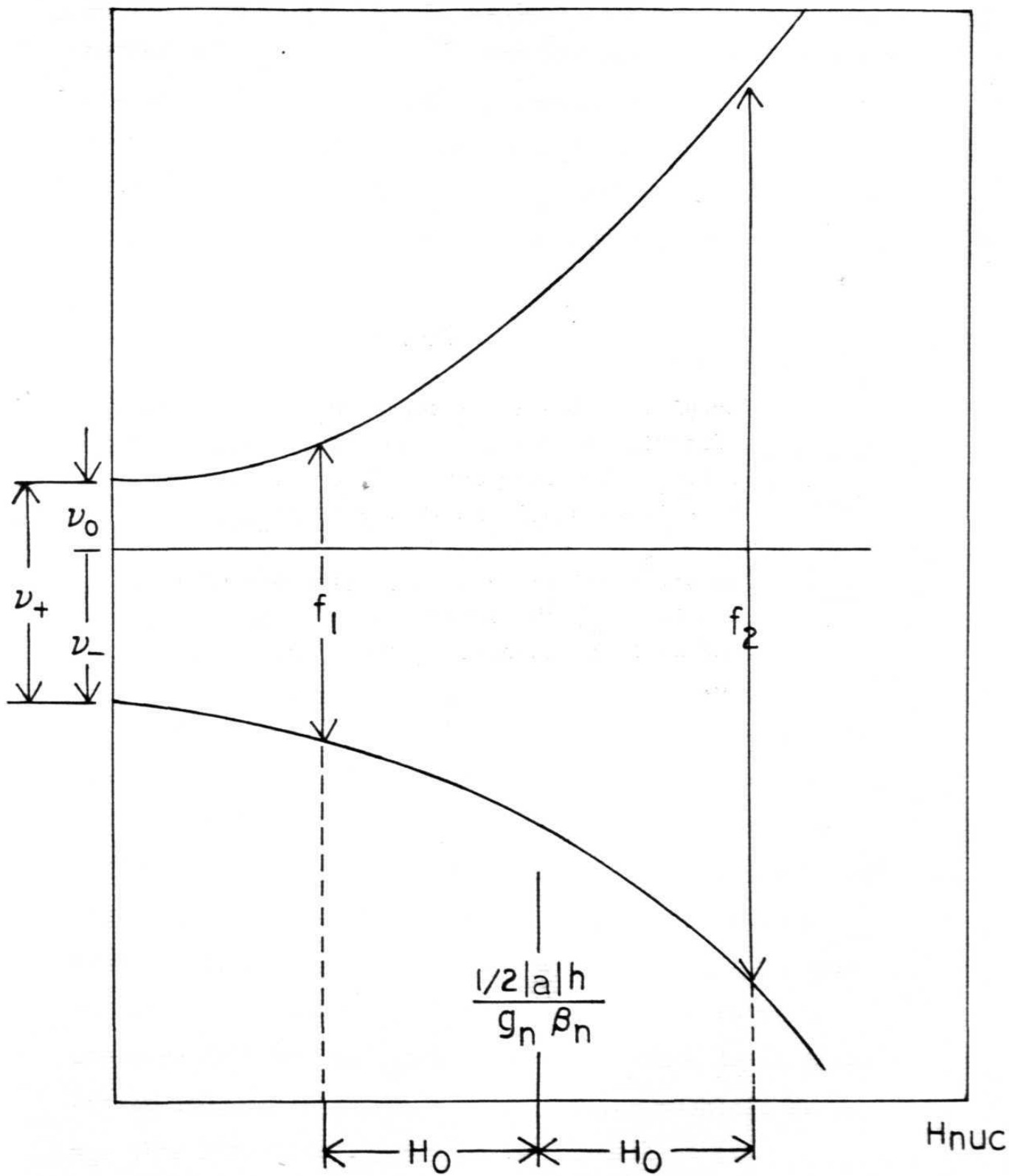
In the present case the modulation is expected from several nuclei with spin $I = 1$ (^{14}N and ^{2}D) and with spin $I = 3/2$ (Cl and Br). From the separations of the frequency components, the hyperfine coupling constant (a) and the quadrupole coupling constant (Q_{zz}) can be calculated. The nuclear Zeeman energy can be calculated because the parameters g_n, β_n, are known.

The quadrupole and hyperfine coupling give rise to splitting in the absence of any magnetic field. Fig. 1 shows the energy level separations for nucleus with $I = 1$. The level separations increase from the zero-field values ν_0, ν_- and ν_+ as a magnetic field H_o is applied. It was shown above that the dipolar and pseudo-dipolar contributions to the echo modulation are very small in relation to the contribution from other effects such as the isotropic coupling. The term which represents this coupling in the spin-Hamiltonian is $aI.S$. The effect of this term on the energy level separation is equivalent to the effect of a magnetic field of value $\frac{1}{2}|a| h/g_n\beta_n$ (for $I = 1$ and $S = \frac{1}{2}$) where g_n and β_n are the nuclear g-factor and nuclear magneton respectively. In effect this term can be regarded as a local magnetic field at the nucleus due to the unpaired spin in the paramagnetic ion. This local field either opposes or reinforces the applied magnetic field H_o. The resultant field seen by the nucleus is

given by

$$H_{nuc} = H_o \pm \frac{1}{2}|a|h/g_n\beta_n \qquad [5]$$

or,

$$H_{nuc} = \frac{1}{2}|a|h/g_n\beta_n \pm H_o \qquad [6]$$

depending on the relative magnitudes of these terms. It can be seen from the figure that the outer levels are relatively insensitive to the orientations of the nuclear quadrupole axes with respect to the orientation of the magnetic field. However, the separation between either of the outer levels and the inner levels is considerably more sensitive to orientations. In such a situation two possibilities can be visualized. If the local field term is large compared to the Zeeman term, we observe transitions such as f_1 and f_2 shown in the energy level diagram. These two lines are separated by the amount $|a|h/g_n\beta_n$. If $H_o \approx \frac{1}{2}|a|h/g_n\beta_n$, then $f_1 \simeq \nu_+$, where ν_+ is the largest of the zero-field nuclear quadrupolar resonance frequencies. In most cases the other zero-field quadrupolar frequencies ν_- and ν_o are also observed as resolved spectral lines. In this case a fourth line is also expected to be seen corresponding to f_2 in the energy level diagram, whose position is given by $H_o + \frac{1}{2}|a|h/g_n\beta_n$.

EXPERIMENTAL:

Crystals of NH_4Cl (Centres I and II) and $NH_4Br(II)$ were grown from saturated solutions of these halides. About 30% by weight of urea was added to the growth solution to prevent dentritic growth. To obtain copper doped crystals, a few drops of 0.01M $CuCl_2$ solution (about 0.01 ml) were added to the growth solution. Centre I crystals were grown by the addition of a few drops of HCl (about 2 or 3 drops for 20 ml of the growth solution) so that the pH was maintained at 2.0. The solutions were kept in a constant temperature bath during the growth period. Crystals of good cubic growth with dimensions of 5 x 2 x 2 mm were obtained. In order to obtain crystals, with Centre II, the pH of the growth solution was maintained at $\approx$ 8.0, by adding a few drops of 28% NH_4OH solution. The solution was kept in a dessicator with pottasium hydroxide pellets as the desiccant.

The deuterated crystals ND_4Cl (Centre II) were grown using ND_4Cl and ND_4OD in an exactly similar way as described above. ND_4Cl was purchased from Sigma Chemicals and ND_4OD was purchased from Stohler Isotope Chemicals. A known amount of $CuCl_2.2H_2O$ solid was dried to remove the water of crystallization and was recrystallized in D_2O to obtain $CuCl_2.2D_2O$. The urea used in growing these crystals was crystallized three times in D_2O to obtain deuterated urea.

The spin echo data were digitized at 20 nsec. interval.
The echo envelope decay was fitted to a sixth degree poly-
nomial. The computations were carried out on a Robotron 5620
computer.

RESULTS AND DISCUSSION:

Electron spin echo envelope modulations have been
recorded for the following single crystals: $NH_4Cl:Cu^{2+}$
(Centre I), $NH_4Cl:Cu^{2+}$ (Centre II), $ND_4Cl:Cu^{2+}$ (Centre II)
and $NH_4Br:Cu^{2+}$ (Centre II). Attempts to grow single crystals
of $ND_4Cl:Cu^{2+}$ (Centre II) and $ND_4Br:Cu^{2+}$ (Centre II) were
unsuccessful. ESEEM were recorded with the magnetic field
parallel to the symmetry axis of the complex and also
perpendicular to it. Three pulse echo modulation patterns
were recorded as a function of T for different values of τ .
The ESEEM data were Fourier transformed using the two methods
of extrapolation to time $\tau' = 0$ and apodization using the
window function as described in Chapter II. Before Fourier
transformation a smooth curve was drawn to simulate the
decay of the echo in the absence of modulation. This was
fitted to a sixth degree polynomial. This polynomial was
then used to divide out the decay from the recorded data.
Extrapolation of the data was accomplished by continuing
the oscillations of the recorded portion of the envelope
to time $\tau' = 0$. Care was taken to make certain that no

Fig. 2

NH$_4$X (X = Cl$^-$ or Br$^-$) lattice in the body centred
phase doped with Cu^{2+}. The Cu^{2+} ion enters the
lattice interstitially. The ligands in the first,
second and third coordinate spheres can be
visualized. Hydrogens and deuterons are not
shown in the figure.

Cu²⁺
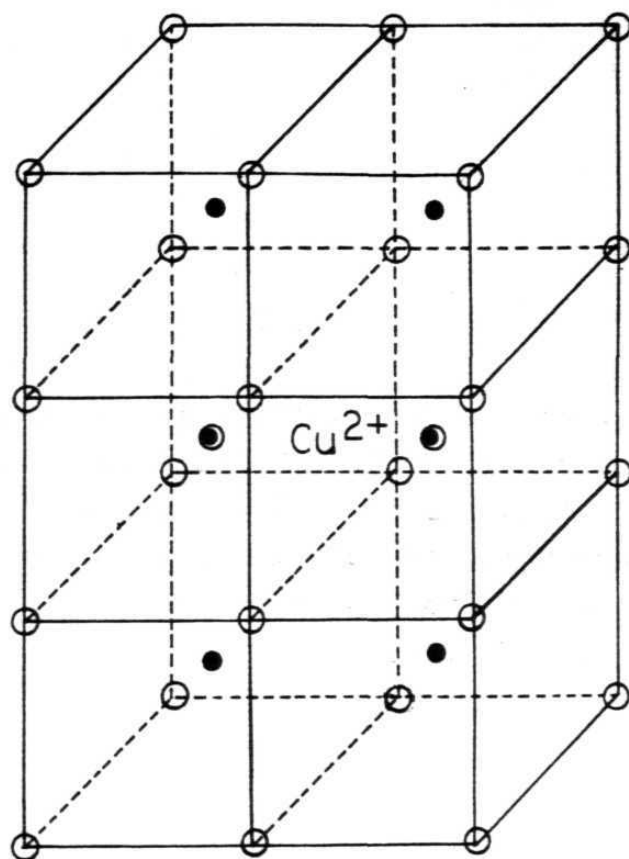
○ X⁻

● NH₄⁺

◐ NH₃

or H₂O

spurious frequency components were introduced and the modulation reached maximum at $\tau' = 0$. Preserving the cosine nature of the modulated envelope. The window function was applied to the unextrapolated time domain data for apodization. The data were Fourier transformed for different values of the window parameter α from 0 to 0.5 in steps of 0.1. The frequency components obtained upon Fourier transformation using these methods yielded consistent results.

Ammonium Chloride ($NH_4Cl:Cu^{2+}$):

1) Centre I $[(CuCl_4)^{2-}:2H_2O]$

A schematic diagram of the lattice of NH_4X (X = Cl,Br) is shown in Fig. 2. As shown in this Figure, Cu^{2+} enters the lattice at an interstitial site surrounded by four chloride ions lying in a plane, and two charge compensating H_2O molecules in a direction perpendicular to the plane[8]. In the case of Centre II the charge compensation is achieved by two ammonia molecules liganded axially.[8]

The three pulse echo modulation from $NH_4Cl:Cu^{2+}$(Centre I), recorded by monitoring the $g_\perp$ region (symmetry axis perpendicular to the magnetic field) for $\tau = 650$ nsec. is shown in Fig. 3. The dotted line is the extrapolated portion of the envelope. The frequency spectrum obtained by Fourier transformation of the modulation after extrapolation is

Fig. 3

The stimulated echo envelope for $NH_4Cl : Cu^{2+}$
(Centre I) for $\tau = 650$ nsec recorded in the $g_\perp$
region. The broken line represents the extra-
polated portion of the envelope. The echo
amplitude is in arbitrary units. $H_o = 0.295$ T,
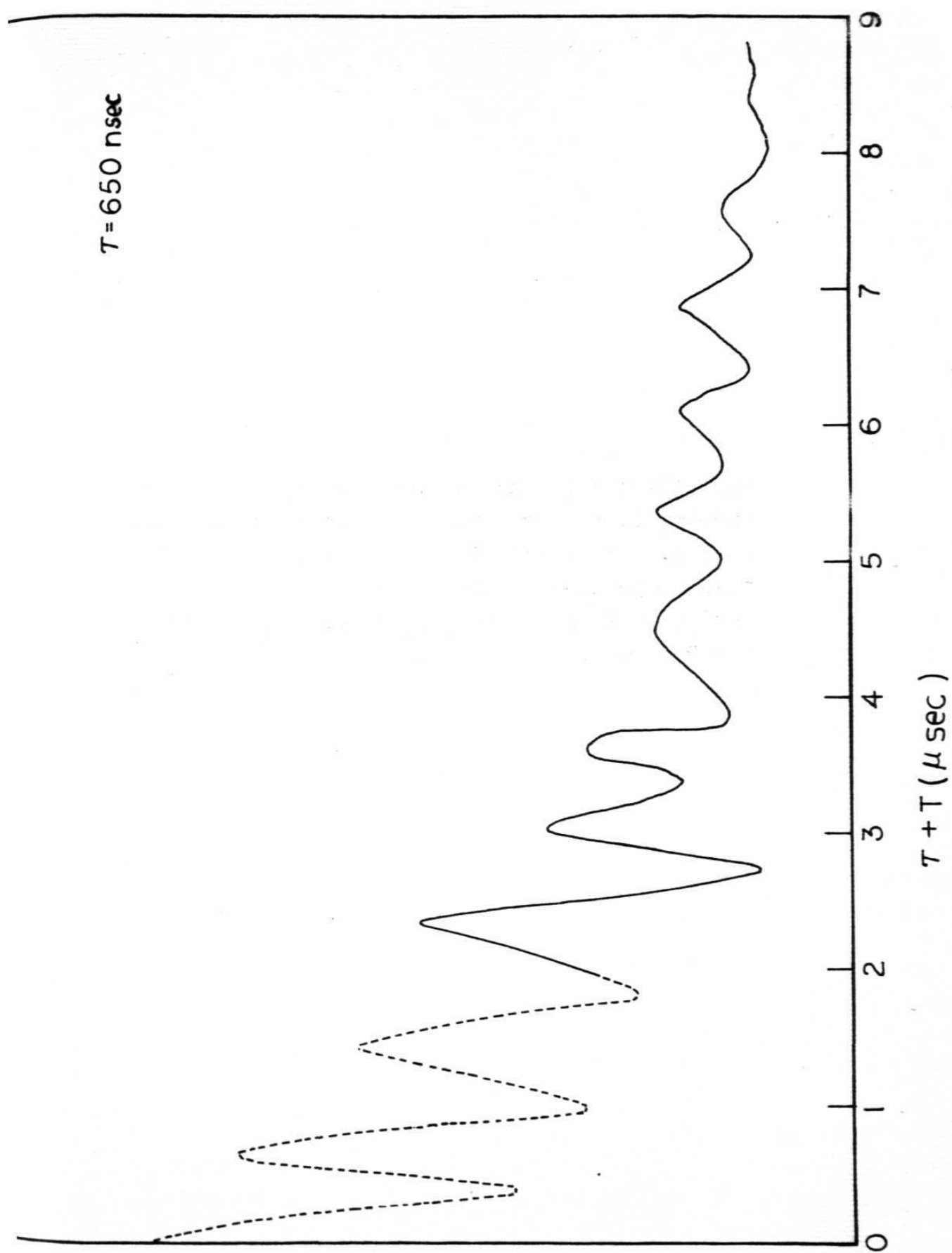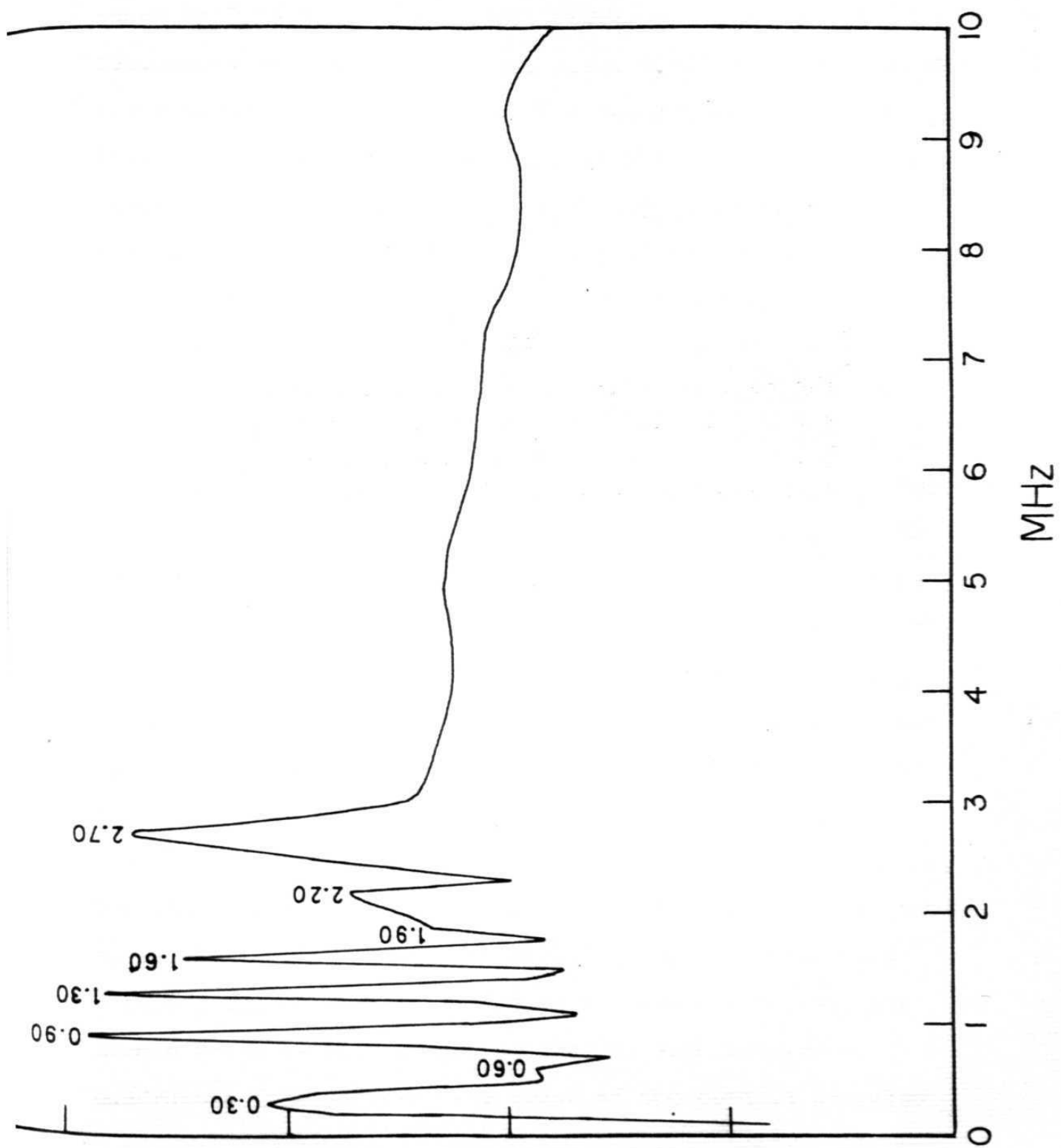$f = 9.44$ GHz.

Fig. 4

The Fourier cosine transform of the envelope
for $NH_4Cl : Cu^{2+}$ (Centre I) shown in Fig. 3.
The noise has been smoothened after 3 MHz. The
peak positions have been indicated.

MHz

shown in Fig. 4. The frequency spectrum shows several
components at 0.30, 0.60, 0.90, 1.30, 1.60, 2.20 and 2.70 MHz
and a broad peak at 1.90 MHz. The modulation does not arise
from the immediately liganded nuclei because the microwave
power used was not sufficient to excite these transitions.
The modulation from protons was eliminated by employing large
pulse widths. In any case the proton modulation is expected
to be weak because of the small value of I. Therefore the
modulation is assumed to be associated with nuclei in the
second and higher coordinate spheres around the central
Cu^{2+} ion. Following the arguments of Mims et al.[3], we interpret
the set of peaks at 0.30, 1.30, 1.60 MHz as arising due to
the zero-field quadrupole frequencies. Two of these peaks
add up to give the third, which is a characteristic of such
peaks[3]. These peaks are usually very sharp, but the large
width of the peak at 0.30 MHz is due to the presence of the
unresolved peak at 0.60 MHz. These frequencies correspond
to the zero-field quadrupolr frequencies ν_0, ν_- and ν_+
and arise due to coupling with nuclei with $I = 1$. It seems,
therefore reasonable to conclude that these peaks arise due
to coupling with nitrogen nuclei. As has been discussed
earlier, the contributions due to the contact and nuclear
Zeeman terms cancel out giving rise to such zero-field
quadrupole frequencies. The value of the contact coupling
can be calculated using the relation $|a| = \dfrac{2Hg_n\beta_n}{h}$. In the
present case, the value of a is 1.81 MHz. Using this value

of $|a|$, the frequency corresponding to f_2 in the energy
level diagram (Fig. 1) was calculated to be $\approx$ 2.71 MHz.
This is in excellent agreement with the 2.70 MHz line
observed in the frequency spectrum. The peak at 0.90 MHz is
the free nuclear precessional frequency arising from distant
nitrogens which have a negligible contact coupling with the
unpaired spin. The other components at 0.60, 1.90 and
2.2 MHz are from couplings with a chloride. These
frequencies would be discussed in detail for the case of
Centre II below where similar chloride frequencies have been
observed. ESEEM have also been recorded at different τ
values (500 nsec. - 950 nsec.). But they yielded
consistently the same frequencies. However, some frequencies
were absent at different τ values and this is due to the
suppression effect discussed earlier.

The ESEEM was also recorded with the static magnetic
field parallel to the symmetry axis for τ = 500 nsec.
This did not change the value of $|a|$, but the frequency
components changed. This is expected because of the change
in the field H.

2) Centre II $[(CuCl_4)^{2-}:2NH_3]$:

Here the ESEEM data have been recorded with the magnetic
field perpendicular to the symmetry axis only. In this case
it was possible to observe all the chloride ENDOR

Fig. 5

The three pulse echo envelope of a single crystal
of NH_4Cl : Cu^{2+} (Centre II) for τ = 350 nsec
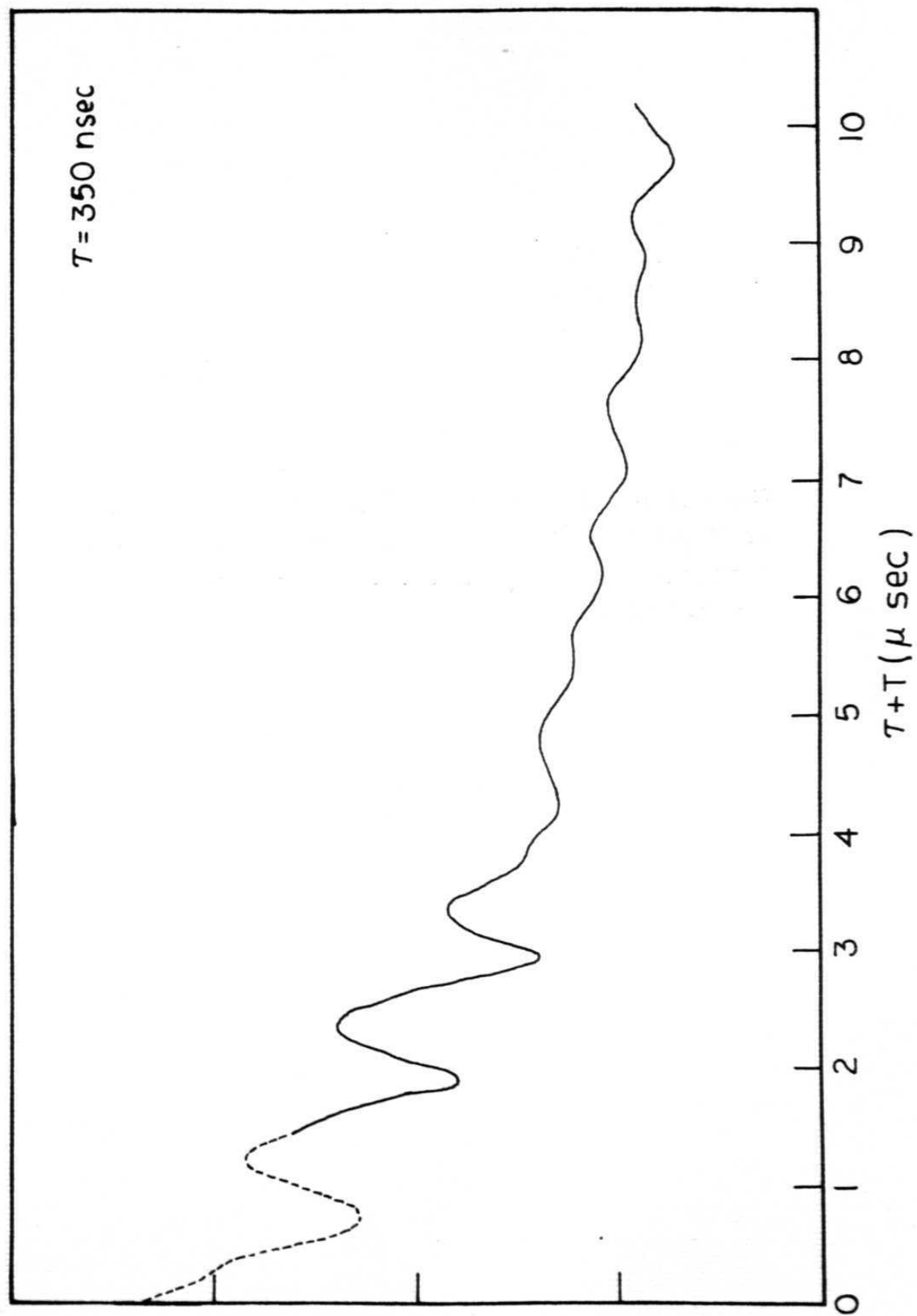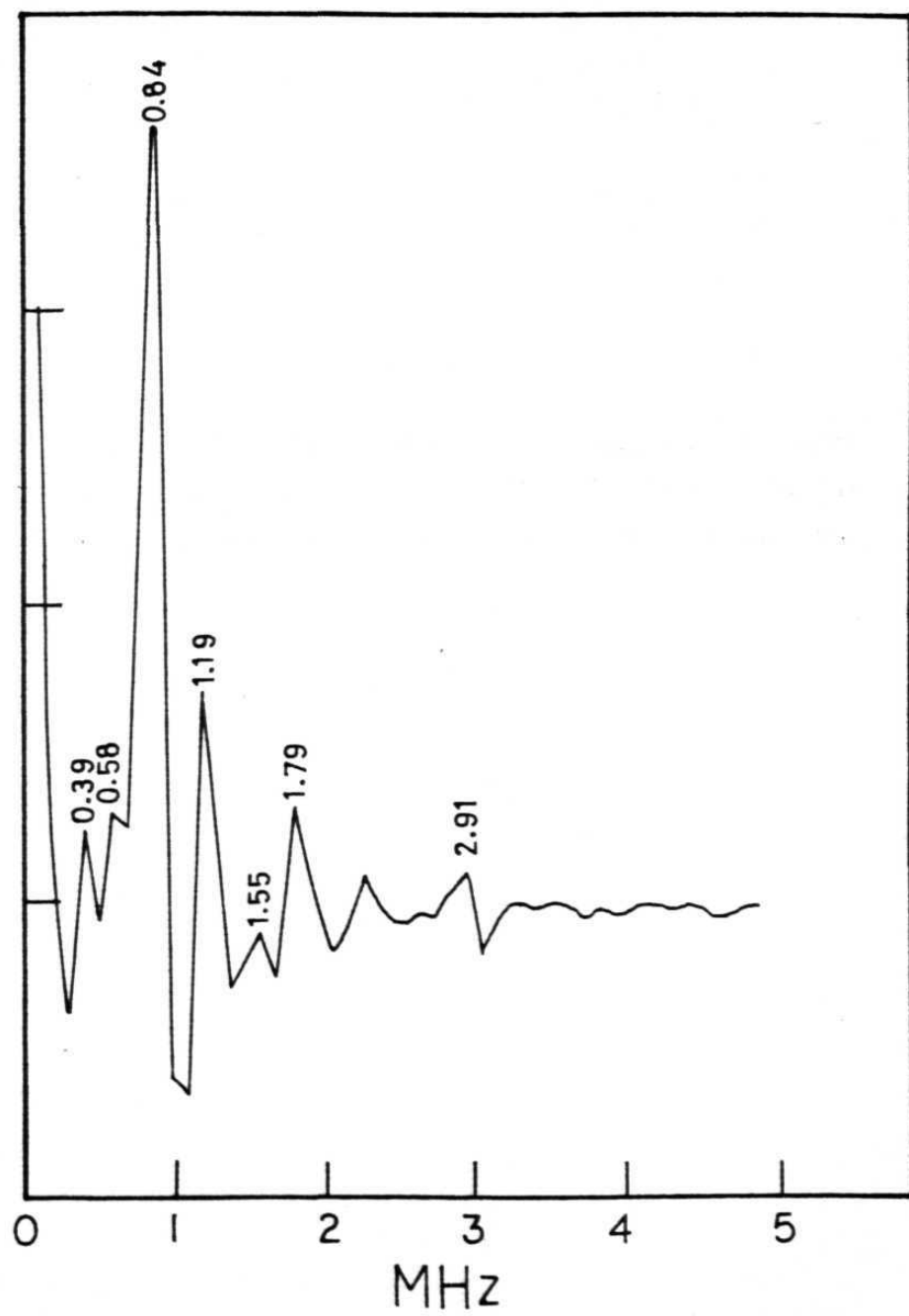recorded in the $g_\perp$ region. H_o = 0.283 T,
f = 8.79 GHz.

Fig. 6

Fourier cosine transform of the modulation of
$NH_4Cl : Cu^{2+}$ (Centre II) shown in Fig. 5. The
frequency components have been indicated.

Figs. 7 - 12

The Fourier cosine transform spectra for the
modulation of NH_4Cl : Cu^{2+} (Centre II) shown in
Fig. 5 after the application of the window
function. The different spectra are obtained
using different values of the window parameter α.

Fig. 7	$\alpha = 0.5$
Fig. 8	$\alpha = 0.4$
Fig. 9	$\alpha = 0.3$
Fig. 10	$\alpha = 0.2$
Fig. 11	$\alpha = 0.1$
Fig. 12	$\alpha = 0.0$ (without window)

The frequency components obtained in each case
have been indicated.

$\alpha = 0.1$

Peak labels: 0.39, 0.58, 0.85, 1.16, 1.55, 1.79, 2.91

$\alpha = 0.0$

MHz
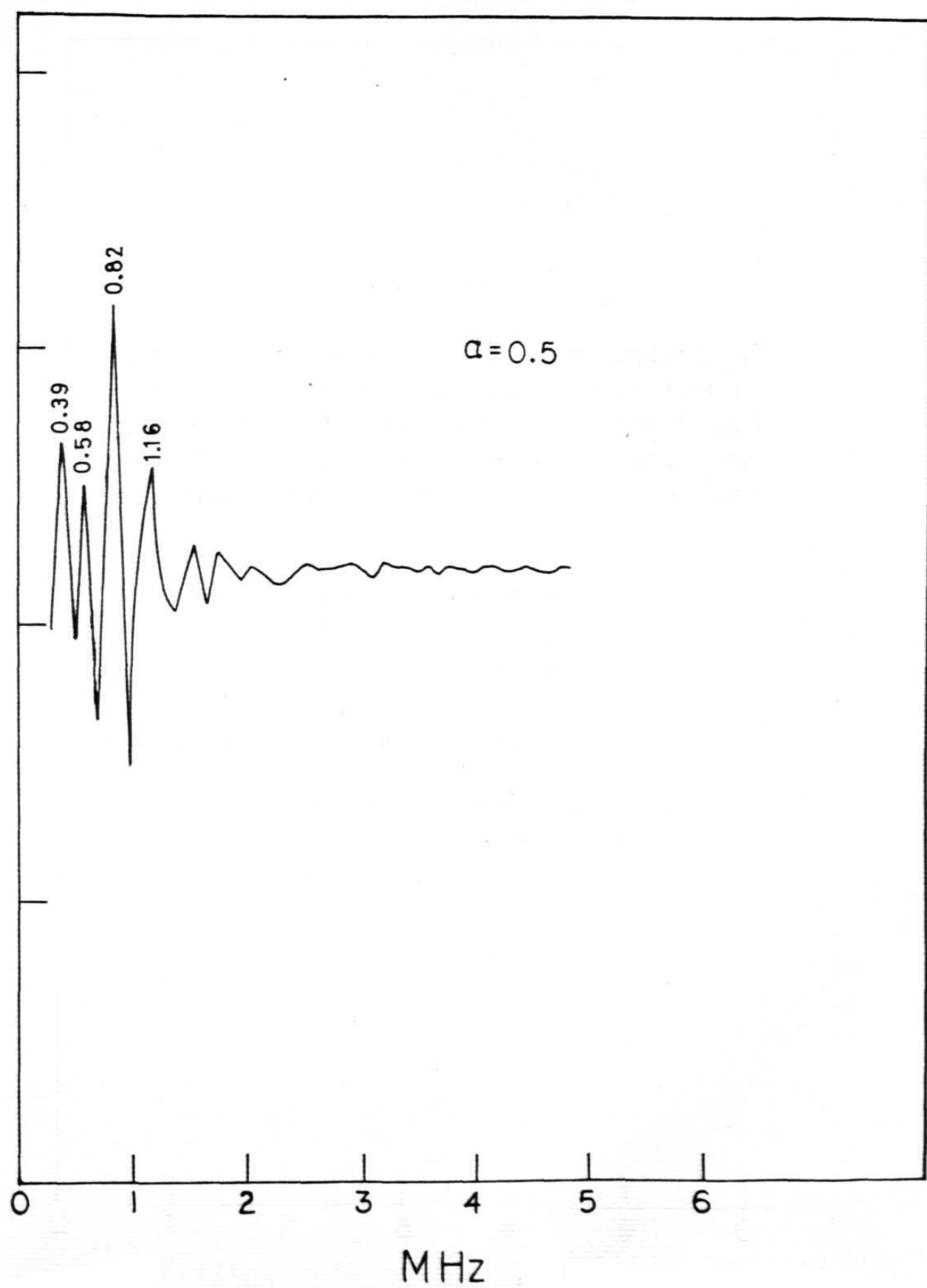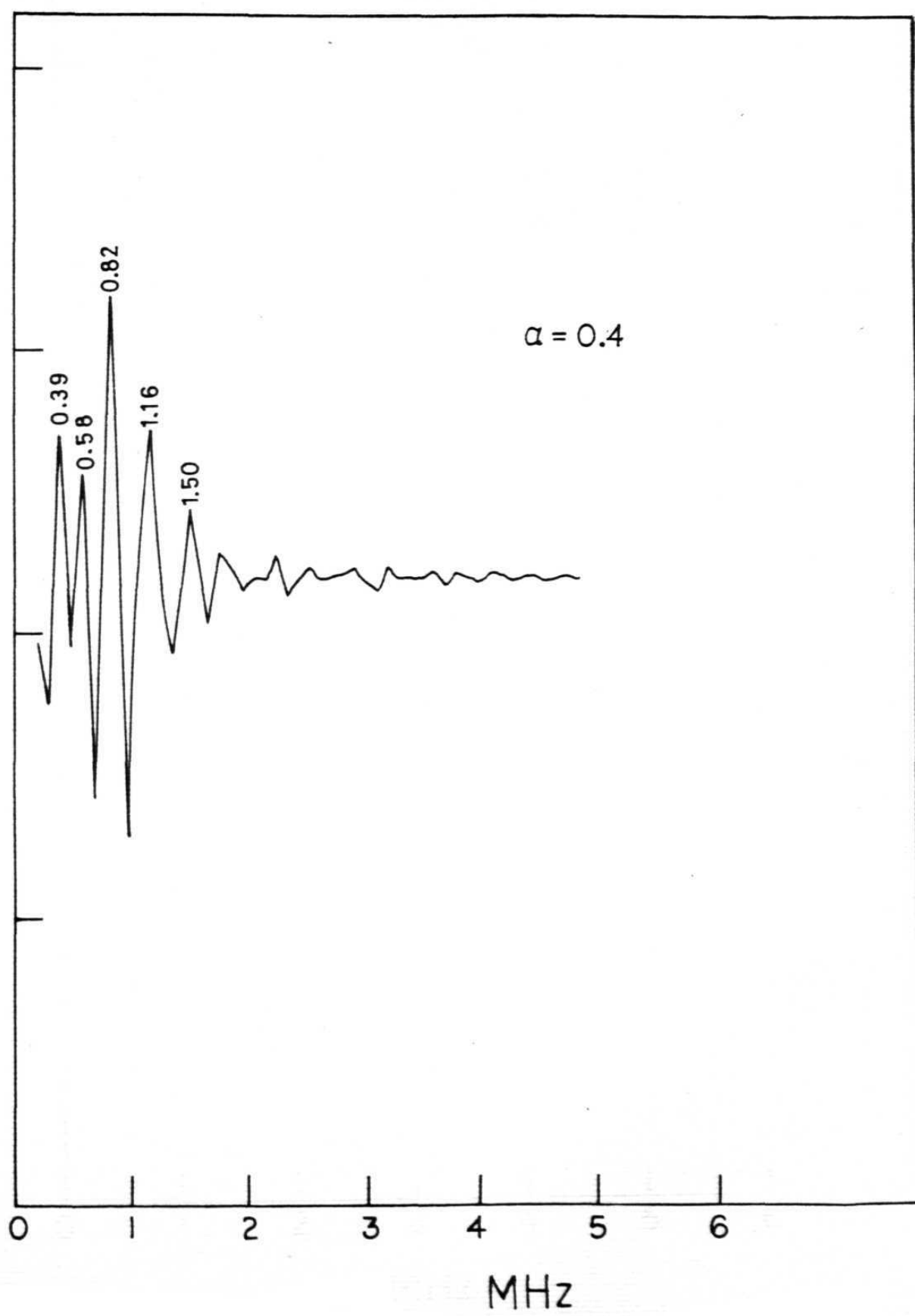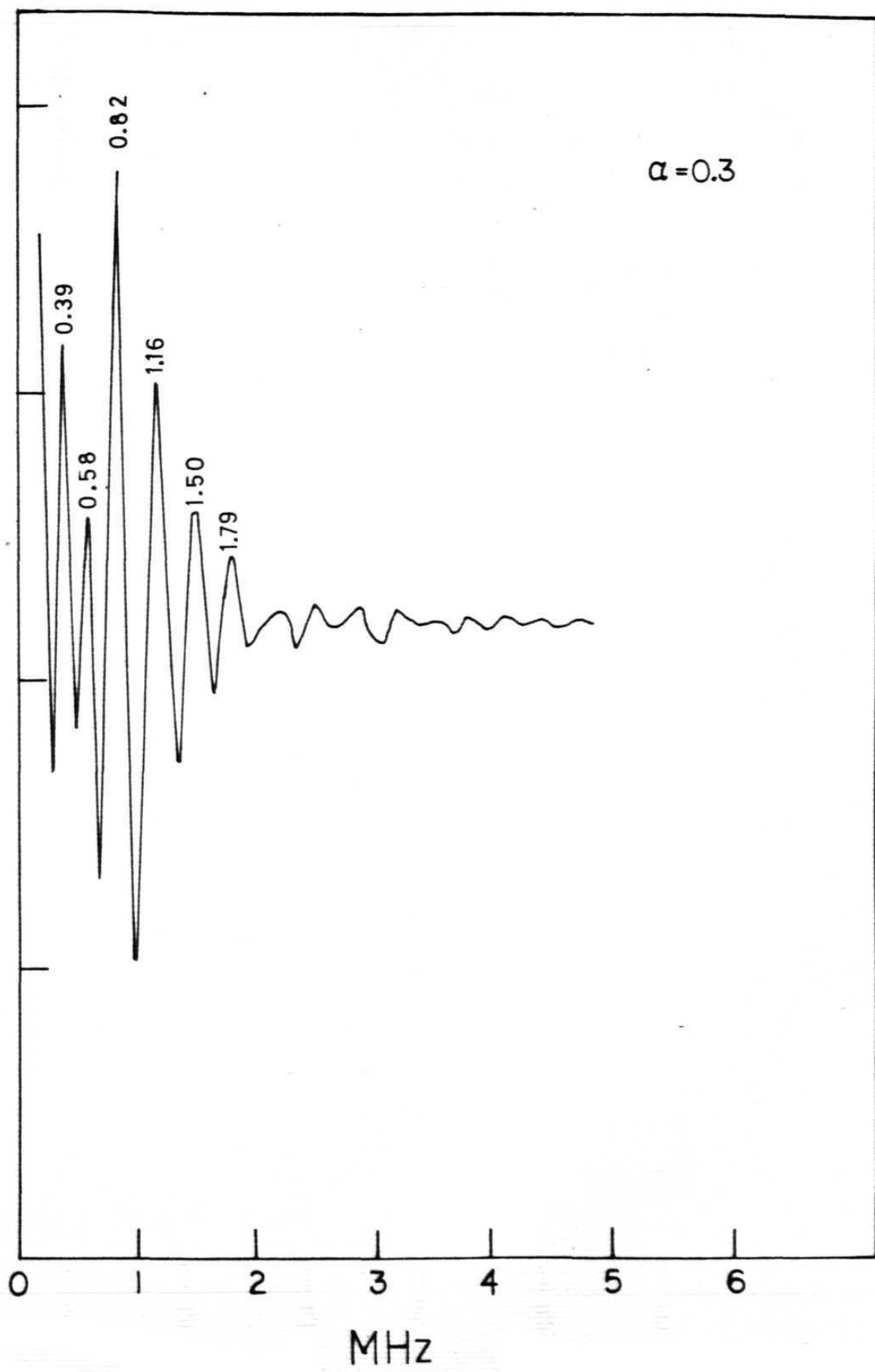
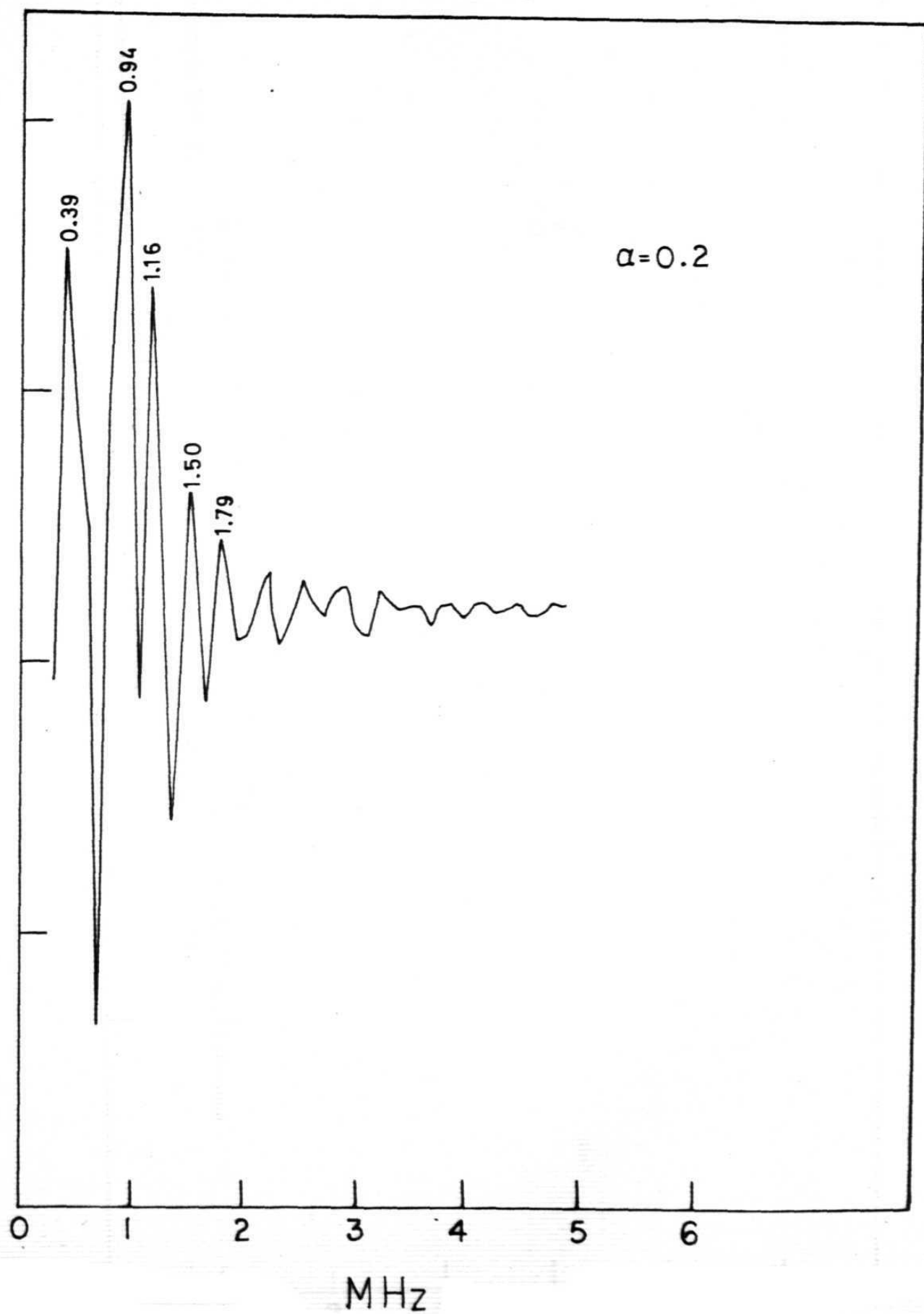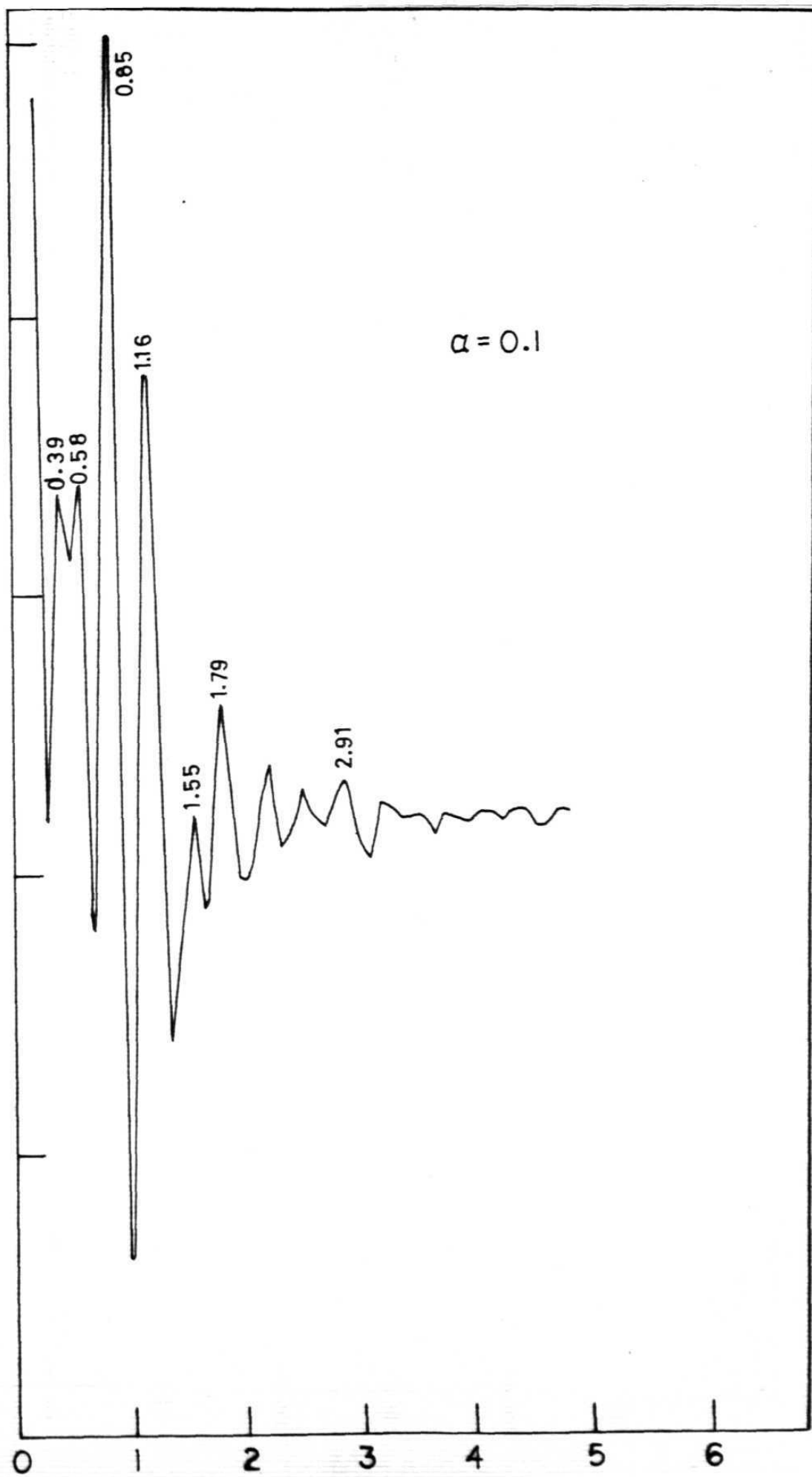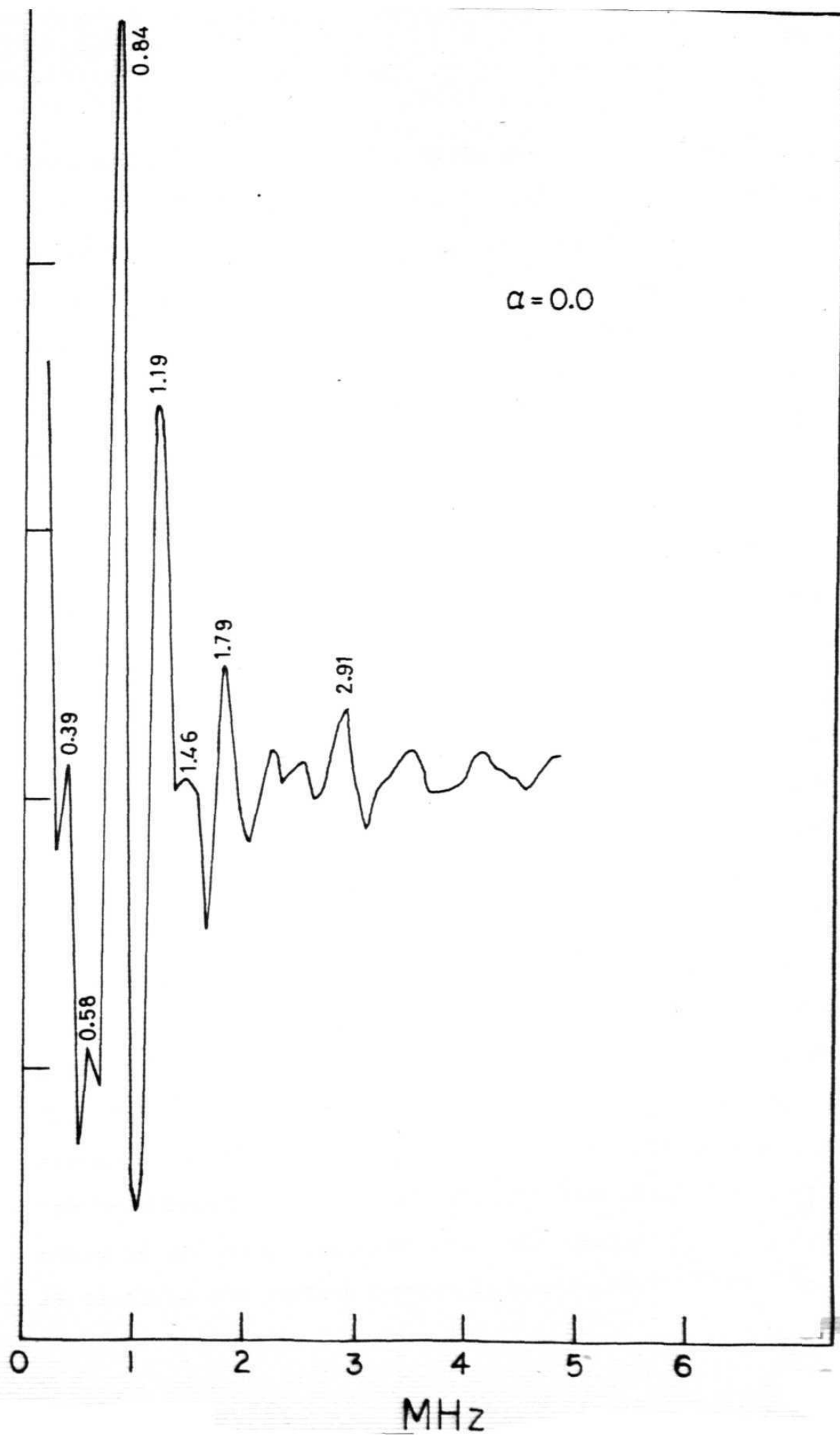frequencies distinctly. The ESEEM for $\tau = 350$ nsec. . is shown in Fig. 5 and its Fourier transform using the extrapolated envelope is shown in Fig. 6. The FT data after multiplying with the window function, with the window parameter $\alpha = 0.5$ to 0.0 are shown in Figs. 7 to 12. The frequency spectrum shows several components at 0.39, 0.58, 0.84, 1.19, 1.55, 1.79 and 2.91 MHz. The data were recorded at a field value of $H = 0.2830T$. The nuclear Zeeman frequencies for Cl^{35} and Cl^{37} at this field are 1.18 MHz and 0.98 MHz respectively. The ENDOR frequencies have been calculated for different values of the isotropic hyperfine coupling constant $|a|$ and the quadrupole coupling $|Q_{zz}|$. The best fit was obtained for values of $|a| = 1.2$ MHz and $|Q_{zz}| = 0.1$ MHz using the Cl^{35} nuclear Zeeman frequency of 1.18 MHz. The calculated frequencies are 0.38, 0.58, 0.78, 1.58, 1.78 and 1.98 MHz. The slight shifts from the observed frequencies might arise from the dipolar couplings which ≈ 0.08 to 0.02 MHz for second and higher coordinated chlorides. The frequency at 0.78 MHz is close to the 0.84 MHz observed. The peak at 0.84 MHz is very broad indicating an overlap of two components which are the 0.78 MHz components from chloride, and the 0.87 MHz component which is the free nitrogen precessional frequency. The 1.98 MHz peak could not be observed in the frequency spectrum and the reason could be the suppression effect. The frequency at 1.19 MHz is close to the nuclear Zeeman frequency of Cl^{35} at this value

of H and appears due to a very small hyperfine coupling with the unpaired spin. The peak at 2.91 MHz could not be clearly accounted for.

The modulation was recorded for other values of τ also. In this case, the suppression effect is more evident than in Centre I. Components higher than 1.18 MHz are suppressed for τ = 300 nsec. and entirely a new set of peaks appeared for τ = 400 nsec. For this value of τ, zero-field quadrupole frequencies due to nitrogens appeared at 0.67, 0.96 and 1.62 MHz. The corresponding contact coupling constant is 1.74 MHz. The corresponding frequency at 2.71 MHz (f_2), could not be observed in the frequency spectrum. The peak at 2.92 MHz for τ = 350 nsec. could be the frequency corresponding to f_2, because f_2 is known to be very sensitive to anisotropies of the electron nuclear coupling[3]. This frequency might have been suppressed at τ = 400 nsec.

Ammonium Bromide : NH_4Br (Cu^{2+})

Centre II: $[(CuBr_4)^{2-} : 2NH_3]$:

Centre II in $NH_4Br:Cu^{2+}$ is similar to Centre II in ammonium chloride[6,10]. For this system also the ESEEM patterns were recorded by monitoring both the $g_\perp$ and the $g_\parallel$ regions. The ESEEM for the $g_\perp$ orientation and for

Fig. 13

The stimulated echo envelope for $NH_4Br : Cu^{2+}$ (Centre II) with $\tau = 400$ nsec recorded in the perpendicular region $H_o = 0.3075$ T, $f = 9.54$ GHz.
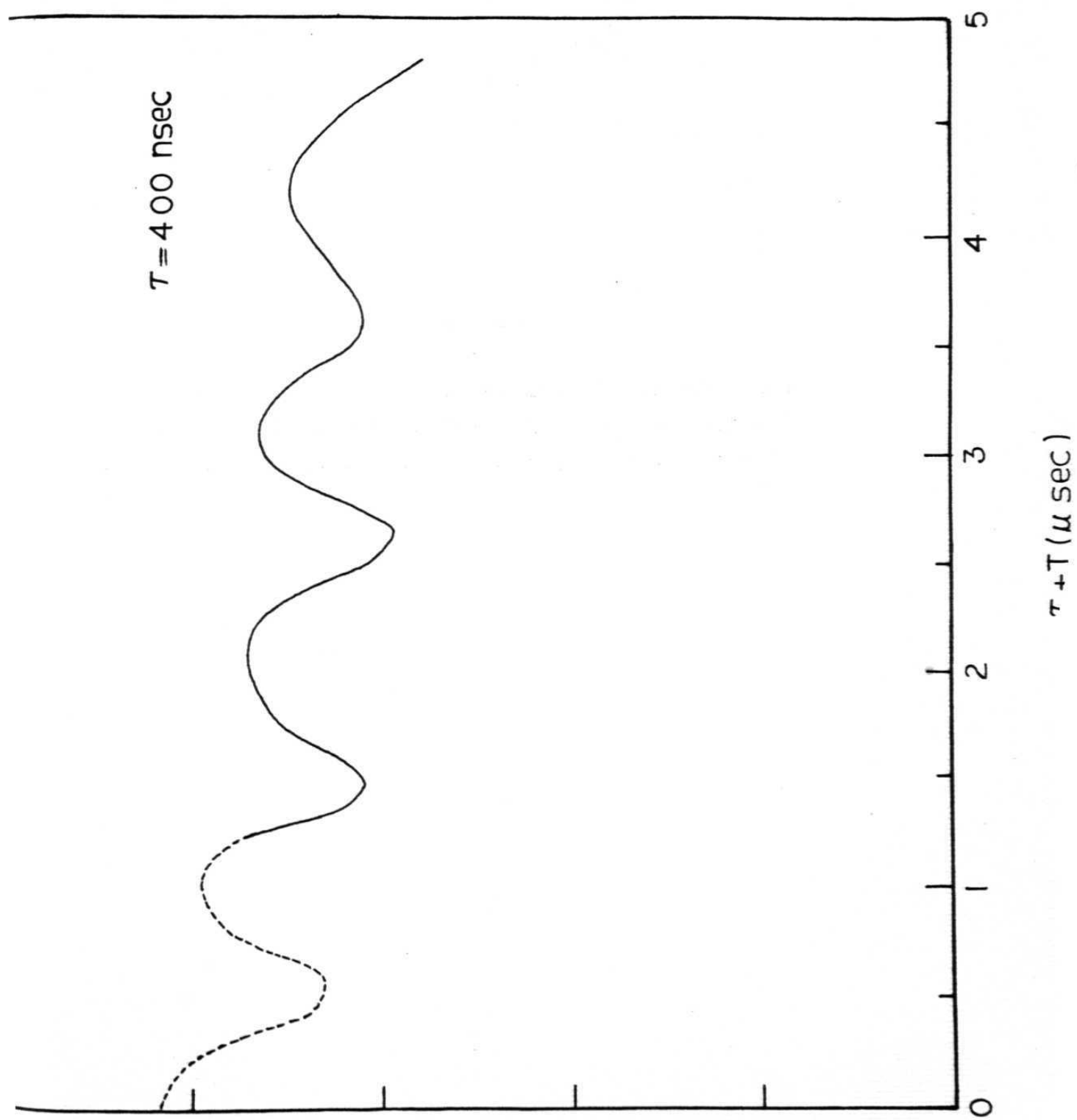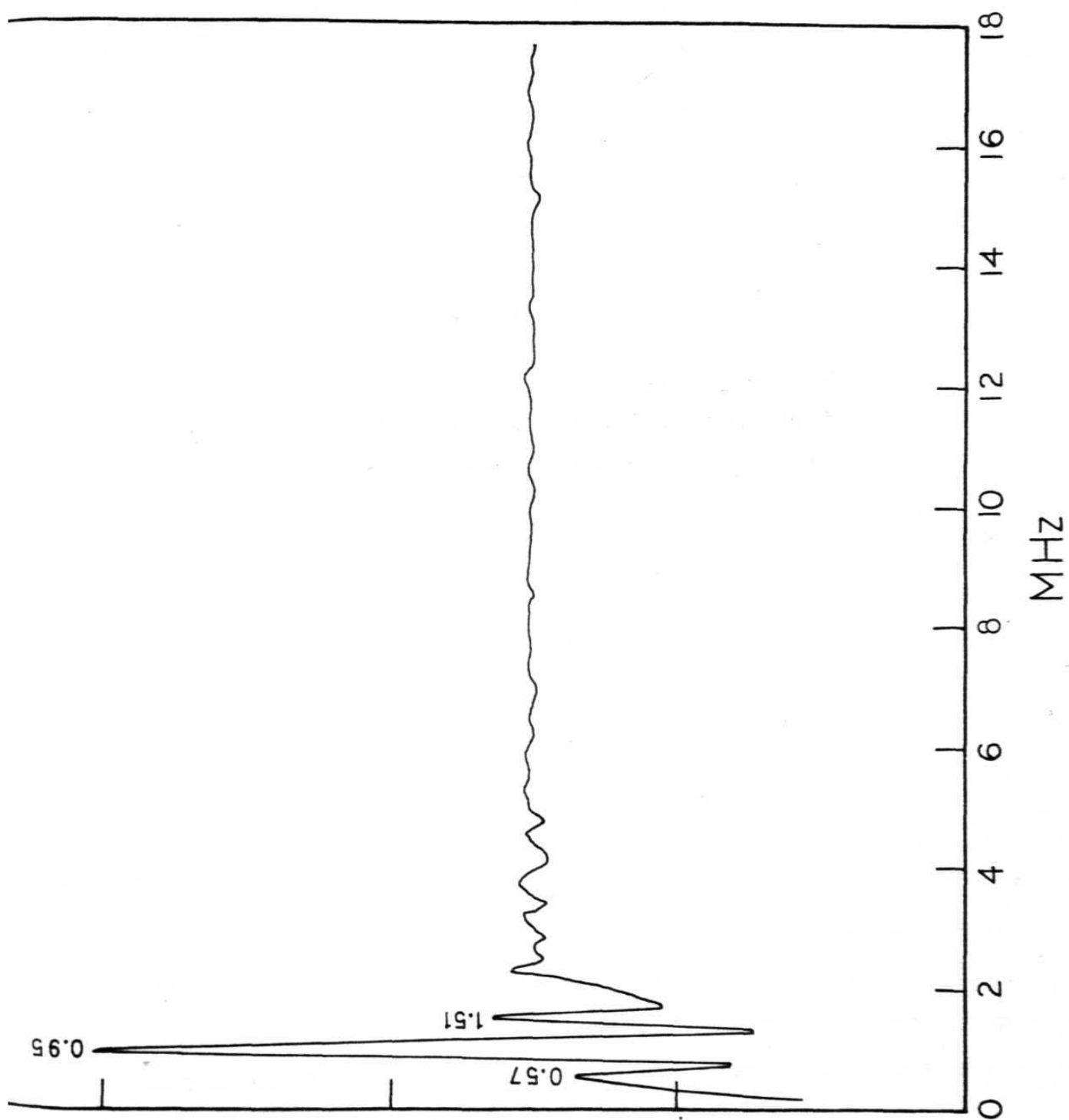
$\tau = 400$ nsec

$\tau + T \, (\mu \, \text{sec})$

Fig. 14

The Fourier transform spectrum for the envelope of NH_4Br : Cu^{2+} (Centre II) shown in Fig. 13. The noise has not been smoothned.

τ = 400 nsec. is shown in Fig. 13 and the corresponding
FT spectrum is shown in Fig. 14. The frequency spectrum
is relatively simple containing only three components at
0.57, 0.95 and 1.51 MHz. Clearly these frequency components
are the zero-field quadrupole frequencies of nitrogen. The
contact coupling constant calculated from these frequencies
was found to be 1.9 MHz. The frequency corresponding to f_2
in Fig. 14 should occur at 2.845 MHz and such a frequency
could not be seen in the FT spectrum. This might be due to
the suppression effect. The ESEEM has also been recorded
at τ = 300 nsec. but the corresponding FT spectrum shows
the same frequencies, except that the 1.51 MHz component
is split into 1.37 and 1.76 MHz.

The modulation for τ = 450 nsec with the tetragonal axis
parallel to the magnetic field is shown in Fig. 15. The
corresponding frequency spectrum is shown in Fig. 16.
From the FT spectrum it can be seen that there are only
three lines which correspond to the zero-field quadrupole
frequencies of nitrogen. The frequency components are 0.50,
0.99 and 1.485 MHz. The contact coupling constant for this
nitrogen is $|a|$ = 2.04 MHz. A comparison of this contact
coupling constant with that obtained from the perpendicular
part shows that the modulation essentially arises from the
same nitrogen in both the cases.

Fig. 15

The stimulated echo envelope for $NH_4Br : Cu^{2+}$
(Centre II) with τ = 450 nsec recorded in the
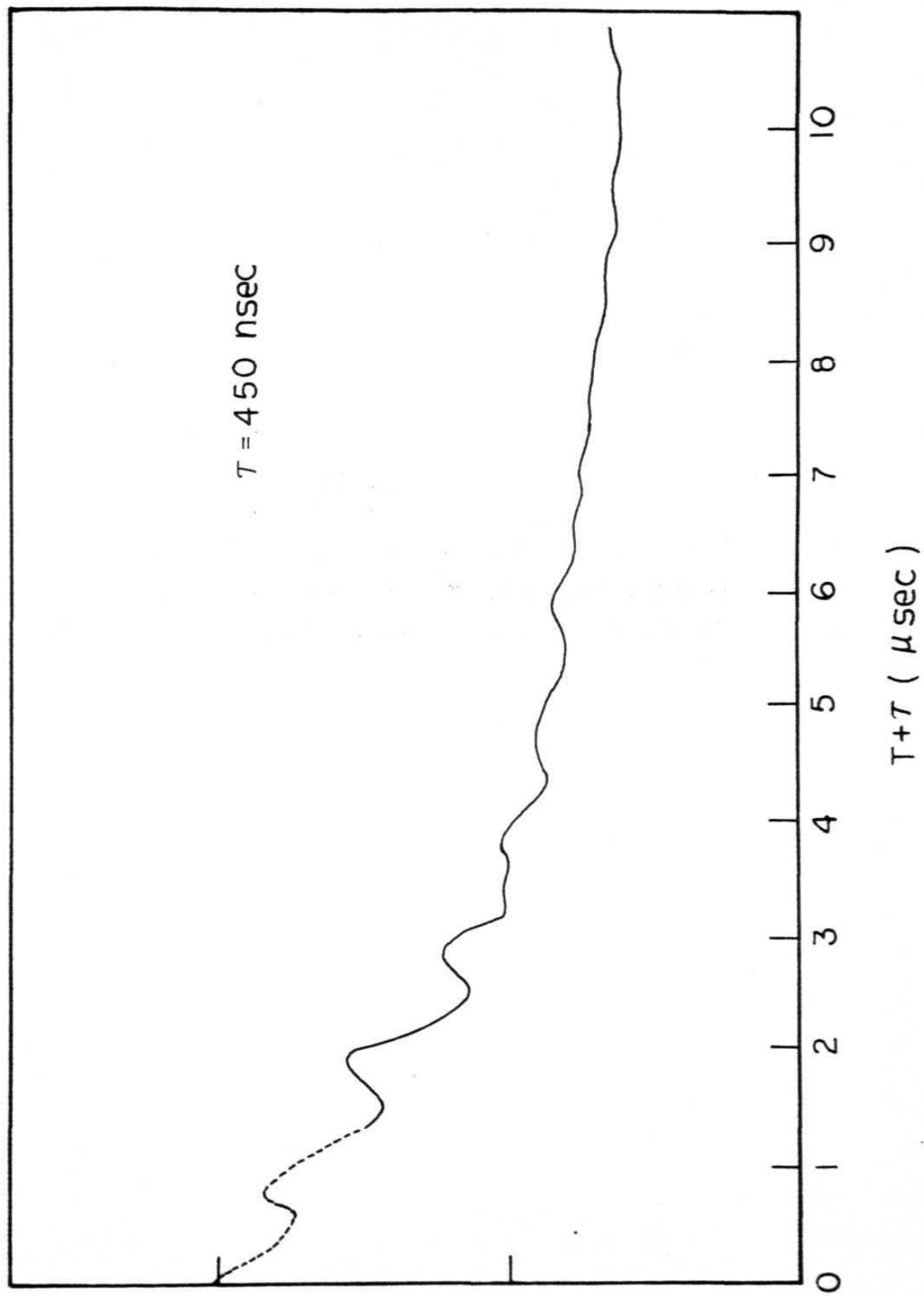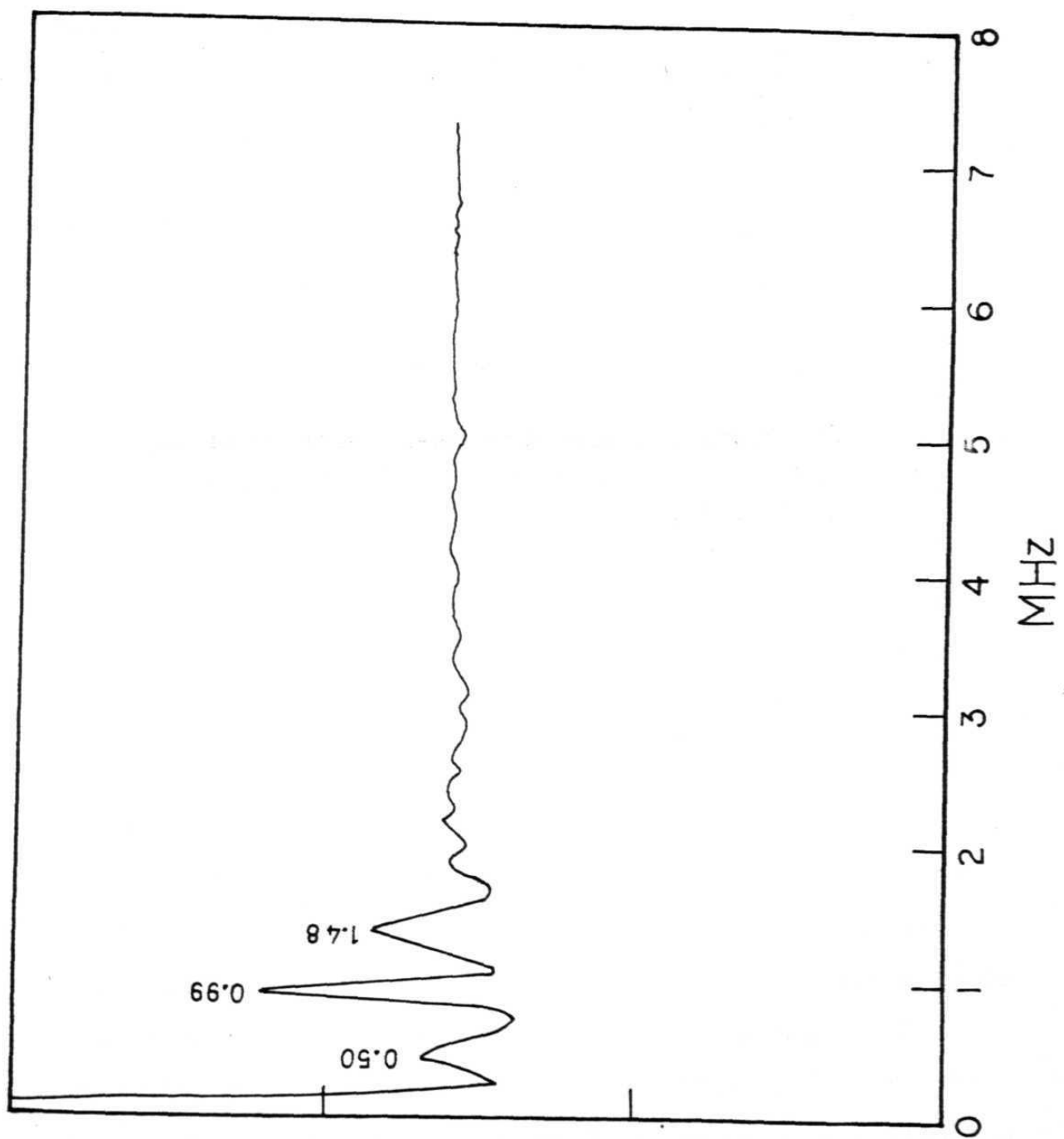parallel region. H_o = 0.333 T, f = 9.32 GHz.

$T = 450$ nsec

$T + T$ (μ sec)

Fig. 16

The Fourier cosine transform spectrum of the
modulation of $NH_4Br : Cu^{2+}$ (Centre II) shown
in Fig. 15.

The modulation could be from the next nearest neighbour nitrogens located at a distance of 0.453 nm. The frequency corresponding to f_2 is 3.06 MHz. It might have been suppressed and could not be seen in the range to the τ-values studied. Frequencies corresponding to bromide modulation did not appear in $NH_4Br:Cu^{2+}$. The reason could be the high Larmor precessional frequencies of bromide ions which are 3.279 and 3.535 MHz in the perpendicular part and 3.551 and 3.829 MHz in the parallel part for ^{79}Br and ^{81}Br respectively. If the contact couplings are small, the frequency components from such nuclei appear at frequencies greater than 2 MHz. Also, the range of τ-values (250 - 400 nsec.) might not have been sufficient to observe all the cycles of modulation from the system and the frequencies from the bromide ions might have been suppressed in this range.

Ammonium Chloride $[ND_4Cl:Cu^{2+}(Centre\ II)]$:

The modulation from ND_4Cl would be more complicated because of the presence of deuterium in large quantities compared to others. Hence the modulation is expected to be rich from contributions from all the nuclei, and the FT analysis of the modulation shows that this is indeed the case. The ESEEM for ND_4Cl have been recorded by monitoring the $g_\perp$ region for different τ-values ranging from

Fig. 17

The three pulse echo envelope for $ND_4Cl : Cu^{2+}$
(Centre II) with $\tau = 300$ nsec recorded in the
perpendicular region. $H_o = 0.3060$ T, $f = 9.50$ GHz.

$\tau = 300$ n sec.
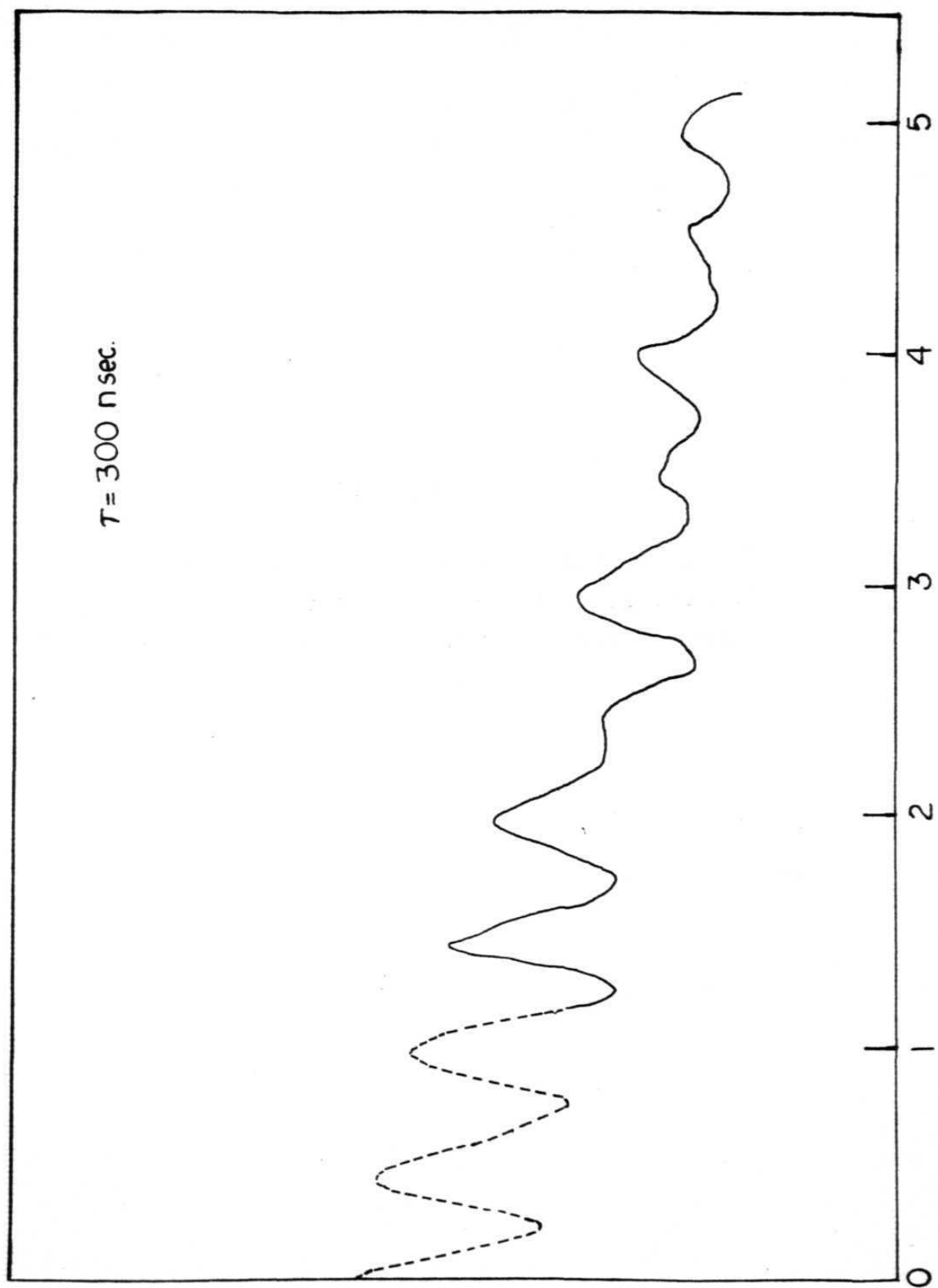
Fig. 18

The stimulated echo envelope for $ND_4Cl : Cu^{2+}$
(Centre II) with $\tau = 450$ nsec recorded in the
perpendicular region. $H_o = 0.3060$ T, $f = 9.50$ GHz.

$\tau = 450$ nsec

$\tau + T$ (μ sec)
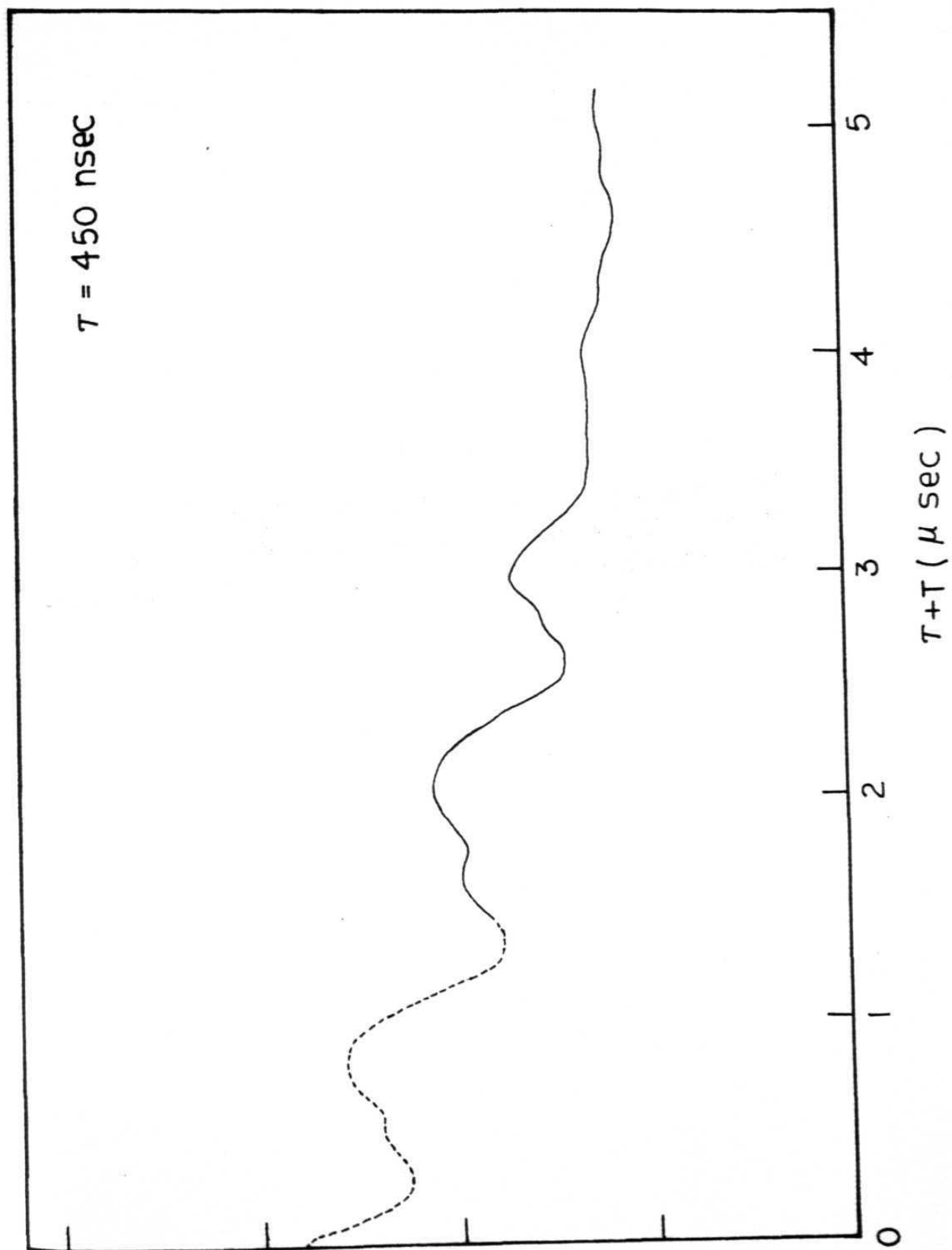
Fig. 19

The Fourier cosine transform spectrum of the
modulation for $ND_4Cl : Cu^{2+}$ (Centre II) shown
in Fig. 17. The noise has not been smoothened.
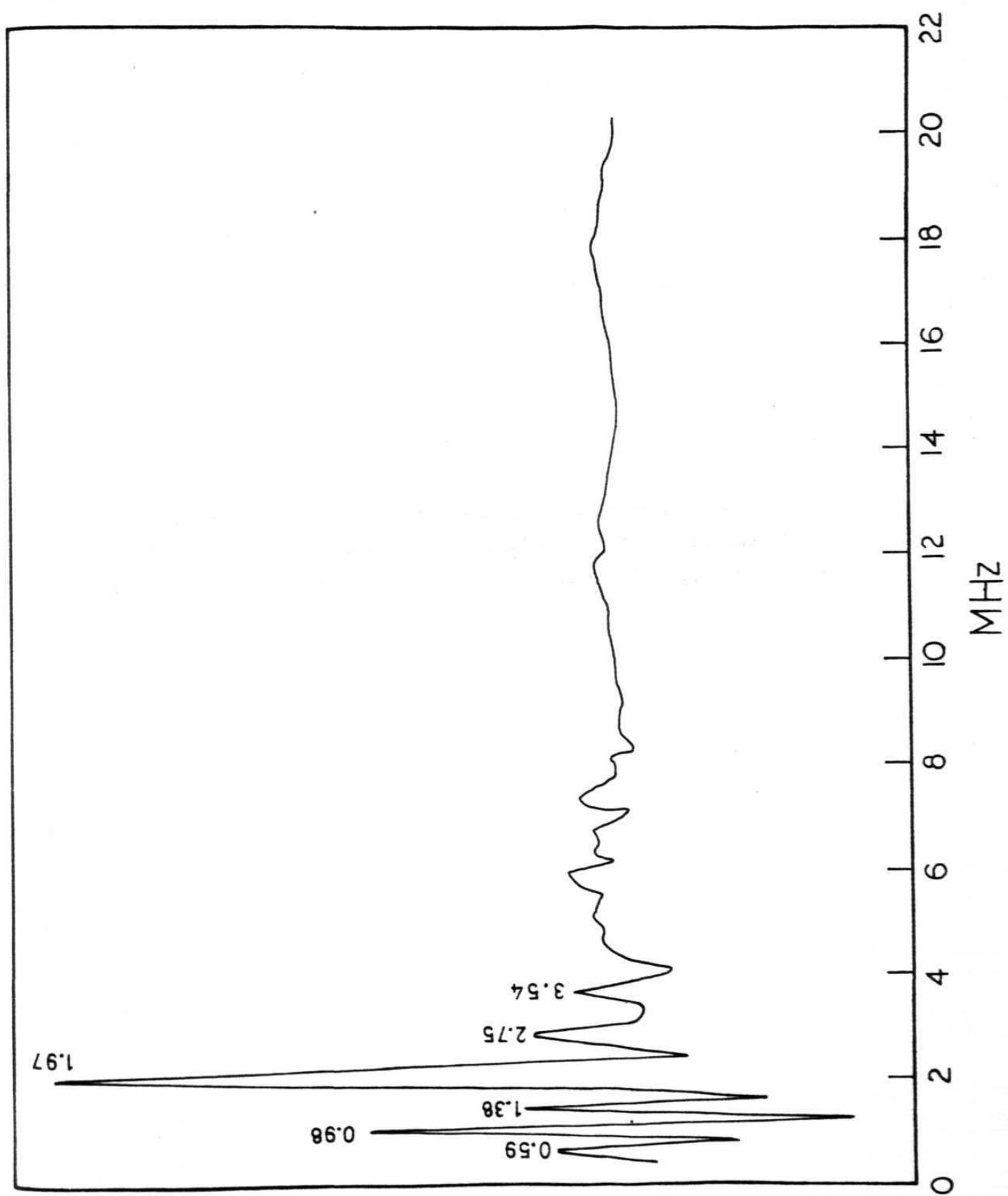
Fig. 20

The Fourier cosine transform of the modulation
for ND_4Cl : Cu^{2+} (Centre II) shown in Fig. 18.
The noise has not been smoothened.
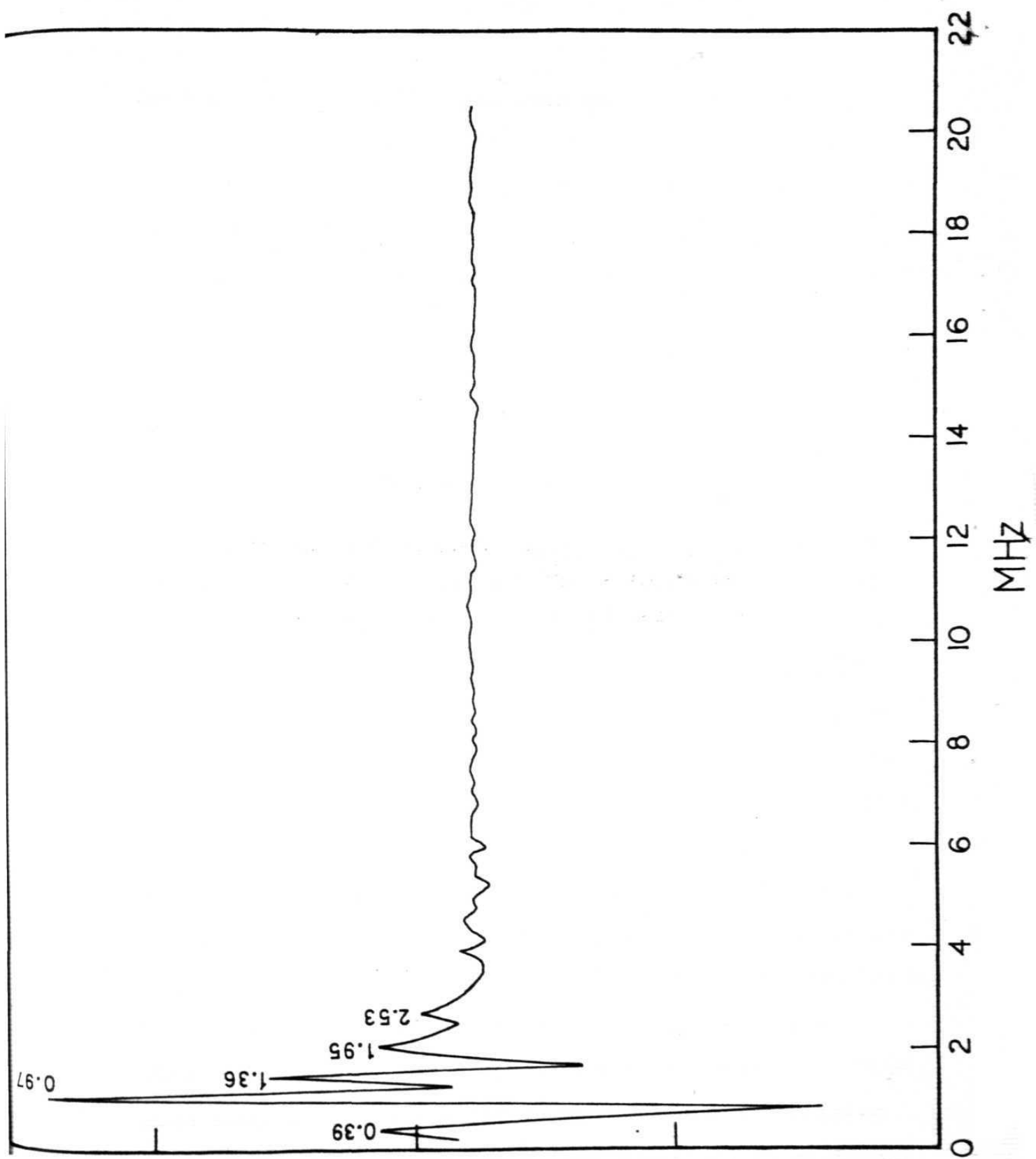
300nsec to 600nsec. The frequency components in the
corresponding FT spectra are given in Table II. The
modulations for the values of τ = 300 and 450 nsec.
are shown in Figs. 17 and 18. The dotted line is, as usual,
the extrapolated portion of the envelope. The corresponding
frequency domain spectra are shown in Figs. 19 and 20
respectively. The frequency spectrum in the case of
τ = 300 nsec. contains the components 0.59, 0.98, 1.38,
1.97, 2.75 and 3.54 MHz. The peak at 0.98 MHz is close to
the free nuclear precessional frequency of 0.94 MHz of the
nitrogen. The shift is due to some small dipolar coupling.
The peaks at 0.59, 1.38 and 1.97 MHz are the zero-field
quadrupole frequencies of an I = 1 nucleus. In the present
case, this nucleus could be a deuteron or a nitrogen.
For a deuteron the isotropic hyperfine coupling constant
calculated for this field setting turns out to be 4 MHz.
The corresponding contact coupling to nitrogen is 1.9 MHz.
The frequency corresponding to f_2 for these cases is 6 MHz
for deuteron and 2.84 MHz for nitrogen. The 2.75 MHz
component may correspond to this frequency f_2, but it has
clearly contribution from deuterons as will be shown below.
The 6 MHz peak is absent in the transformed spectra
throughout. These frequencies appear in almost all ESEEM
data recorded for different τ -values. The frequencies
1.97, 2.75 and 3.54 MHz occur from couplings to deuterons
whose isotropic coupling constant, $|a|$ = 0.50 MHz, and the

quadrupole coupling constant, $Q_{zz} \approx 0.25$ MHz. This value of Q_{zz} is consistent with the value of 0.18 MHz reported from NMR studies on ND_4Cl^{11}. The peak at 1.97 MHz has contributions from zero-field quadrupole frequencies and the ENDOR frequencies of deuteron. Apart from these it is also seen to be very close to the nuclear Zeeman-frequency of a deuteron. From Table II it can be seen that similar frequency components appear in ESEEM recorded for other values of τ also. In the case of the ESEEM with $\tau = 450$ nsec., the deuteron ENDOR frequencies occur at 1.36, 1.95 and 2.53 MHz. Another set of zero-field quadrupole frequencies appear at 0.39, 0.97 and 1.36 MHz. A comparison of these zero-field frequencies with those obtained from NH_4Br (H = 0.3075T whereas here H = 0.3060T) shows that the former frequencies might owe their origin to a nitrogen nucleus. In that case, the frequencies at 0.39, 0.97 and 1.36 MHz must have been from a deuteron. The frequency at 1.28 MHz for $\tau = 400$ nsec. is the free nuclear precessional frequency of a Cl^{35} nucleus at this field value (0.306T). Also the frequencies around 2.02 MHz and 0.98 MHz are nuclear Zeeman frequencies of deuterons and nitrogens respectively. Thus the modulation in the case of NH_4Cl appears to be dominated by deuterons. However, the frequencies pertaining to chlorides and nitrogen have clearly been seen. In the case of $\tau = 450$ nsec. the FT spectrum shown in Fig. 21b is obtained by using the window function with $\alpha = 0.1$.

It is seen that the 0.39 MHz peak disappeared. Instead a peak at 0.58 MHz appears. This situation is the same for other values of α also. But the truncated data without the window function gives no peak at either 0.39 or 0.58 MHz. It is possible that both the frequencies are present in the modulation and the resolution of the FT spectrum is not good enough to show both the peaks distinctly.

Since the modulation does not arise from the directly coupled nuclei, it should be the result of coupling to the nuclei in the second and higher coordination spheres. Hence, the dipolar couplings, as shown in the beginning, do not appear to influence the frequency components in any manner. However, the deuterons with a contact coupling constant $|a| = 4$MHz appear to be very close to the unpaired spin. These deuterons are most likely coordinated to the immediate ligands and could be pointing towards one of the halides which are coordinated directly to copper.

Thus these ammonium halides have shown superhyperfine frequencies from several nuclei due to couplings with the unpaired spin. In almost all the cases studied the free nuclear precessional frequencies of nitrogen appeared. Also two sets of deuteron frequencies have been observed. One with a large isotropic hyperfine constant of 4 MHz and the other/with a smaller isotropic hyperfine coupling constant of about 0.5 MHz. There is a wealth of data on the zero-

field quadrupole coupling frequencies of nuclei with $I = 1$,
viz., nitrogen and deuteron. The nitrogen contact coupling
varies from 1.74 MHz to 2.04 MHz depending on the crystal
being studied. The differences in frequencies and coupling
constants indicate the change of environment due to the
host lattice. Most of the modulation seems to arise from
nuclei in the second coordination sphere which are located
at a distance of about $4A^{\circ}$ from the Cu^{2+}ion. One significant
observation is that the coupling parameters derived from the
observed superhyperfine frequencies turn out to be the same
when measured from $g_{\perp}$ or $g_{\parallel}$ settings. This shows that the
observation of the finer structural details is not
influenced by the g-setting. It only influences the SHF
frequencies which depend on the field, but not the coupling
constants. The low value of the dipolar couplings makes
the interpretation of the SHF spectrum simple. However, the
influence of the dipolar coupling and the single crystal
nature of the spectrum can be seen from a consideration of
the linewidths of the SHF frequencies. The effects of the
suppression effect are seen in several cases but it is more
prominent in the case of chloride frequencies and especially
at low τ values. The effect of the window function can be
clearly seen by referring to Fig. 21(a to f). These figures
refer the different values of the window parameter α. Some
of the peaks are shifted when compared to the peak positions
in the FT spectrum from the extrapolated envelope. The

Fig. 21

The Fourier cosine transform spectra for the
modulation from ND_4Cl : Cu^{2+} (Centre II) with
τ = 450 nsec shown in Fig. 18. The truncated
time domain data has been Fourier transformed
using the window function with α = 0.0 to 0.5.

a
α = 0.0

b
α = 0.1

MHz   MHz

c
α = 0.2

d
α = 0.3

e
α = 0.4

f
α = 0.5

2   4   6   8
MHz

0   2   4   6   8
MHz
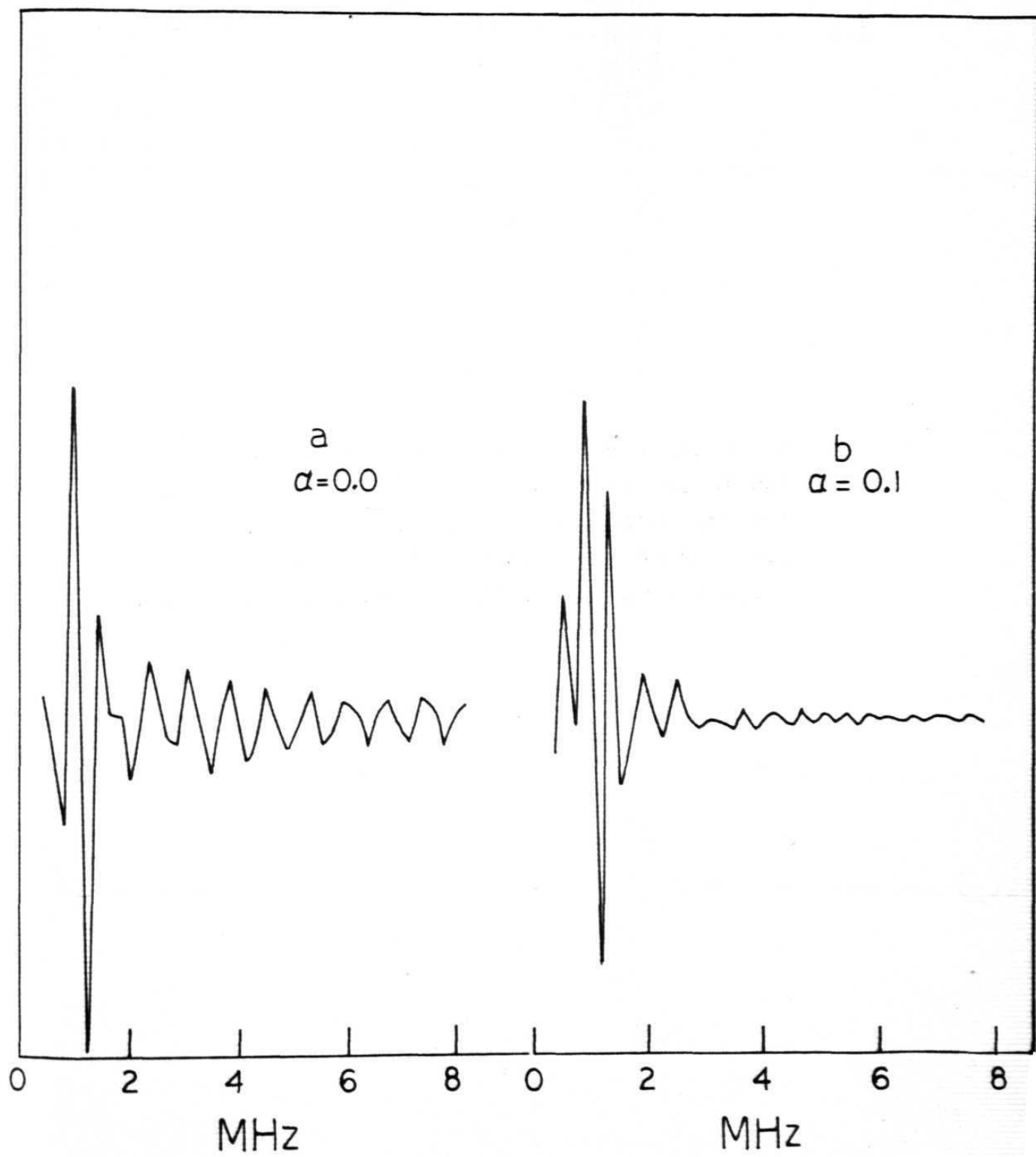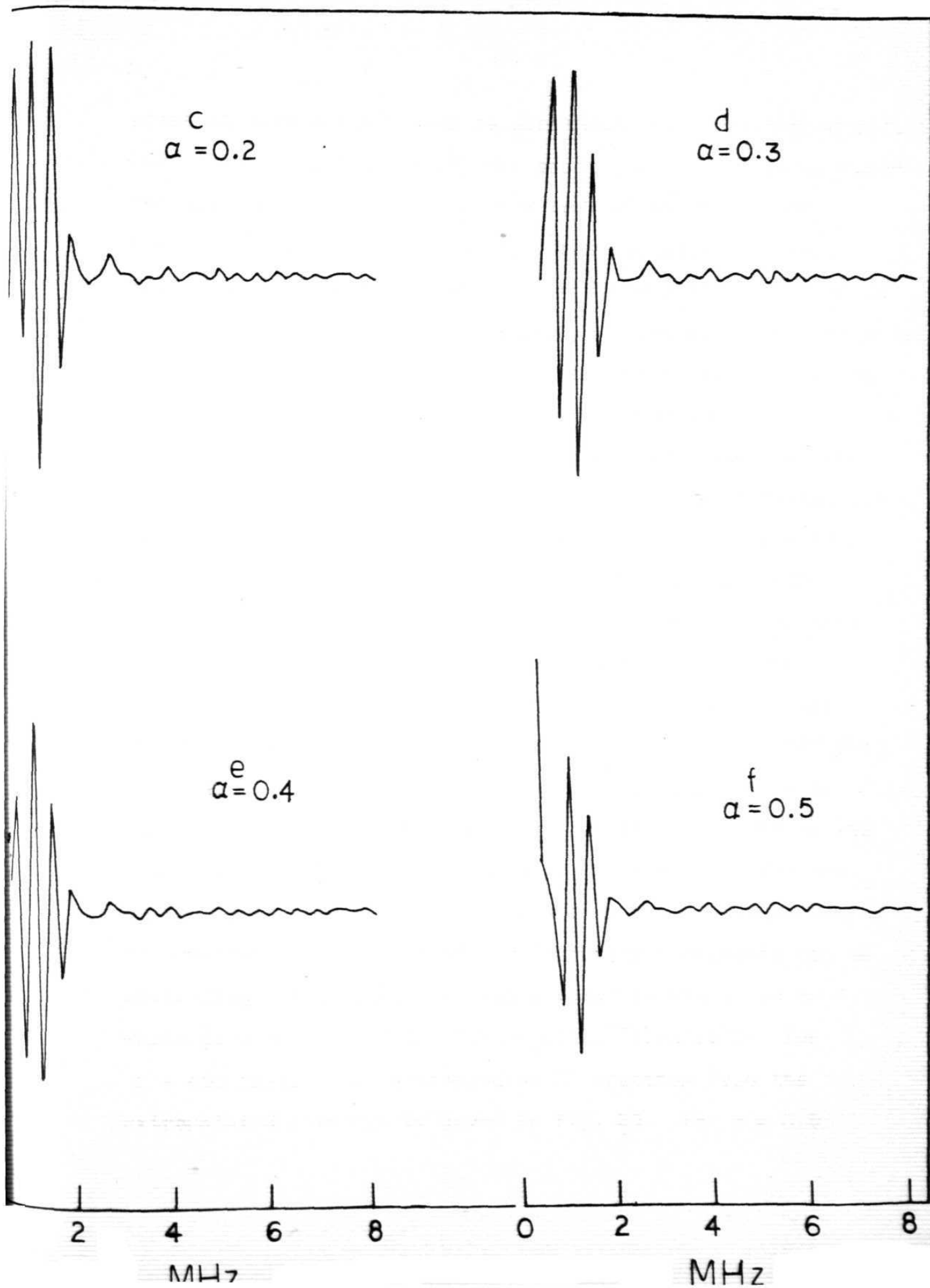
peaks at 0.39 and 0.58 MHz retain their positions throughout.
The peaks at 0.84 and 1.188 MHz shift their position to 0.824
and 1.164 MHz for $\alpha = 0.5$. The rest of the peaks are
suppressed for this value of α. From comparison of the
frequencies, line shapes and line positions for different αs
(i.e. $\alpha = 0.0$ to 0.5) a few conclusions can be drawn. Firstly,
it is seen that as the value of α increases, suppression of
the sidelobes and low frequency noise increases. However,
there is loss of main line amplitude coupled with a decrease
of sidelobe amplitudes. Also peaks with low intensities are
suppressed. This is clearly evident in Fig. 21f where only
four frequency components are seen whereas in Fig. 21b
eight frequency components are seen. As mentioned before,
there is a shift of frequencies with respect to those
obtained from the extrapolated envelope and also a similar
shift is seen with the α-value. Thus the peak at 0.824 MHz
for $\alpha = 0.5$, shifts to 0.848 for $\alpha = 0.1$. This shift is
characteristic of α, and the amount of shift depends on the
resolution in the frequency domain. This in turn depends
on the phase memory times of the system under consideration.
In some cases this shift of the frequency components can be
misleading. This point is illustrated in Figs. 21a to f
which give the FT spectra for $NH_4Cl:Cu^{2+}$(Centre II) for
$\tau = 450$ nsec. The corresponding FT spectrum from the
extrapolated envelope is given in Fig. 20. For $\alpha = 0.5$

(shown in Fig. 21f) the peak at 0.39 MHz is not clearly resolved. There is a peak at 1.75 MHz for α = 0.4 to 0.2 and this actually shifts to 1.95 MHz for α = 0.1. As has been discussed earlier this peak arises from a deuterium nucleus. Thus α = 0.1 seems to give the best results in both the cases considered here. One advantage of the FT of the extrapolated curve is that it reproduces the peaks in the truncated data without any shifts. But the resolution of the peaks in the apodized FT. spectra is better than that in the FT spectra obtained from extrapolated data. Also the baseline stability is very good in the apodized spectra.

The frequency shifts observed in the apodized spectra depend on the resolution in the frequency domain. The resolution is dependent on the time upto which the ESEEM could be recorded. The length of the recorded ESEEM data is in turn dependent on the phase memory time of the system, being longer for large phase memory times. For sufficiently long phase memory times the shifts could become negligible. Also, if the lines overlap with sidelobes from others, the shape of the lines is no longer Lorentzian, and might be important when effects of varying α are to be considered.

The values of $|a|$ and $|Q_{zz}|$ obtained from the ESEEM studies do not seem to tally well with those obtained from ENDOR studies by Boettcher and Spaeth[8]. SHF frequencies from the immediately liganded nuclei could not be observed in the present case. The interaction constants obtained by them for the distant nuclei are much smaller than those obtained from the present ESEEM studies and we do not have any explanation for this.

In these ammonium halides electron spin echoes disappeared when the crystal is tilted a little away from its axis. Similar phenomena have been observed by Grischkowsky and Hartmann[12,13]. The disappearance of the echo was explained by the loss of dephasing effects of the modulating nuclei. The modulating nuclei provide an incoherent quasiperiodic fluctuating magnetic field at the site of the unpaired spin depending upon the magnitude and orientation of the applied magnetic field. The periodic nature of the field produces dephasing effects. Echoes are observed only when the magnitudes of such fields are at a minimum.

TABLE 1

Calculated dipolar couplings for the modulating nuclei (Cl^-, Br^-, N) in NH_4X ($X = Cl^-, Br^-$) single crystals. The cell parameters used are from Wycoff at room temperature. The g- values are taken at the lowest possible temperature wherever available. The angle θ has been deduced from the geometry.

    * Closest nuclei

    ** Second neighbour nuclei

The details of the relavant data used in these calculations are:

$NH_4Cl:Cu^{2+}$ a = 0.38756 nm   Centre I $g_{\parallel}$ = 2.022
                                              $g_{\perp}$ = 2.287

                                         Centre II $g_{\perp}$ = 2.220

$NH_4Br:Cu^{2+}$ a = 0.40590 nm   Centre II $g_{\parallel}$ = 2.000
                                              $g_{\perp}$ = 2.217

$ND_4Cl:Cu^{2+}$ a = 0.38632 nm   Centre II $g_{\parallel}$ = 2.219

Modulating Nucleus	Distance r	Angle θ	NH₄Cl:Cu²⁺				NH₄Br:Cu²⁺			ND₄Cl:Cu²⁺	
			Distance nm	Centre I		Centre II	Distance nm	Centre II		Centre II	
				$g_\parallel$ Dipolar coupling MHz	$g_\perp$ Dipolar coupling MHz	$g_\perp$ Dipolar coupling MHz		$g_\parallel$ Dipolar coupling MHz	$g_\perp$ Dipolar coupling MHz	$g_\perp$ Distance r(nm)	Dipolar coupling MHz
Nitrogen (^{14}N)	$a/2$*	$0°$	0.1938			1.74	0.2029	1.36	1.51	0.1932	1.7
	$a\sqrt{5}/2$**	$63°$	0.4333	− 0.03	− 0.03	− 0.02	0.4538	0.02	0.03	0.4319	− 0.0
	$3a/2$	$90°$	0.5813	− 0.03	− 0.02	− 0.01	0.6088	0.02	0.03	0.5795	− 0.0
Chloride ^{35}Cl ^{37}Cl	$a/\sqrt{2}$*	$90°$	0.2740	− 0.38	− 0.43	− 0.42				0.2732	− 0.4 / − 0.3
	$a\sqrt{3}/\sqrt{2}$**	$35°$	0.4747	0.07 / 0.06	0.08 / 0.07	0.08 / 0.07				0.4731	0.0 / 0.0
	$a\sqrt{10}/2$	$90°$	0.6128	− 0.03 / − 0.03	− 0.04 / − 0.03	− 0.04 / − 0.03				0.6108	− 0.0 / − 0.0
Bromide ^{79}Br ^{81}Br	$a/\sqrt{2}$*	$90°$					0.2870	− 0.84 / − 0.90	− 0.93 / − 1.00		
	$a\sqrt{3}/\sqrt{2}$**	$35°$					0.4971	0.16 / 0.17	0.18 / 0.19		
	$a\sqrt{10}/2$						0.6418	− 0.07 / − 0.08	− 0.08 / − 0.09		

TABLE II

Frequency components from FT-ESEEM of $ND_4Cl:Cu^{2+}$(Centre II), with H_o = .306 T. The free nuclear precession frequencies are ν_D = 2.00 MHz, ν_N = 0.94 MHz, $\nu_{Cl}{}^{35}$ = 1.276 MHz, and $\nu_{Cl}{}^{37}$ = 1.062 MHz.

S.No.	τ(nsec)	Frequencies (MHz)
1	300	0.59, 0.98, 1.38, 1.97, 2.75, 3.54
2	350	0.49, 0.98, 1.37, 1.65, 2.04
3	400	0.55, 0.92, 1.28, 1.65, 2.02, 2.57
4	450	0.39, 0.97, 1.36, 1.95, 2.53
5	500	0.55, 0.92, 1.65
6	600	0.55, 0.92, 1.47, 2.02, 2.57

References

1. W.B. Mims and J. Peisach, J. Chem. Phys. 69, 492 (1978).

2. T. Shimizu, W.B. Mims, J. Peisach and J.L. Davis, J. Chem. Phys. 70, 2249 (1979).

3. J. Peisach, W.B. Mims and J.L. Davis, J. Biol. Chem. 254, 12379 (1979).

4. W.E. Blumberg, W.B. Mims and D. Zuckerman, Rev. Sci. Instrum. 44, 546 (1973).

5. R.P.J. Merks and R. de Beer, J. Mag. Res. 37, 305 (1980).

6. S.H. Hagen and N.J. Trappeniers, Physica, 47, 165 (1970).

7. E. Antonini and M. Brunori, 'Hemoglobin and Myoglobin in Their Reactions with Ligands', North Holland, Amsterdam, 1971.

8. F. Boettcher, and J.M. Spaeth, Phys. Stat. Sol.(b) 61, 465, (1974).

9. N. Kuroda and A. Kawamori, J. Phys. Chem. Sol. 32, 1233 (1971).

10. M.D. Sastry and P. Venkateswarulu, Proc. Ind. Acad. Sci. 66, 208 (1967).

11. V. Hovi and P. Pyyki, Phys. Kondens. Mater 5, 1 (1960).

12. D. Grischkowsky and S.R. Hartmann, Phys. Rev. Lett. 20, 41 (1968).

13. N.A. Kurnit, I.D. Abella and S.R. Hartmann, Phys. Rev. Lett. 13, 567 (1964).

CHAPTER IV

FOURIER TRANSFORM STUDIES OF DEUTERON MODULATION OF ELECTRON
SPIN ECHO ENVELOPE OF SILVER ATOM IN DEUTERATED ICE
AND METHANOL GLASSES

INTRODUCTION:

The irradiation of silver salts in aqueous systems and alcohol glasses produces silver atoms by the reaction of silver cations with radiation-produced electrons[1,2]. In aqueous ice the silver atom is initially produced in the cation environment which is a non-equilibrium environment. Gentle thermal excitation induces attainment of an equilibrium environment for the silver atom[3]. From EPR studies Kevan, Hase and Kawabata[3] concluded that each Ag^o is surrounded by four water molecules and the equilibrium environment differs from the non-equilibrium environment in the rotation of water molecules. Later electron spin echo modulation studies by Ichikawa, Kevan and Narayana[4] have indicated that only one water molecule is involved in the rotation. This conclusion has been arrived at by the analysis of the ESEEM in both equilibrium and non-equilibrium environments. The time domain analysis of the modulation in the non-equilibrium configuration indicates that each silver atom is surrounded by eight equivalent deuterium nuclei located at a distance of 0.31 nm with a negligible isotropic hyperfine coupling. This corresponds to four water molecules surrounding each Ag^o. In the equilibrium environment, the time domain analysis of this data indicates that each Ag^o interacts with two groups of non-equivalent deuterium nuclei. One group contains a

single deuterium nucleus located at a distance of 0.17 nm
and has an isotropic coupling constant of 1.8 MHz while the
second group of nuclei consists of seven deuterium nuclei
located at a distance of 0.31 nm and exhibits negligible
isotropic hyperfine coupling. Thus the complexity increases
in going from a non-equilibrium configuration (site I) to
an equilibrium configuration (site II) and therefore would
be an excellent system for Fourier transformation studies.
On the other hand Ag^o in methanol does not show any conversion
from a non-equilibrium to an equilibrium environment and is
presumably formed in the equilibrium configuration[5]. In
this chapter the Fourier transform studies of the ESEEM
of Ag^o in CH_3OD and CD_3OH glasses and D_2O ice are described.
Since the modulation arising from deuterium nuclei is
stronger compared to protons[6], a more intense FT spectrum
is obtained by the substitution of hydrogen with deuterium.
It is for this reason that deuterated compounds have been
used. The problem of the truncation of the data has been
investigated by both extrapolating the data back to zero time
and by apodization[8]. The results have been compared with
those obtained from time domain analysis[4]. The advantages
of the FT analysis over the time domain analysis have been
pointed out.

THEORY:

Since the modulation is relatively simple only two pulse echo modulation has been used for the Fourier transformation studies. As mentioned earlier the modulation pattern is completely dominated by the interaction with deuterium nuclei (with nuclear spin I = 1) and the proton modulation is completely eliminated by using slightly longer pulsewidths. Therefore only the modulation arising from deuterium nuclei would be considered. The expression for normalized two pulse echo modulation with $S = \frac{1}{2}$ and I = 1 is given by

$$
\begin{aligned}
V(\tau) = {}& (1-\tfrac{4}{3}k+\tfrac{3}{4}k^2)+(\tfrac{2}{3}k-\tfrac{1}{2}k^2)(\cos\omega_{ab}\tau+\cos\omega_{bc}\tau+\cos\omega_{de}\tau+\cos\omega_{ef}\tau) \\[2mm]
& -(\tfrac{1}{6}k-\tfrac{1}{6}k^2+\tfrac{1}{6}k(1-k^2)^{1/2}][\cos(\omega_{ab}+\omega_{de})\tau+\cos(\omega_{ab}-\omega_{de})\tau \\[2mm]
& +\cos(\omega_{bc}+\omega_{ef})\tau+\cos(\omega_{bc}-\omega_{ef})\tau]-[\tfrac{1}{6}k-\tfrac{1}{6}k^2-\tfrac{1}{6}k(1-k^2)^{1/2}] \\[2mm]
& \cos(\omega_{bc}+\omega_{de})\tau+\cos(\omega_{bc}-\omega_{de})\tau+\cos(\omega_{ab}+\omega_{ef})\tau+\cos(\omega_{ab}-\omega_{ef})\tau] \\[2mm]
& +\tfrac{1}{4}k^2(\cos\omega_{ac}\tau+\cos\omega_{df}\tau)+\tfrac{1}{24}k^2[\cos(\omega_{ac}+\omega_{df})\tau+\cos(\omega_{ac}-\omega_{df})\tau \\[2mm]
& -\tfrac{1}{12}k^2\cos(\omega_{de}+\omega_{ac})\tau+\cos(\omega_{de}-\omega_{ac})\tau+\cos(\omega_{df}+\omega_{ab})\tau+\cos(\omega_{df}-\omega_{ab} \\[2mm]
& +\cos(\omega_{df}+\omega_{bc})\tau+\cos(\omega_{df}-\omega_{bc})\tau+\cos(\omega_{ef}+\omega_{ac})\tau \\[2mm]
& +\cos(\omega_{ef}-\omega_{ac})\tau]
\end{aligned}
$$

[1]

where τ is the time interval between the two pulses. Fig. 5 of Chapter II shows the energy level diagram for an $S = \frac{1}{2}$ and $I = 1$ spin system corrected for quadrupole coupling to a first order. The frequencies ω_{ij} are the frequency separations between the energy levels, and are defined in Eq. (35b) of Chapter II.

If Δ is the appropriate quadrupole coupling, which of course, is angularly dependent, we can express $\omega_{ab} = \omega_\alpha + \Delta, \omega_{bc} = \omega_\alpha - \Delta, \omega_{ef} = \omega_\beta + \Delta, \omega_{de} = \omega_\beta - \Delta$, where ω_α and ω_β are the average hyperfine splittings in the absence of quadrupole coupling and are associated with $|M_S = \frac{1}{2}>$ and $|M_S = -\frac{1}{2}>$ states respectively. The parameter k in the above equation has the same meaning as given in Chapter II.

It has already been shown in Chapter II that if each Ag^o interacts simultaneously with n nuclei Eq. (1) could be rewritten after incorporating the relaxation effects as

$$E(\tau) = F_o(\tau) \left\{ 1 - \sum_i a_i [1 - F_i(\tau) \cos \omega_i \tau] \right\} \qquad [2]$$

where ω_i are superhyperfine frequencies. In the absence of nuclear quadrupole coupling for an $S = \frac{1}{2}$, $I = 1$ system we expect to see two transitions one at ω_α, and the second at ω_β from each of the interacting nuclei. In the presence

Fig. 1

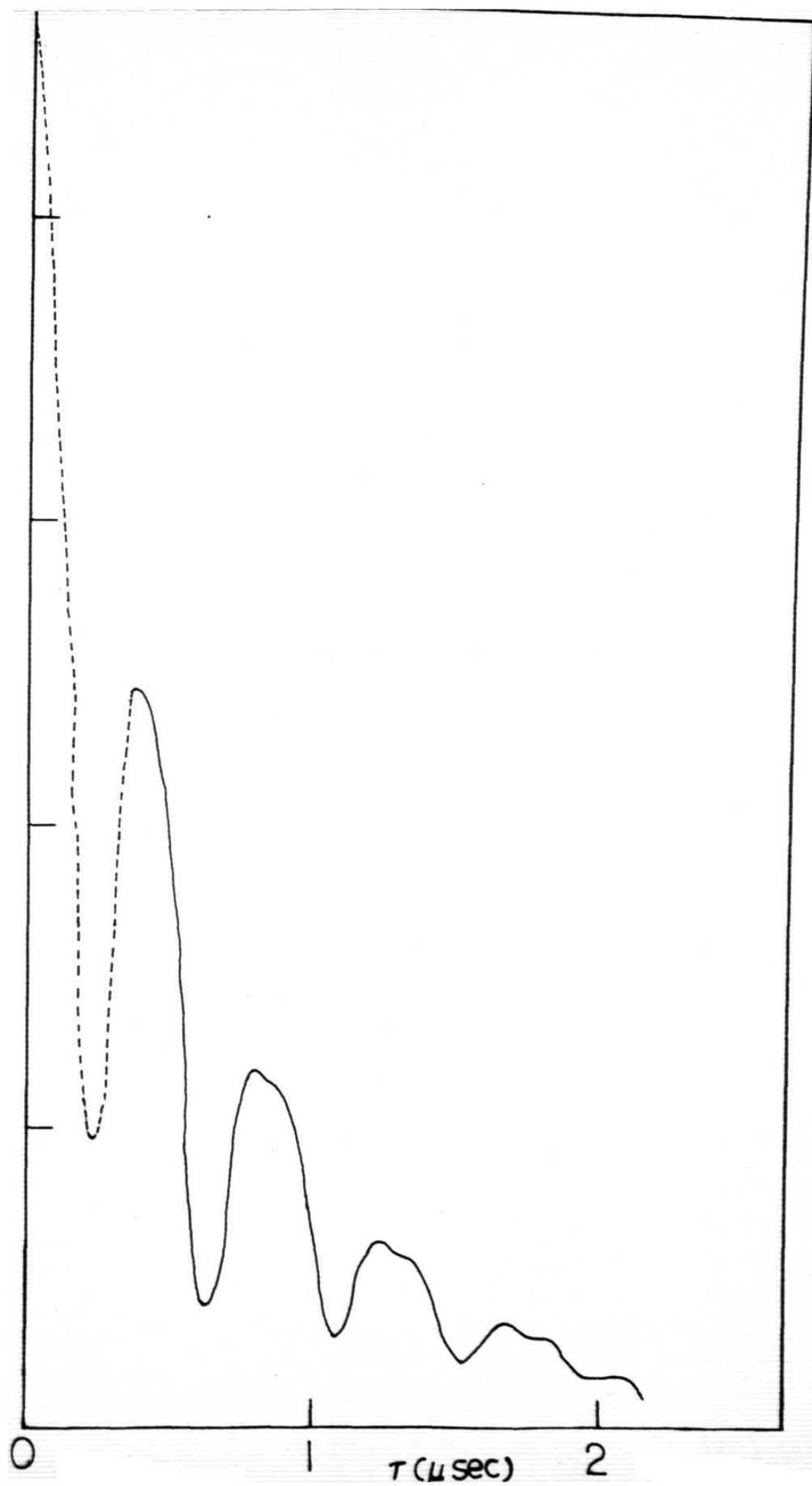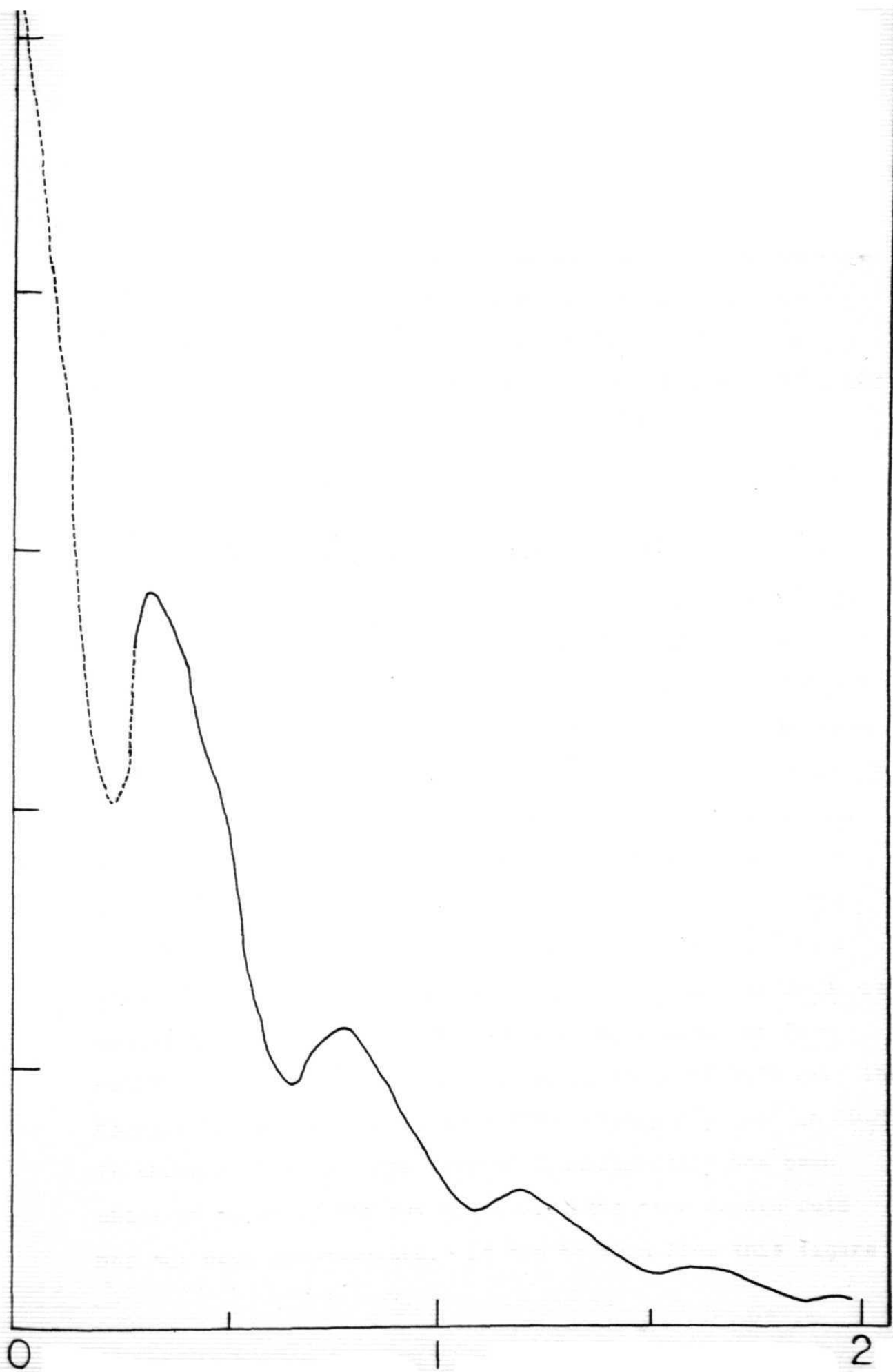The two pulse echo envelope of Ag^0 in CD_3OH

Fig. 2

The two pulse echo envelope of Ag^0 in CH_3OD

of a small quadrupole coupling we expect to see four transitions at $\omega_\alpha \pm \Delta$ and $\omega_\beta \pm \Delta$ for each nucleus. In Eq. (2) a_i is the amplitude of the line at frequency ω_i. The significance of the decay functions $F_o(\tau)$ and $F_i(\tau)$ has been discussed earlier.[11] Fourier transformation of the time domain data has been carried out by extrapolation[6,7,10], and by apodization[9] using the window function[12] given in Chapter II (Eq. [50] of Chapter II).

RESULTS AND DISCUSSION:

The spin echo modulations from Ag^o in CD_3OH and CH_3OD are shown in Figs. 1 and 2. The dashed line in these figures is obtained by extrapolating the modulation subject to the constraints discussed in Chapter II. As can be seen from these figures the modulation is fairly simple and shows only two frequency components with periods 0.4 and 0.2 μs. The time domain analysis[5] shows that the modulation essentially arises from only one type of nucleus. In the case of CH_3OD this corresponds to four hydroxyl deuterons located at a distance of 0.33 nm and in the case of CD_3OH it corresponds to 12 methyl deuterons arising from the four methyl groups located at an average distance of 0.33 nm. The Fourier transformation of the ESEEM arising from Ag^o in CD_3OH is shown in Fig. 3. The Fourier transformation has been obtained by using the raw data, i.e. the time domain data has not been preprocessed. It can be seen from this figure

Fig. 3

The Fourier cosine transform of the truncated
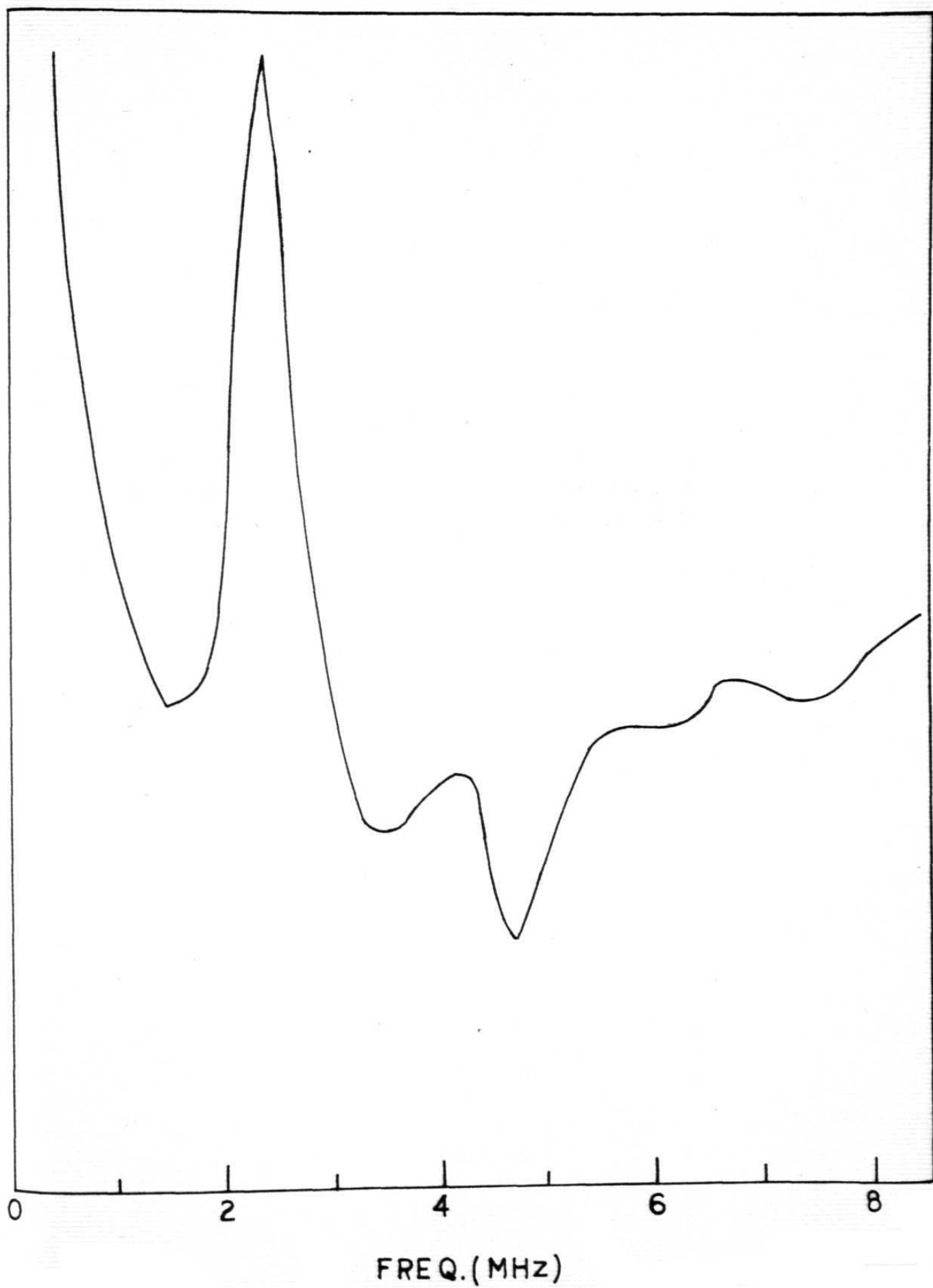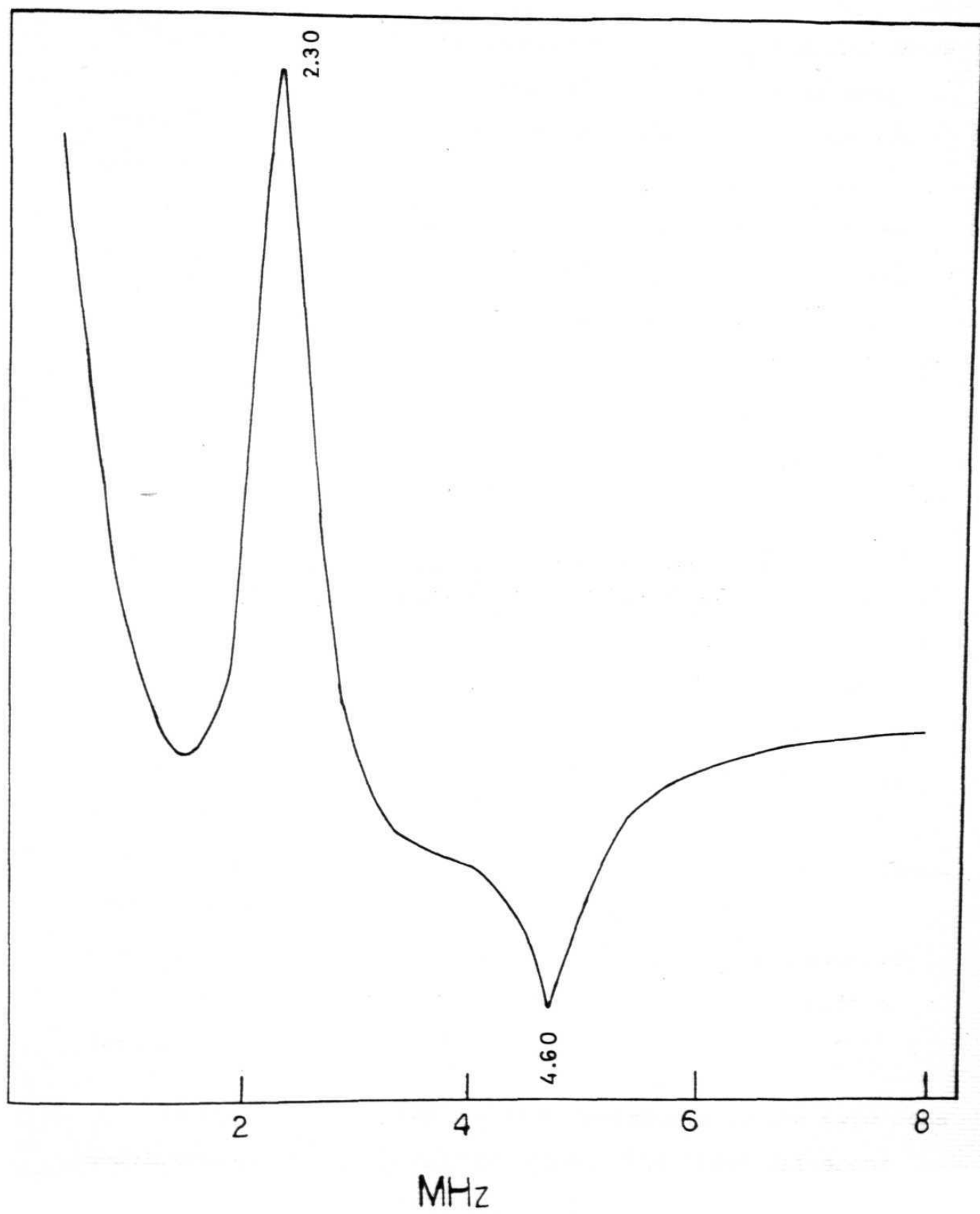data of Ag^0 in CD_3OH shown in Fig. 1.

FREQ. (MHz)

Fig. 4

The Fourier cosine transform of the data of Ag^{0} in CD$_3$OH after extrapolating to $\tau = 0$.

that besides observing the two peaks at 2.3 and 4.6 MHz there
are a number of spurious peaks. It can also be seen that
there is a large dc component which very strongly overlaps
with these peaks. The peaks at 2.3 and 4.6 MHz can be
identified with the periods 0.4 and 0.2 μs observed in the
time domain respectively. From the expression for the two
pulse echo modulation it can be seen that four frequency
components located at $\omega_\alpha, \omega_\beta, \omega_\alpha \pm \omega_\beta$ are expected. However, if
the hyperfine coupling is small compared to nuclear Larmor
frequency, we have, $\omega_\alpha \approx \omega_\beta \approx \omega_I$ and $\omega_\alpha - \omega_\beta \simeq 0$ $\omega_\alpha + \omega_\beta \simeq 2\omega_I$. Thus
the observed frequencies correspond to ω_I and $2\omega_I$. In Fig. 4,
the same Fourier transformed spectrum is shown after extra-
polating the data back to $\tau = 0$. On comparison with Fig. 3,
it is seen that the spurious peaks which were present in the
truncated data have disappeared in the FT spectrum. Also
the baseline is more stable and the resolution is enhanced.
In Figs. 5a to 5e the FT spectra from the apodized data are
shown for different values of the window parameter α. As
has been observed in Chapter II, it is seen that the sidelobes
and other spurious peaks decreased with increasing α.
However, this decrease in sidelobe amplitude is accompanied
by a decrease in the amplitude of the genuine peaks with a
loss of resolution.

In Fig. 6, the cosine Fourier transforms of the spin echo
modulation of Ag^0 in CH_3OD are shown. The three different

Fig. 5

The Fourier cosine transform of the envelope of Ag^o in CD_3OH using the window function for different values of the window parameter

$$
\begin{aligned}
&(a) \quad \alpha = 0.1 \\
&(b) \quad \alpha = 0.2 \\
&(c) \quad \alpha = 0.3 \\
&(d) \quad \alpha = 0.4 \\
&(e) \quad \alpha = 0.5
\end{aligned}
$$
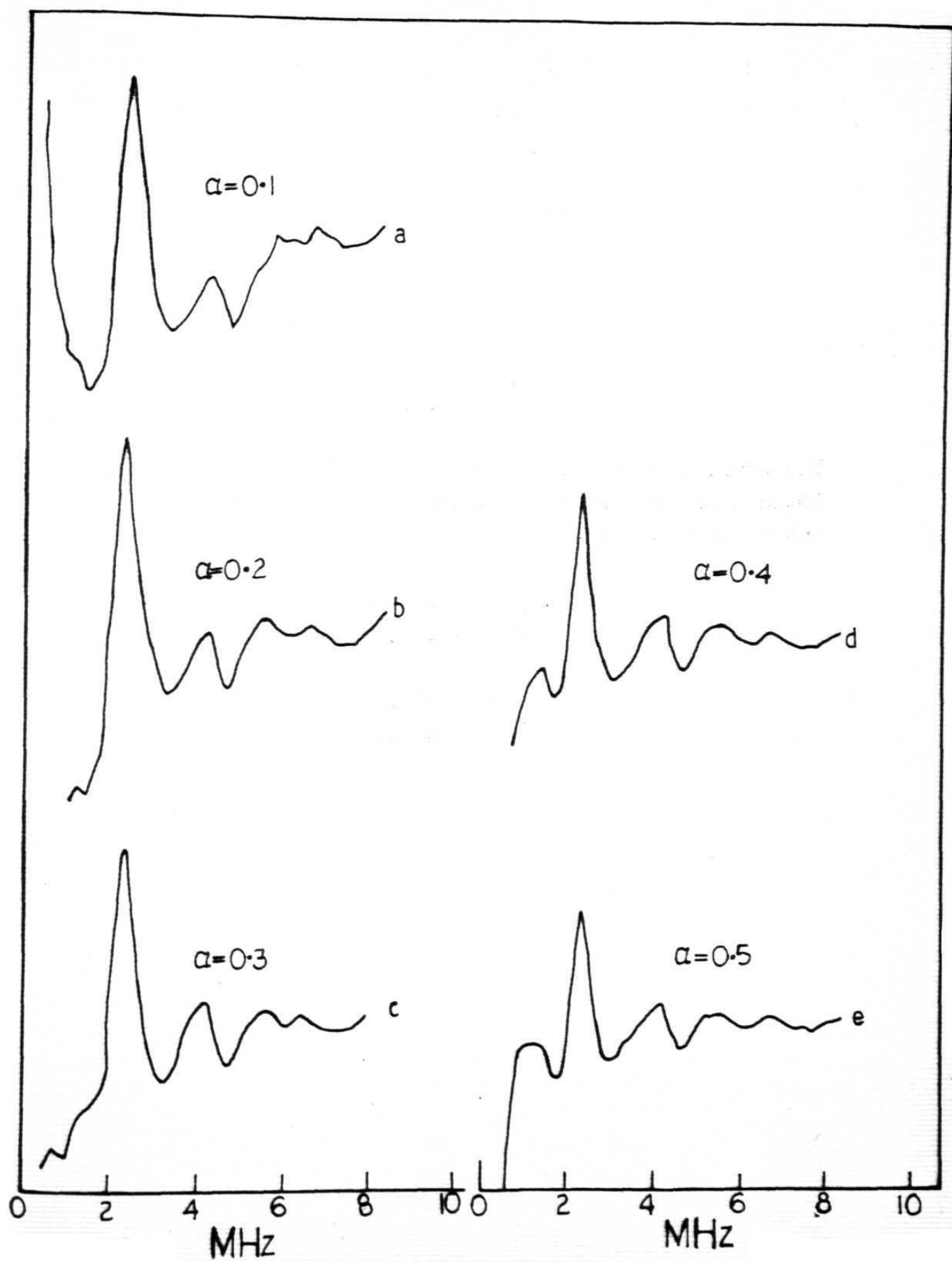
Fig. 6

The Fourier cosine transform of the modulation in Ag$^\circ$ in CH_3OD

(a) _____ FT of the truncated data

(b) _ . _ . _ FT of the truncated data after multiplication with the window function defined in Eq. [5].

(c) _ _ _ _ _ FT after extrapolation of the experimental curve to $\tau = 0$.

Fig. 7

Two pulse echo envelope for Ag^0 in Ice (site I) in
the non equilibrium configuration.

$\tau \, (\, \mu \; \text{sec})$

Fig. 8

Two pulse echo envelope for Ag^0 in Ice (site II) in
the equilibrium configuration.

$\tau \ (\mu \ \text{sec})$

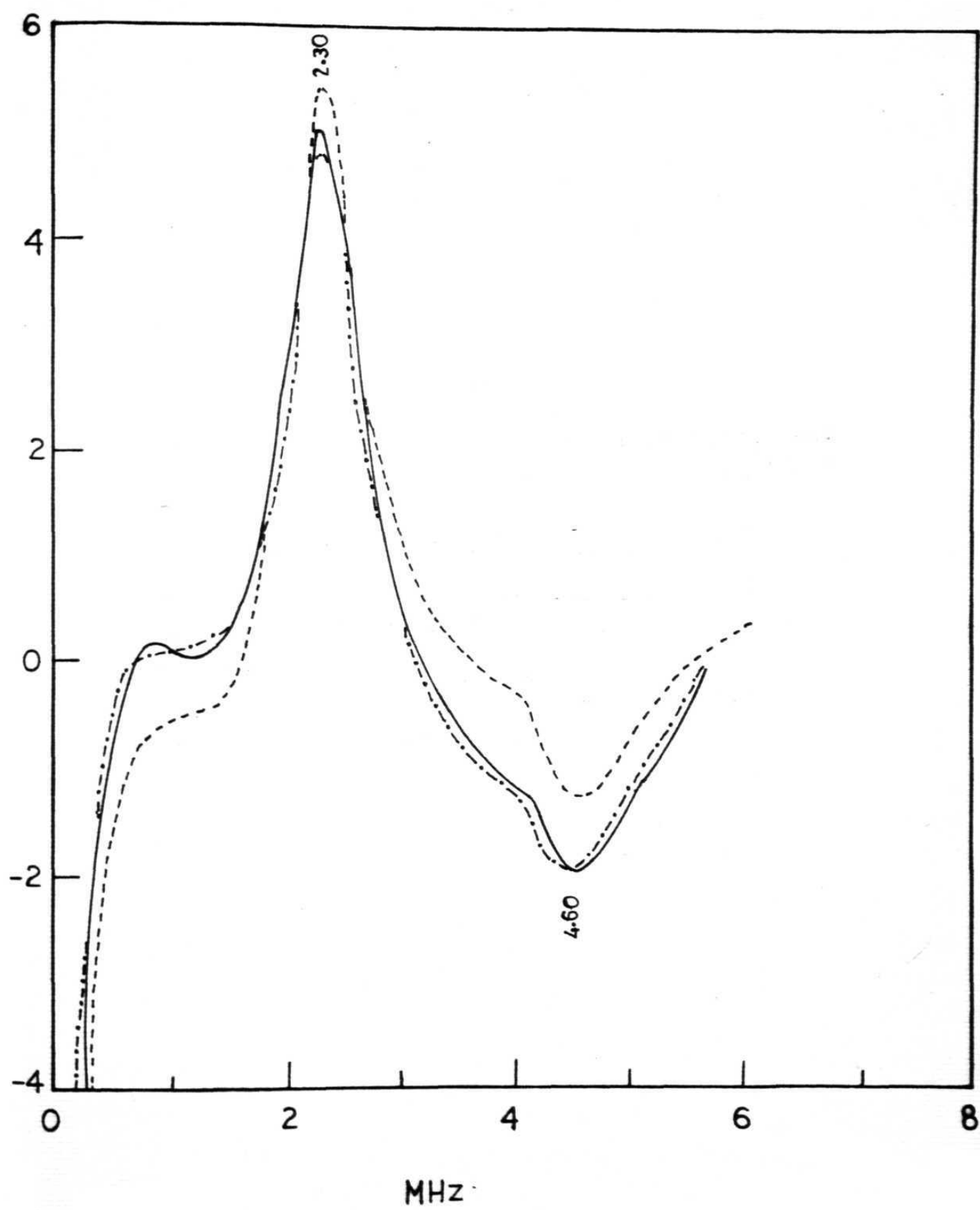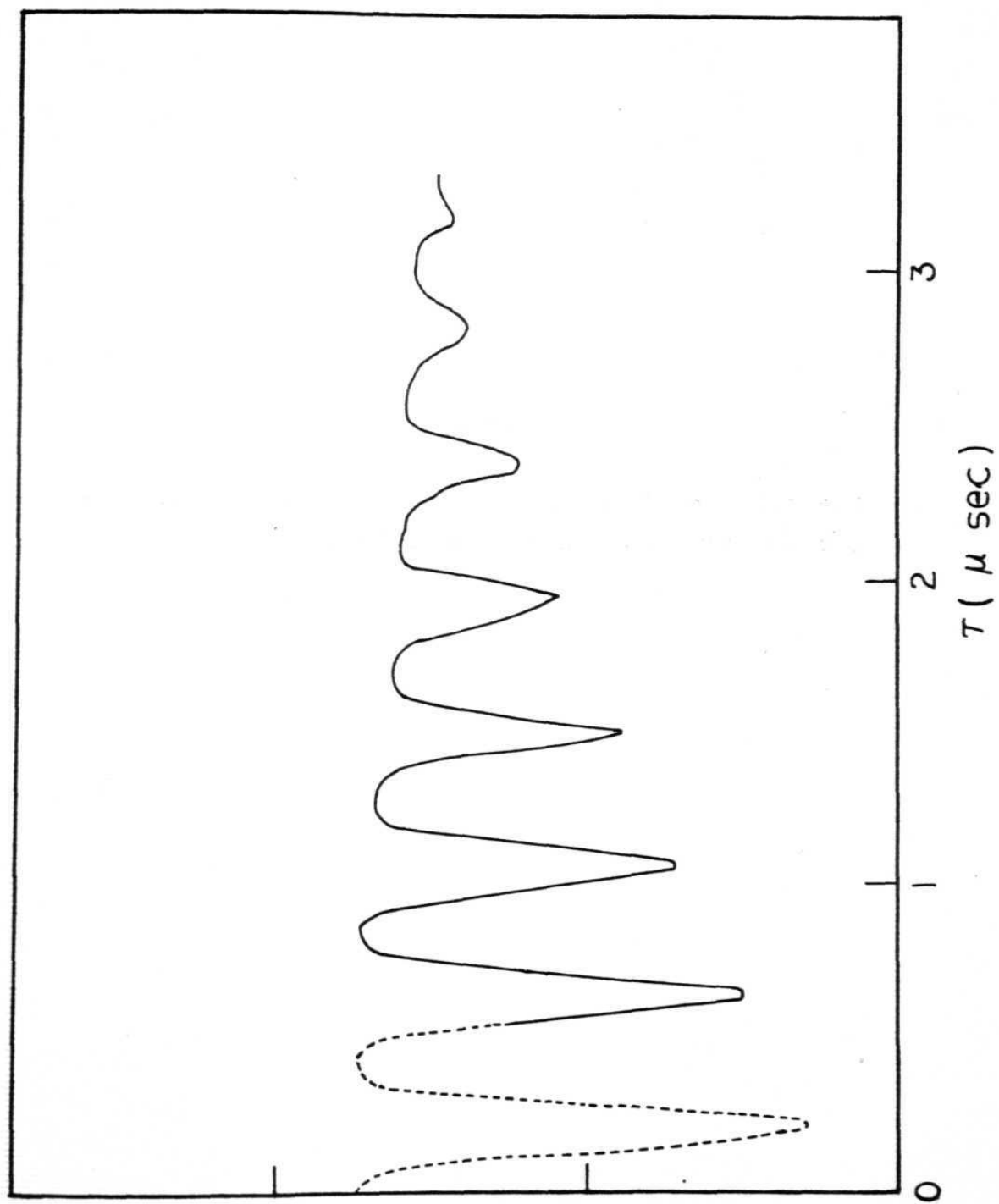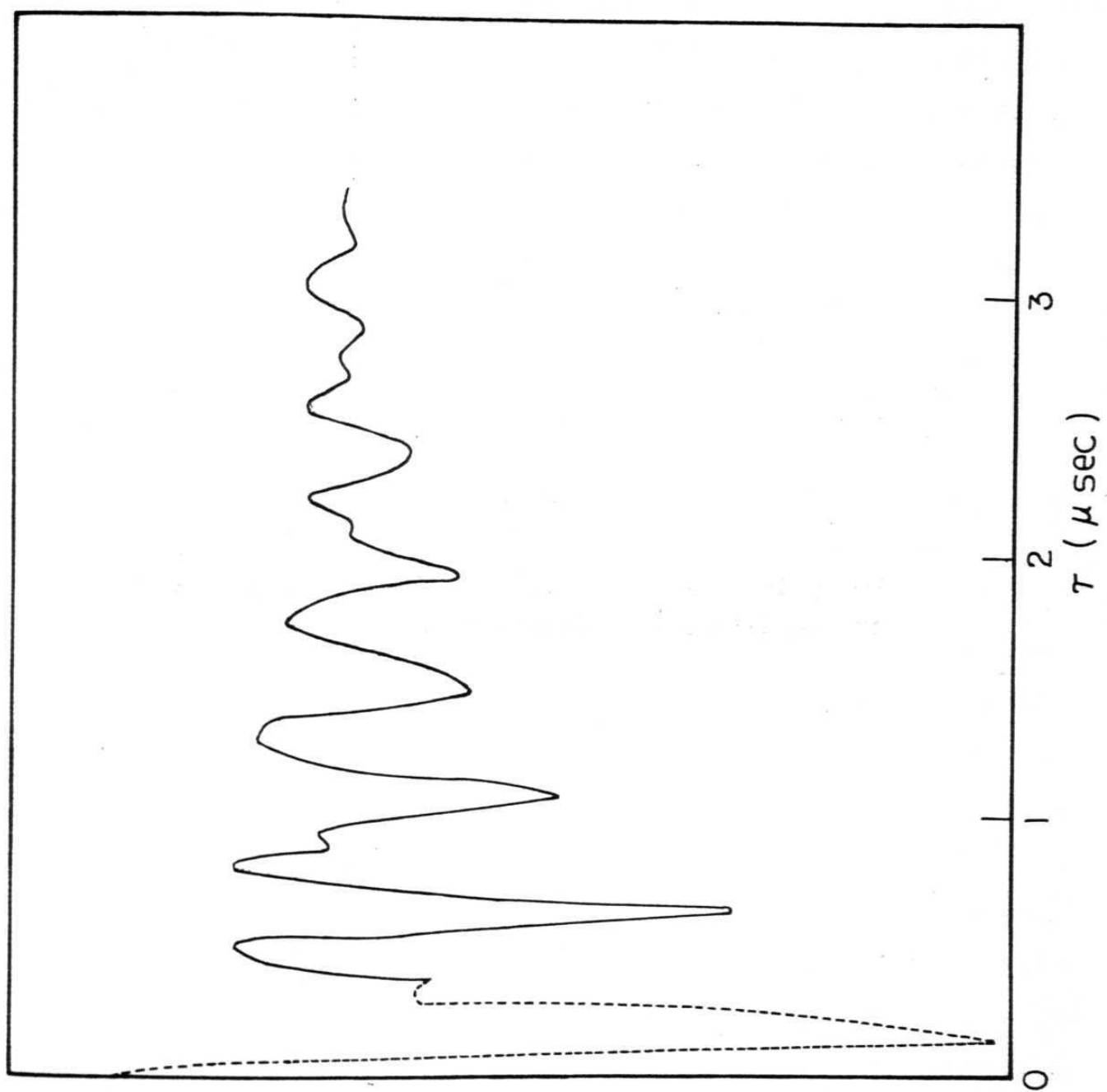curves correspond to the three methods used in Fourier transformation, viz., a) FT of the truncated data, b) FT of the data apodized using the window function with $\alpha = 0.1$, and c) FT of the extrapolated data. It can be concluded from Fig. 6 that the FT of the data with extrapolation to time $\tau = 0$ gives better resolution when compared to the other two methods of preprocessing the data.

The modulations from the polycrystalline samples, Ag^o in ice in site I and Ag^o in site II are shown in Figs. 7 and 8. It can be seen from Fig. 7 that the modulation shows two periods of 0.4 and 0.2 µs corresponding to two frequency components of 2.3 and 4.6 MHz. The Fourier spectrum of the truncated data again shows a large dc component and a number of spurious peaks besides the two frequency components at 2.3 and 4.6 MHz. The FT spectrum has been obtained by apodizing the data for various values of α. It is observed that the spurious peaks are suppressed for increasing values of α. This is however accomplished at the expense of linewidth and amplitude. In Fig. 9b the FT spectrum of the extrapolated time domain data for site I is shown. This shows clearly two peaks at 2.3 and 4.6 MHz which correspond to components at ω_I and $2\omega_I$. This compares well with the time domain analysis which indicates that the silver atom interacts with only one type of deuterium nucleus and has practically zero isotropic coupling.

Fig. 9

Fourier cosine transform of the envelope of Ag^o:
D_2O (site I)

a) – – – –   FT of the truncated data without the window

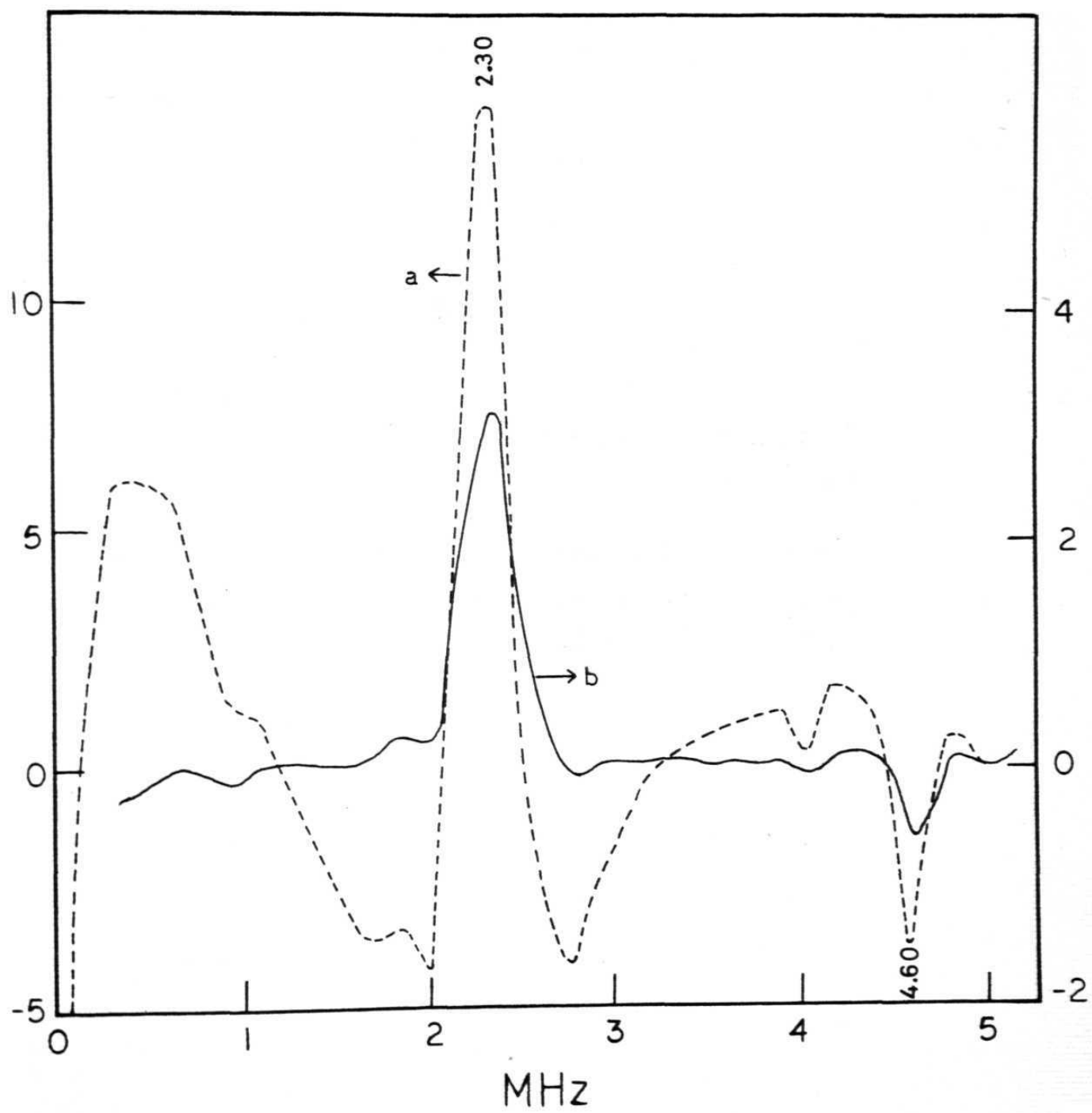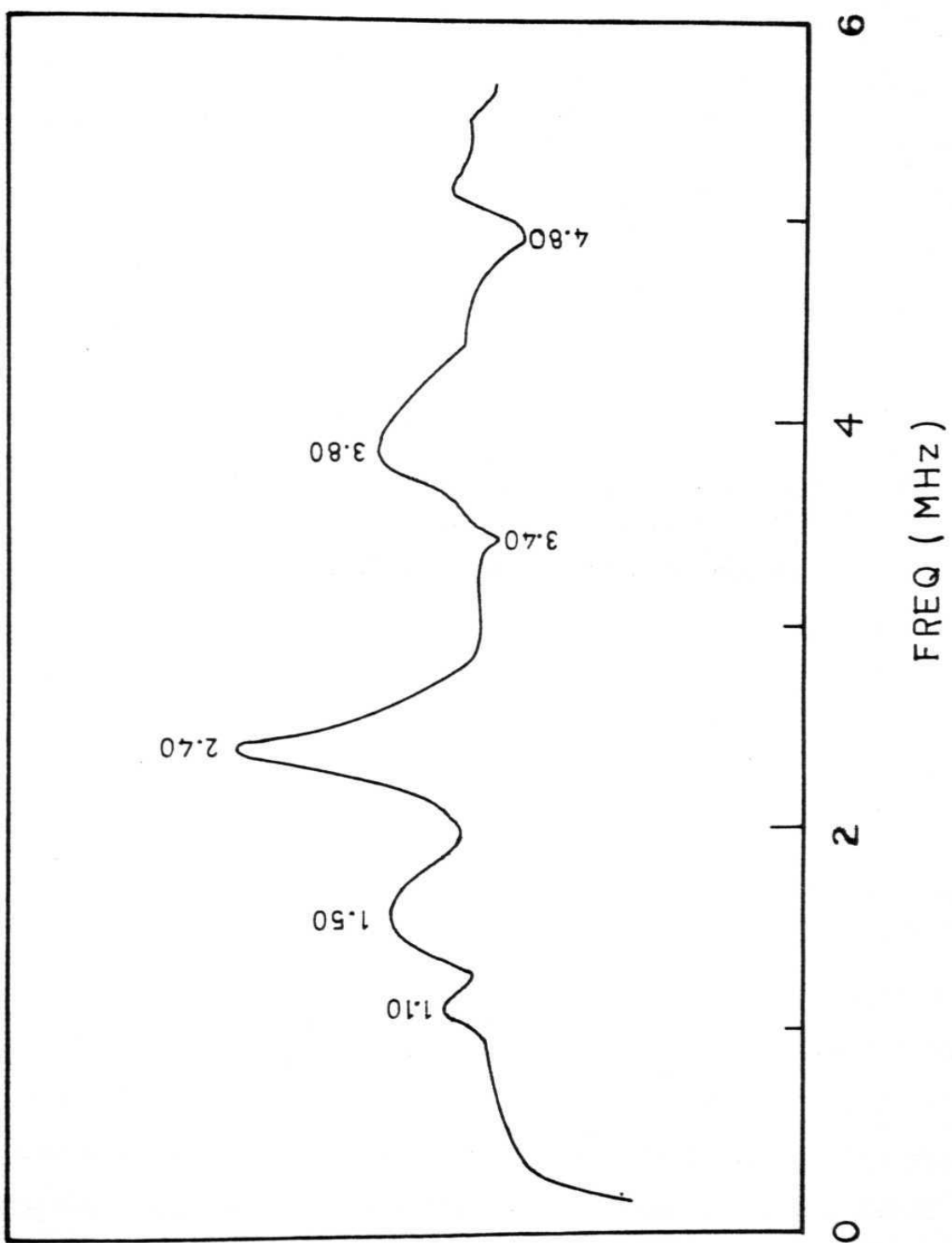b) ———   FT of the modulation after extrapolating
to $\tau = 0$.

Fig. 10

Fourier cosine transform of the envelope for
Ag^O: D_2O (site II) after extrapolating the
experimental curve to $\tau = 0$.

FREQ (MHz)

Site II exhibits a little more complex modulation. It can be seen that there are additional glitches present at lower values of τ. The time domain analysis indicates that these glitches arise from the closer deuteron [4]. The closer deuteron appears because of the rotation of a water molecule. The Fourier spectrum of the truncated data shows very broad peaks which could not be clearly identified. The apodization of the data did not improve the situation significantly. However the FT spectrum of the extrapolated data clearly shows a number of peaks at 1.1, 1.5, 2.4, 3.4, 3.8 and 4.8 MHz. The FT spectrum of the extrapolated data is shown in Fig. 10. The peaks at 2.4 and 4.8 MHz correspond to the interaction of Ag^{o} with farther deuterons because these frequencies correspond to ω_I and $2\omega_I$: This is also consistent with the fact that the 4.8 MHz peak has opposite phase compared to the peak at 2.4 MHz. From the time domain analysis we know that each silver atom also interacts with a deuterium nucleus which has a significant isotropic hyperfine coupling. Therefore the interaction with this deuterium nucleus gives rise to two peaks at $\omega_I + a/2$ and $\omega_I - a/2$, where 'a' is the isotropic hyperfine coupling constant. But the frequency spectrum shows not two peaks but four peaks at 1.1, 1.5, 3.4 and 3.8 MHz besides the peaks at 2.4 and 4.8 MHz which correspond to ω_I and $2\omega_I$ components respectively. The four peaks could be accounted for if we assume the presence of a small quadrupole coupling Δ. In the presence of a small

quadrupole coupling four peaks are expected at
$\omega_I + |a/2| + |\Delta|$, $\omega_I + |a/2| - |\Delta|$, $\omega_I - |a/2| + |\Delta|$ and
$\omega_I - |a/2| - |\Delta|$. Solving these equations we get a = 2.3 MHz
and Δ = 0.2 MHz. Thus it was possible for us to resolve
the very small quadrupole coupling by using the FT analysis.
The value of the isotropic coupling 2.3 MHz obtained from
the FT analysis differs from the value of 1.8 MHz obtained
from the time domain analysis. This discrepancy arises
because the time domain analysis neglects the quadrupole
coupling completely. It should be pointed out here that the
value of the quadrupole coupling parameter Δ = 0.2 MHz
compares very well with the value obtained from nuclear
quadrupole resonance sutdies of deuterated ice[13].

These studies thus clearly show that for glassy and
polycrystalline substances the FT ESEEM is a very reliable
method for measuring small hyperfine couplings. By using
this technique small quadrupole shifts could also be measured
whose presence is not obvious from the time domain analysis.
Another conclusion that could be drawn from these studies is
that extrapolation, whenever possible, is a better method for
obtaining high resolution spectrum compared to apodization.
This is especially so when the modulation does not contain
more than two or three periods and the phase memory time is
relatively small. This is understabdable because for systems
exhibiting long phase memory times the amount of data lost due
to truncation forms an insignificant fraction of the total
data available.

References

1. B.L. Bales and L. Kevan, J. Chem. Phys. 55, 1327 (1971).

2. D.R. Brown and M.C.R. Symons, J. Chem. Soc. Faraday Trans., 173, 1490 (1977).

3. L. Kevan, H. Hase and K. Kawabata, J. Chem. Phys. 66, 3843 (1977).

4. T. Ichikawa, L. Kevan and P.A. Narayana, J. Chem. Phys. 71, 3792 (1979).

5. T. Ichikawa, L. Kevan and P.A. Narayana, J. Phys. Chem. 83, 3378 (1979).

6. W.B. Mims, J. Peisach and J.L. Davis, J. Chem. Phys. 66, 5536 (1977).

7. T. Shimizu, W.B. Mims, J. Peisach and J.L. Davis, J. Chem. Phys. 70, 2249 (1979).

8. D. Shaw, 'Fourier Transform NMR Spectroscopy', Elsevier, Amsterdam (1976).

9. R. Bracewell, 'Fourier Transform and Its Application', McGraw Hill, NY (1965).

10. W.E. Blumberg, W.B. Mims and D. Zuckerman, Rev. Sci. Instrum. 44, 546 (1973).

11. P.A. Narayana and L. Kevan, J. Mag. Res. 46, 84 (1982).

12. C. Bingham, M.B. Godfrey and J.W. Tukey, IEEE Trans. Audio Electroacoust. 15, 56 (1967).

13. D.T. Edmonds and A.L. Mackay, J. Mag. Res. 20, 515 (1975).

CHAPTER V

FOURIER TRANSFORM STUDIES OF ESEEM OF HEMOGLOBIN DERIVATIVES

INTRODUCTION

In the last two chapters the FT ESEEM studies of single crystals, and polycrystalline and glassy complexes have been discussed. The usefulness of the technique in measuring small hyperfine couplings which are sometimes not revealed in ENDOR spectra has been demonstrated. Also, the resolution of quadrupole coupling parameters of ^{14}N, ^{2}D in the frequency spectrum was clearly demonstrated. In this chapter, the technique of FT ESEEM has been applied to one of the most important proteins, viz. hemoglobin (Hb) and its derivatives

Hemoglobin is the red pigment of the blood, whose function is to transport oxygen and carbon dioxide. It is a protein whose structure and function depend upon several factors such as the oxidation state of iron to which various ligands bind, the pH value, the concentration of organic phosphates, etc. The protein contains four subunits, each having an active site called 'heme'. The iron is embedded in the heme crevice and binds several ligands depending mainly upon its oxidation state and the conformational state of the protein. It binds molecules like O_2, CO, and NO in its Fe^{2+} state and CN^-, N_3^-, F^- and H_2O, etc. in its Fe^{3+} state. All the derivatives of hemoglobin in the Fe^{3+} state and the NO derivative in the Fe^{2+} state are paramagnetic and therefore could be studied using electron paramagnetic

resonance. Also the protein exhibits an important physiological property where the affinity for oxygen in the sixth position increases in a subunit of the protein when there is oxygen bound in other subunits. This is called 'Cooperativity'. This property facilitates hemoglobin to bind oxygen reversibly. The protein can exist in two different quaternary conformations, the fully liganded or R-conformation and the unliganded or T-conformation. Therefore it is important to investigate the electronic structure of the heme and the conformational influences on ligand binding as a function of the ligand. Such an understanding may throw some light on the effects of very subtle conformational changes on the function of hemoglobin.

A number of spectroscopic studies have been carried out on these derivatives in order to study the effects of these ligands on the structure-function relationship of the protein[1-6]. In particular a large number of electron paramagnetic resonance studies have been reported[7-10]. But the information from the EPR studies has been rather limited. In general, the low spin derivatives of hemoglobin give rise to EPR spectra which do not depend on the sixth ligand. Therefore, the same set of EPR spin-Hamiltonian parameters describe the EPR spectral features irrespective of the ligand. This is also the case with high spin derivatives of hemoglobin. Thus EPR spectra are insensitive to the changes

of ligands in the sixth position. The ligand field and molecular orbital (MO) calculations based on these results also do not show significant differences from ligand to ligand. Recently many ENDOR studies have been reported on various derivatives of hemoproteins and other porphyrin compounds[11-13]. Here also the studies have been classified as low-spin and high-spin studies. As has already been pointed out in the general introduction, ENDOR, when applied to polycrystalline substances, does not give a high enough resolution to obtain finer structural details. Nevertheless ENDOR studies have shown significant differences in the ENDOR frequencies of nuclei such as ^{57}Fe, ^{14}N, ^{37}Cl and protons[14]. Also studies on hemin compounds have observed a shift of ^{14}N ENDOR frequencies in protohemin chloride and bromide[15]. This shift of the ENDOR frequencies is related to the replacement of the ligand from chloride to bromide. But no such ENDOR studies have been carried out on actual physical systems. Nuclear magnetic resonance studies have shown such differences in the electronic structures of the heme with ligand[16]. But the structural information is limited in this case because of the difficulty in separating various contributions to the paramagnetic shift such as the pseudo-contact and contact contributions[17]. Moreover, in cases such as HbNO, the lines are too broad to be observed[18]. It was therefore felt that FT ESEEM would be a good technique to study some of the low spin derivatives of hemoglobin

such as HbN_3^-, $HbCN^-$, HbNO, and HbNO+IHP (inositol
Hexaphosphate). Of these derivatives, HbNO is particularly
interesting because it resembles oxyhemoglobin in most of
its properties. It can also be switched to the deoxy
conformation on binding by inositol hexophosphate. Such a
conformational change has been observed using several
techniques including EPR[29,34,35]. Thus one can study the
influence of the quaternary conformational change at the
heme site. Since FT ESEEM has been shown to resolve very
small hyperfine couplings, it is possible to obtain useful
information on Hb and its derivatives. This also would
provide further support for the suitability of this technique
in the case of complex biological samples. Previous studies
by Peisach, Mims and Davis[19] on myoglobin and other low spin
heme complexes indicate that this may indeed be the case.

In the case of hemoglobin the iron in the heme is
coordinated to four nitrogens of the porphyrin pyrroles and
to a nitrogen (N1) of the imidozole of the proximal histidine
(HisF8) as shown in Fig. 1. Also, all the ligands considered
here i.e. CN^-, N_3^- and NO have nitrogens as part of them.
This makes the ESEEM for such a system very complex because
of the contributions from these nitrogens (^{14}N) which have
large quadrupole couplings. The noncollinearity of the
principal axes of various tensors present in the interaction
Hamiltonian makes the situation even more complex. As has

Fig. 1

The active site of hemoglobin — the heme together
with the proximal (His F8) and distal (His E7)
histidines. The iron is bonded to four nitrogens
of the porphyrin ring and to a nitrogen (N1) of
the imidazole of His F8. The shaded area indicates
the position of the sixth ligand (like CN^-, N_3^-, NO,
considered here). Most of the modulation is from
the remote nitrogen (N3) of His F8.

his E 7

his F8
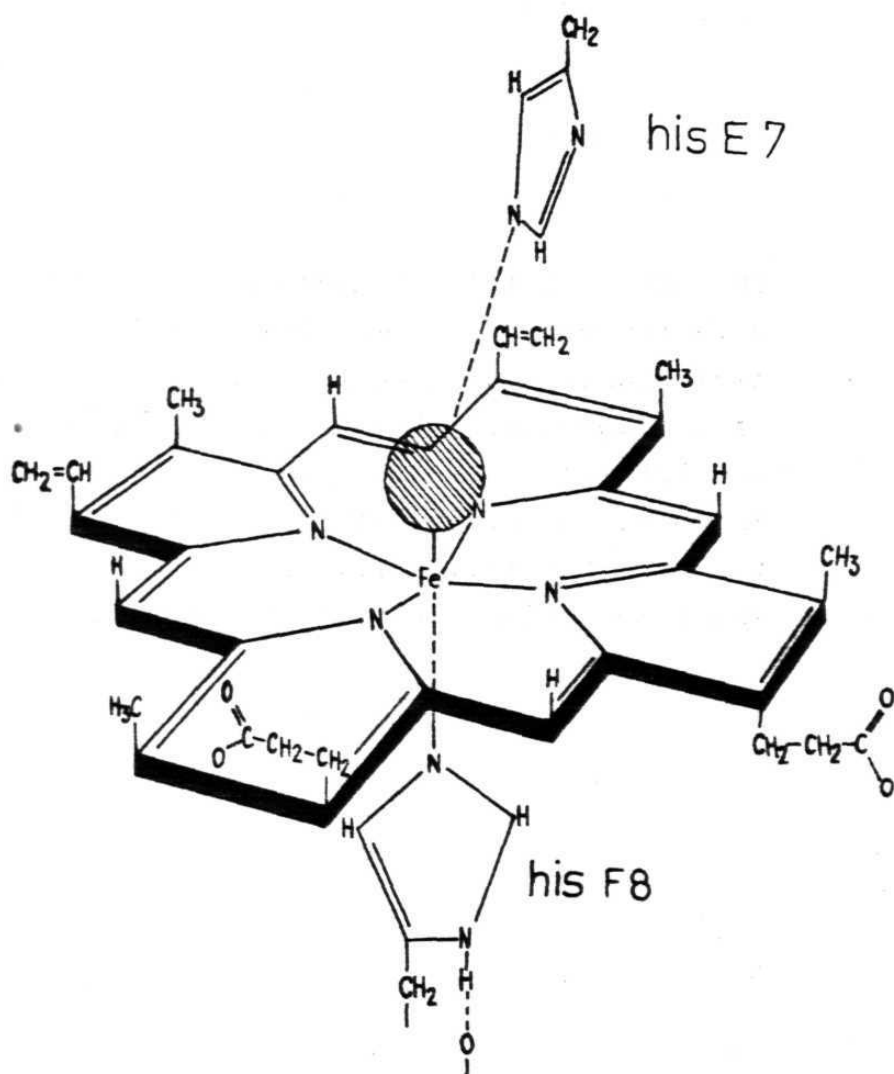
been pointed out in Chapter 3, the time domain analysis for
such a system is very difficult. The presence of the samples
in polycrystalline form adds to the complexity of the
situation. In such a case Fourier transform techniques are
essential for an analysis of the ESEEM. Various peaks in
the frequency spectrum obtained by Fourier transformation
are assigned to specific nuclei in the heme complex by
comparing the frequencies with the results obtained in model
systems. Fourier transformation was carried out by
preprocessing the data by 1) apodization of the data with a
smoothly varying window function, and 2) extrapolating the
data to time $\tau' = 0$.

Preparation of samples:

Preparation and purification of hemoglobin:

Hemoglobin stock solutions were prepared using a
modified method of Drabkin and Perutz[20-21]. About 20 ml of
human blood was drawn at a time, from a healthy non-smoking
individual, like the author. About 3.75 ml of 3.2% sodium
citrate solution (75 ml/400 ml of blood) was used as the
anticoagulant. The blood was centrifuged at 4000-5000
revolutions per minute (rpm) for about ten minutes to
separate the plasma from the red blood cells. All the
centrifugations were carried out at $4^{\circ}C$. After the
centrifugation, the supernatant plasma was pipetted out.

The red blood cells settled to the bottom of the tube. The
cells were then washed three or four times by saline solution
(0.9% NaCl) till the supernatant solution was colorless.
After each washing the red blood cells were collected by
centrifugation at 5000 rpm with a centrifugation time of
about ten minutes each time.

After washing the red blood cells, they were hemolysed
by an equal volume of cold, doubly distilled water. The
solution was left to stand for about half an hour and the
concentration of salt in the solution was brought to 2% by
the addition of 9% NaCl solution. The solution was
immediately centrifuged at 17000 rpm in a Servall refrigerated
centrifuge to separate hemoglobin from the red cell debris.
After the centrifugation the red cell ghosts settled to the
bottom of the tube leaving hemoglobin in the supernatant
solution. It was carefully decanted and the remaining
solution was centrifuged again and hemoglobin was collected.
The hemoglobin solution obtained by the above procedure
contained inorganic ions and organic phosphates such as 2,3-
diphosphoglycerate (2,3:DPG). The hemoglobin solution
obtained by the above process was dialyzed against excess
of 0.1 M phosphate buffer (pH=6.8) at 4°, overnight. This
removes the excess inorganic ions present in the solution.

In order to separate the hemoglobin from the organic phosphates, two procedures were followed. In the first[22], the solution was chromatographed through a 2.5 x 30 cm Sephadex G-25 column, equilibrated with 0.1 **M** phosphate buffer pH 8.0. The column was eluted with the same buffer at a rate of about 3 to 4 drops per minute. When the red hemoglobin band was approximately three or four centimeters from the bottom, fractions were collected in 2 ml. quantities. Only the fractions with highest hemoglobin concentrations measured optically at 577 nm were retained for experimental purposes. The hemoglobin thus obtained was devoid of phosphates and was dialysed against 0.1M phosphate buffer, pH 7.0, overnight and was stored at 4°C as the stock solution.

The second method for the removal of organic phosphates[23] makes use of ion-exchange and ion-retardation resins. The ion-exchange chromatography was performed with the ion-retardation resin AG 11-A8 and the mixed-bed resin AG 501-X8 (D), both obtained from Bio-Rad, Richmond, Calif. These two resins were used in conjunction with each other. The ion retardation resin contains positive and negative charges in a self absorbed form and is predominantly used to desalt proteins. The resin was washed with 5 vols. of 1M NH_4Cl and thereafter with 20 vol. of distilled water as specified by the manufacturer. The general procedure of operating the column was the same as described for gel

Fig. 2

A typical column showing gel (or resin) particles
packed against gravity used in the preparation and
purification of hemoglobin derivatives.
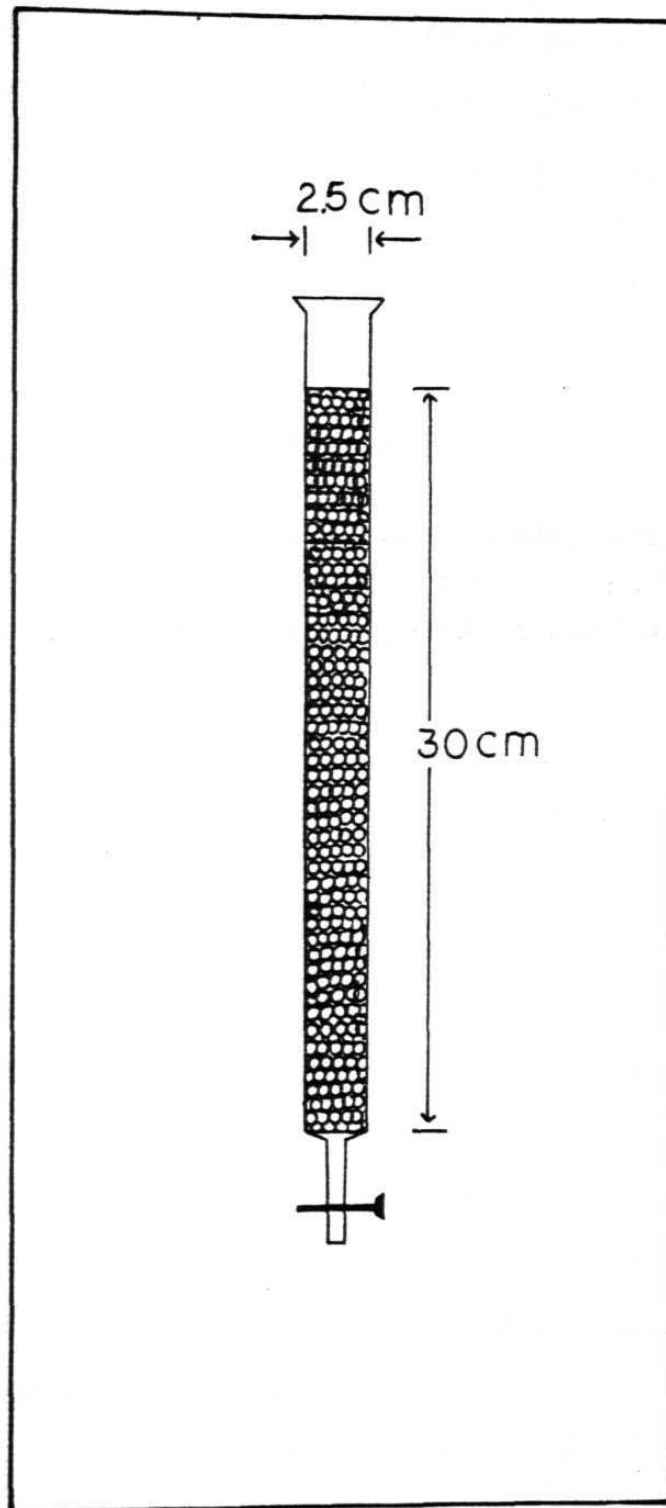
filtration above, except that water was used to elute hemoglobin. The hemoglobin solution was passed through these resins successively and eluted. The protein after this treatment was essentially free of salts. At this point any salt or buffer was added through dialysis and the hemoglobin solution was stored at $4^{o}C$. A typical column used for these purposes is shown in Fig. 2.

Preparation of Met hemoglobin (Met Hb):

The hemoglobin solution obtained by the above method essentially consisted of oxyhemoglobin. For the preparation of some of the derivatives it has to be converted to the met form. This was obtained by oxidizing the Fe^{2+} of oxyhemoglobin by potassium ferricyanide to Fe^{3+}. A portion of the hemoglobin solution was allowed to stand for a few minutes with a slight excess of $K_3Fe\,(CN)_6$. The reaction was complete after a few minutes as was clearly indicated by a change in color of the protein solution. The ferro-cyanide formed in the course of the reaction binds to hemoglobin. It was remove by passing the solution through a 2.5 x 30 cms. Sephadex G-25 column, equilibrated with 0.1 M phosphate buffer, pH 7.0. The solution was eluted by the same buffer.

Preparation of hemoglobin azide and cyanide:

To the met Hb prepared by the above procedure, excess
of 1 M NaN$_3$ solution was added dropwise. The reaction takes
place immediately and could be clearly observed optically
by a change of colour of the solution. The solution was then
dialysed against 0.1 M phosphate buffer, pH 7.0 to remove the
excess azide. The pH of the solution was changed by dialyzing
the solution against phosphate buffer of the desired pH at
least for twelve hours.

HbCN$^-$ was also prepared in an exactly similar manner
except that sodium cyanide was used in the place of NaN$_3$ to
obtain the cyanide derivative.

Preparation of HbNO and HbNO + IHP:

Met Hb prepared by the above procedure was used in the
preparation of HbNO and HbNO+IHP. Met Hb solution was taken
and the concentration of Met Hb in the solution was deter-
mined. Nitrogen gas was passed through the solution for ten
minutes. A stoichiometric amount of buffered ascorbic acid
was added to the Met Hb solution. Any insoluble material,
if formed, was removed by centrifugation and a stoichiometric
amount of solid NaNO$_3$ was added. The reaction was allowed
to proceed for 5 minutes and the pH of the solution was
determined. For the preparation of HbNO+IHP, the same
procedure was followed except that a stoichiometric amount

of IHP (disodium salt) was added to the solution along with ascorbic acid. The pH was adjusted with a buffer solution and the sample tube was immediately sealed.

All the derivatives have been characterized by spectrophotometry. The extinction coefficients[5,6] with the absorption maxima are given in Table 1. All the preparations and purifications were performed at $4^{\circ}C$ and the Hb solutions were stored at $4^{\circ}C$. Derivatives prepared were used within ten days from the day on which blood was drawn.

RESULTS AND DISCUSSION:

As pointed out earlier, in a three pulse echo envelope modulation the suppression effect may remove or reduce the amplitude of some of the frequency components. This problem can be eliminated by performing a two-dimensional FT analysis. This gives a complete ENDOR spectrum[25]. A two dimensional FT analysis requires that the time domain data be recorded both as a function of τ and T. In the case of hemoglobin the phase memory time is quite short and therefore enough data as a function of τ does not exist to perform a complete two-dimensional analysis. An alternate approach is to record the three pulse echo data for different values of τ and Fourier transform each one of them. This way it is possible to recover all the frequency components present eventhough their relative intensities can not be preserved. This

Fig. 3

Stimulated echo envelope for hemoglobin azide at
pH = 7.0 and for τ = 530 nsec. The broken line
represents the extrapolated portion of the
envelope. Magnetic field H_o = 0.23 T.
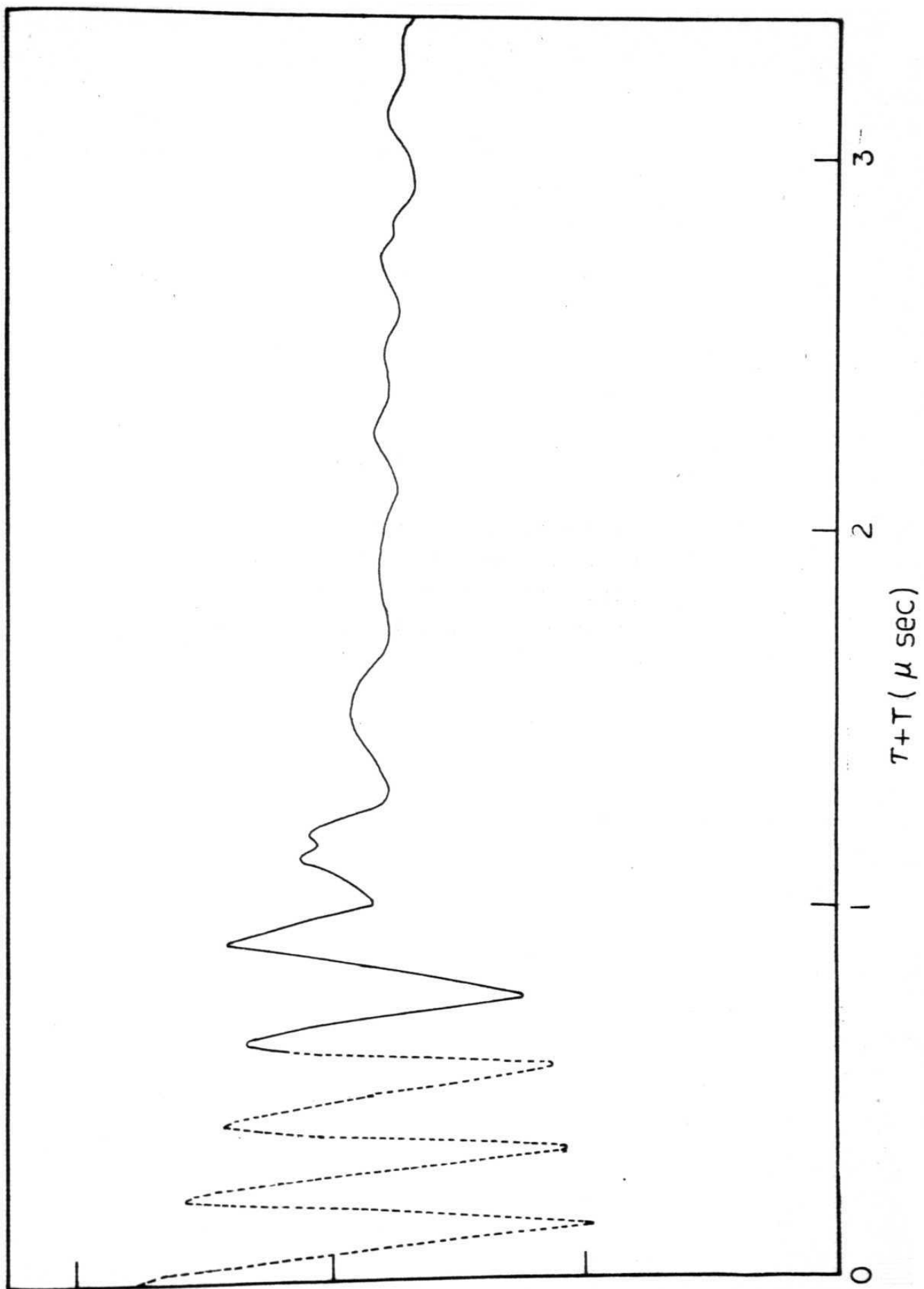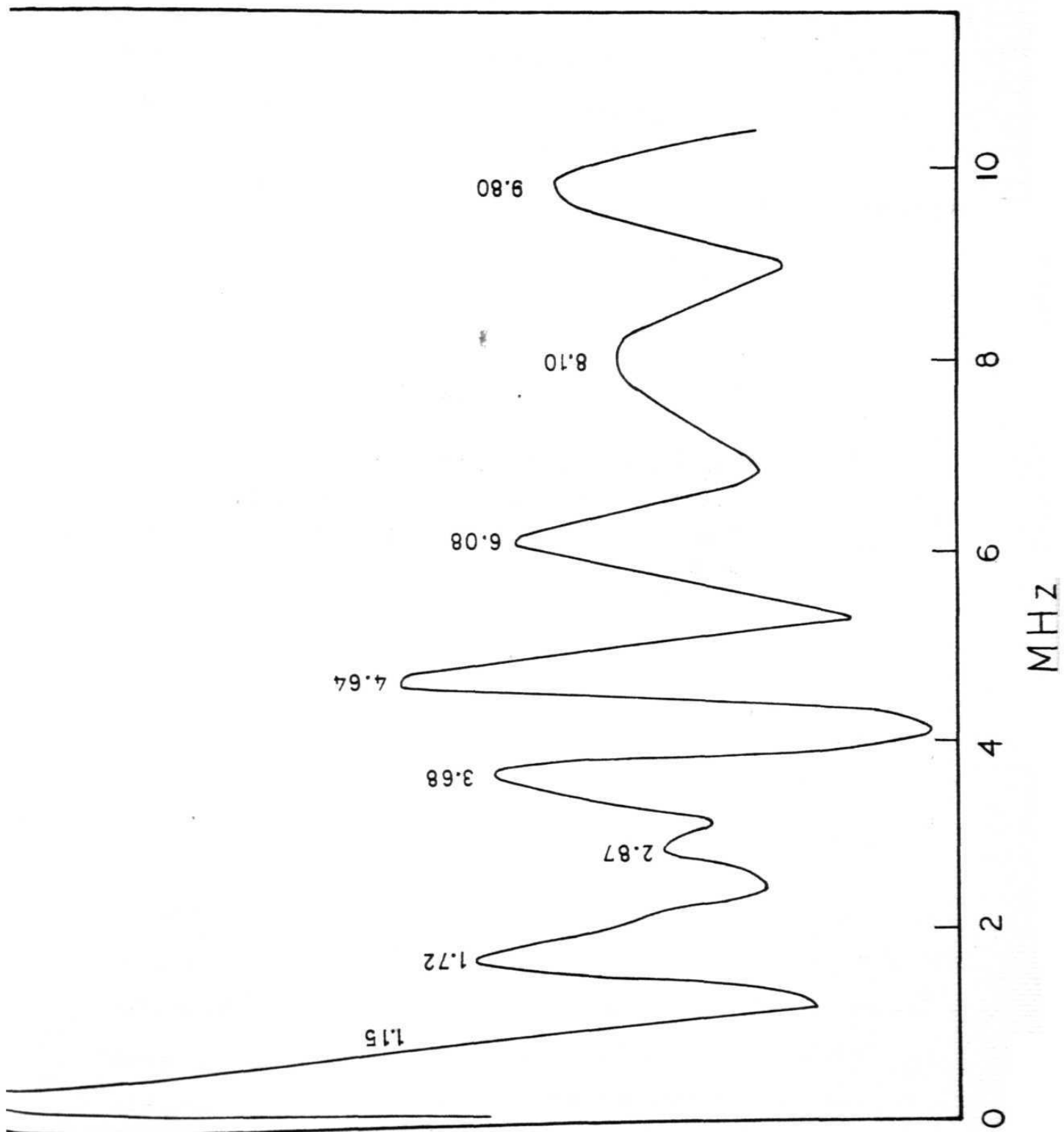
$\tau + T \, (\mu \, \text{sec})$

Fig. 4

Fourier cosine transform of the echo envelope
for hemiglobin azide shown in Fig. 3. The
frequencies have been indicated on top of the
peaks.

procedure has been followed in this chapter. In many instances it is possible to chose values of τ such that all the frequency components of interest are present. Again the relative intensities do not have any physical significance. The results obtained for different derivatives of Hemoglobin are discussed below.

Hemoglobin azide (HbN_3^-):

The three pulse echo modulation arising from HbN_3^- is shown in Fig. 3. The pH of the sample was 8.0 and the value of τ was 530 nsec. The broken line shows the extrapolated portion of the envelope. The Fourier transform of this envelope is shown in Fig. 4. It contains peaks at 0.29, 1.15, 1.72, 2.87, 3.68, 4.64, 6.08, 8.10 and 9.80 MHz. It was verified that none of these peaks arises due to the interaction of the unpaired spin with protons by changing the microwave power and pulse width. The modulation therefore arises solely due to interaction with ^{14}N nuclei. The frequency spectrum is very complex and in order to interpret the spectrum it is necessary to rely on the studies with similar model compounds like the mercaptoethanol and other low spin heme complexes studied by Peisach et al[19]. Also the information concerning the nuclear quadrupole frequencies on several imidazole complexes studied by M.J. Hunt et al[24] and C.H. Ashby et al[26] have been used.

Based on these studies carried out on these compounds, the first three peaks at 0.29, 1.15 and 1.72 MHz are identified with the zero-field quadrupole frequencies. The origin of these frequencies has already been discussed in detail in Chapter III. The value of the isotropic coupling constant (a) estimated from these frequencies is $\approx$ 2.0 MHz. The peak at 2.87 MHz arises due to a combination of the 1.15 and 1.72 MHz components. The lines at 3.68 and 6.08 MHz arise from a porphyrin ^{14}N with an isotropic coupling constant of approximately 4.5 MHz. The assignment has been arrived at from a comparison of the frequency components obtained from the model compounds, particularly heme-mereaptocthanol and bisimidazole complexes[19]. In this case the isotropic coupling is very large compared to the nuclear Zeeman term ($\approx$ 1 MHz at 0.3 Tesla) and from the energy level diagram (Fig. 1 of Chapter III) it can be seen that only two lines, f_1 and f_2 are expected at positions $\frac{1}{2}|a|h/g_n\beta_n + H_o$ and $\frac{1}{2}|a|h/g_n\beta_n - H_o$. The line at 9.80 MHz may be due to a combination of these two frequencies. Such combination frequencies might arise when there are a number of similar interacting nuclei. The peaks at 4.64 and 8.10 MHz are from a nucleus with a large isotropic coupling, probably from a nitrogen of the azide ligand. The modulation in the case of hemoglobin azide did not change with the magnetic field setting. All the modulations have been recorded by monitoring the g = 2.19 ESR line at different pH values.
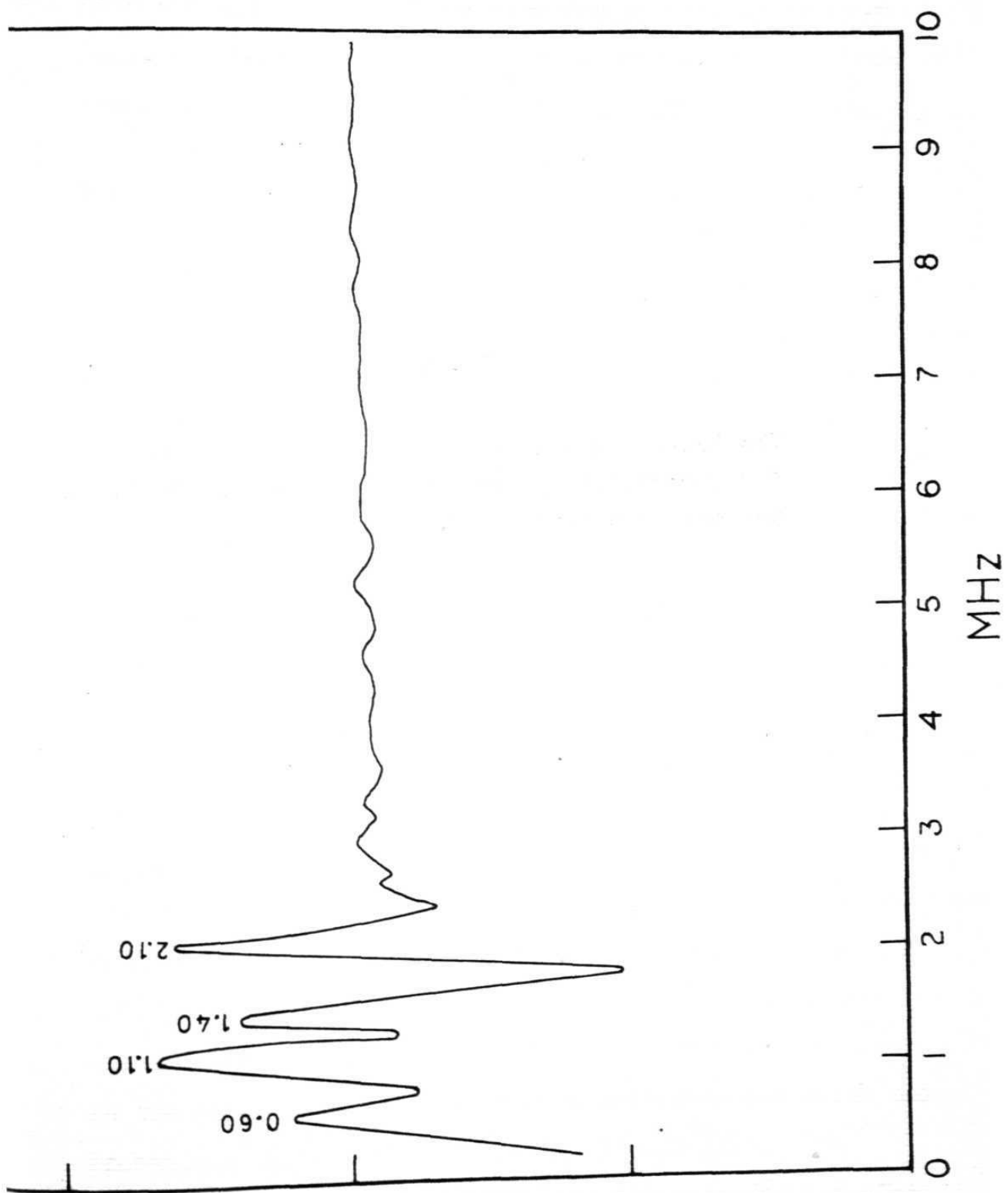
Fig. 5

The three pulse echo envelope for hemoglobin
cyanide for $\tau = 300$ nsec and at pH = 6.8. The
broken line indicates the extrapolated portion
of the envelope. $H_o = 0.32$ T.

$\tau = 300$ nsec
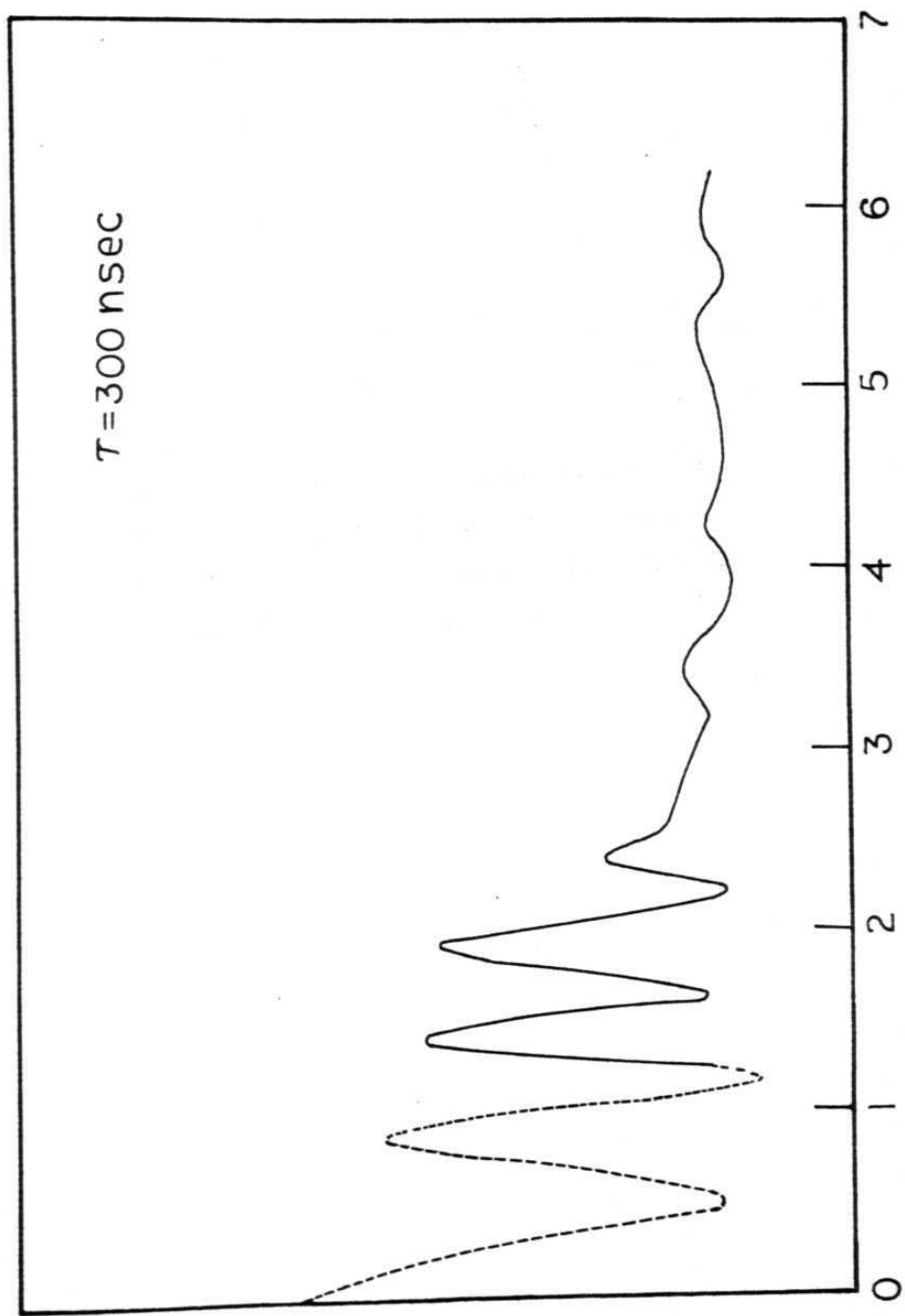
$\tau + T$ (μ sec)

Fig. 6

The Fourier cosine transform of the echo envelope
for hemoglobin cyanide shown in Fig. 5. The noise
has not been smoothened.

Also the modulation did not show any pH dependence in the range studied (pH 6-9). This shows that azide ion binds to hemoglobin strongly and is consistent with other studies[5].

Hemoglobin Cyanide (HbCN):

In Fig. 5 the ESEEM of HbCN⁻ with γ = 300 nsec. is shown. The extrapolated portion is shown by a dashed line. The pH of the sample is 6.8. The Fourier spectrum for this modulation is shown in Fig. 6. It shows four frequency components at 0.6, 1.1, 1.4 and 2.1 MHz. A comparison of these frequencies with those reported for imidazole nitroxide complexes and mercaptoethanol complexes[19] reveals that the frequencies at 0.6, 1.4 and 2.1 MHz are zero-field quadrupolar frequencies. These arise from the nitrogen N3 of the proximal histidine. The peak at 1.1 MHz is due to the free nuclear Zeeman interaction from one of the several nitrogens present. The zero-field quadrupole frequencies arise because the contact and the Zeeman terms have almost equal values as in the case HbN_3^-. The modulation from HbCN⁻ is relatively simple when compared with that of HbN_3^-. It involves contributions only from the distant nitrogen (N3) of the proximal imidazole whereas modulation in the case of HbN_3^- arises due to porphyrin nitrogens and probably from nitrogens of the N_3^- ligand also. The modulation in the case of HbCN⁻ is also recorded for other

values of τ and at different pH values. It did not show any additional frequency components. Moreover, the modulation did not change with pH showing the stability of the derivative. This is consistent with the conclusions derived using other techniques[5].

Hemoglobin Nitroxide (HbNO) and HbNO+IHP:

The modulation data from these derivatives of hemoglibin have shown several interesting features. In both these cases modulations have been recorded for values of τ ranging from 200 - 700 nsec., and the modulations have been Fourier transformed both using a window function and extrapolating the data to $\tau + T = 0$. All the modulations have been recorded for samples at pH 6.8.

Fig. 7 shows the modulation from HbNO with $\tau = 300$ nsec. The broken line is the extrapolated portion of the envelope. Fig. 8 shows the Fourier transformed spectrum. It shows frequencies at 0.40, 0.80, 1.30, 1.75, 5.0 and 8.0 MHz. ESEEM data with other τ values also gave rise to the same frequencies, though some of the frequencies were suppressed for different τ values. From an examination of the frequencies it is clear that the 0.40, 1.30, 1.75 MHz frequency components form a set of zero-field quadrupole frequencies. Similar frequencies have been observed to arise from the nitrogen N3 of the proximal histidine in

Fig. 7

The stimulated echo envelope for hemoglobin
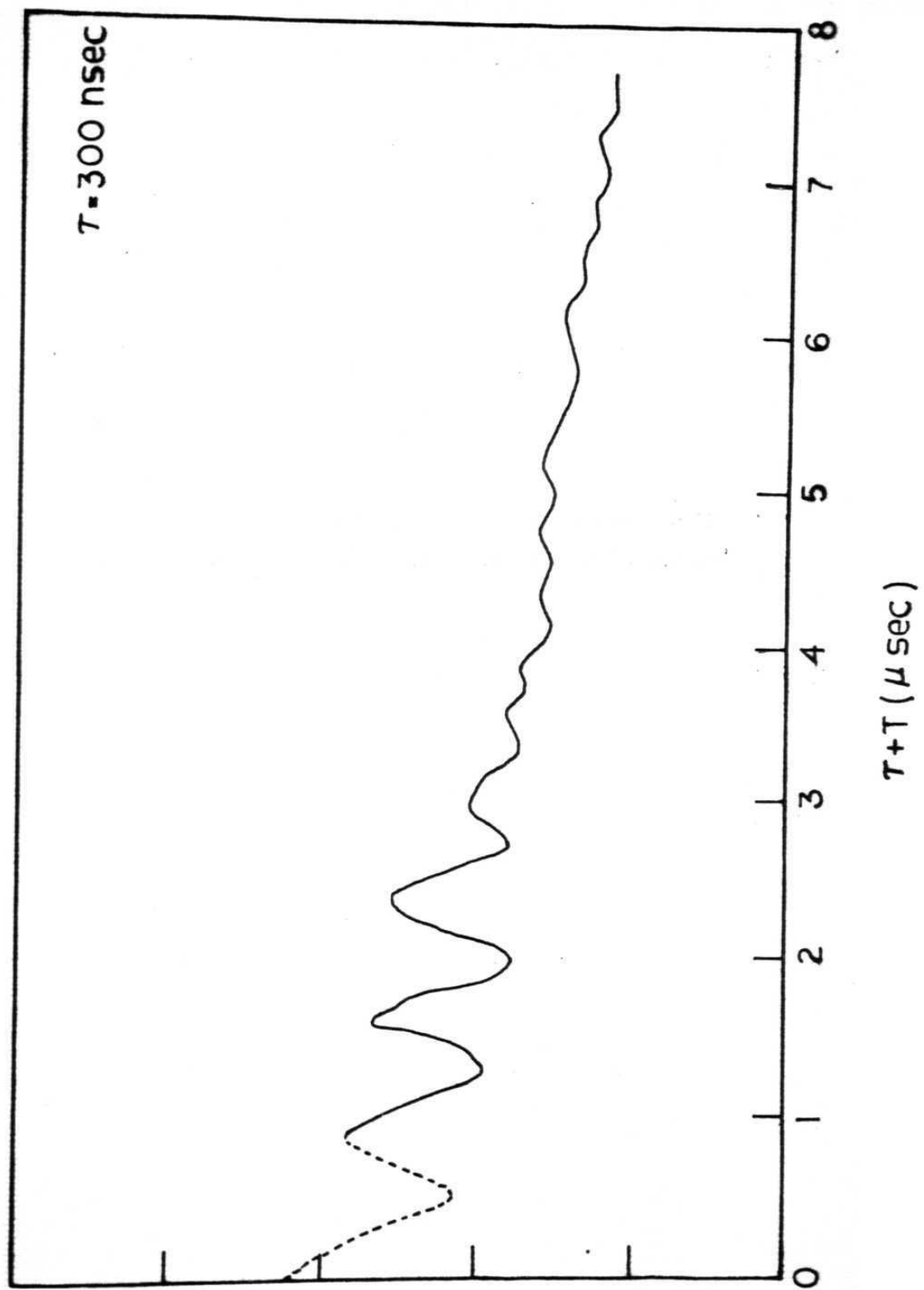nitroxide at pH = 6.8 and τ = 300 nsec.

Fig. 8

The Fourier cosine transform of the echo envelope
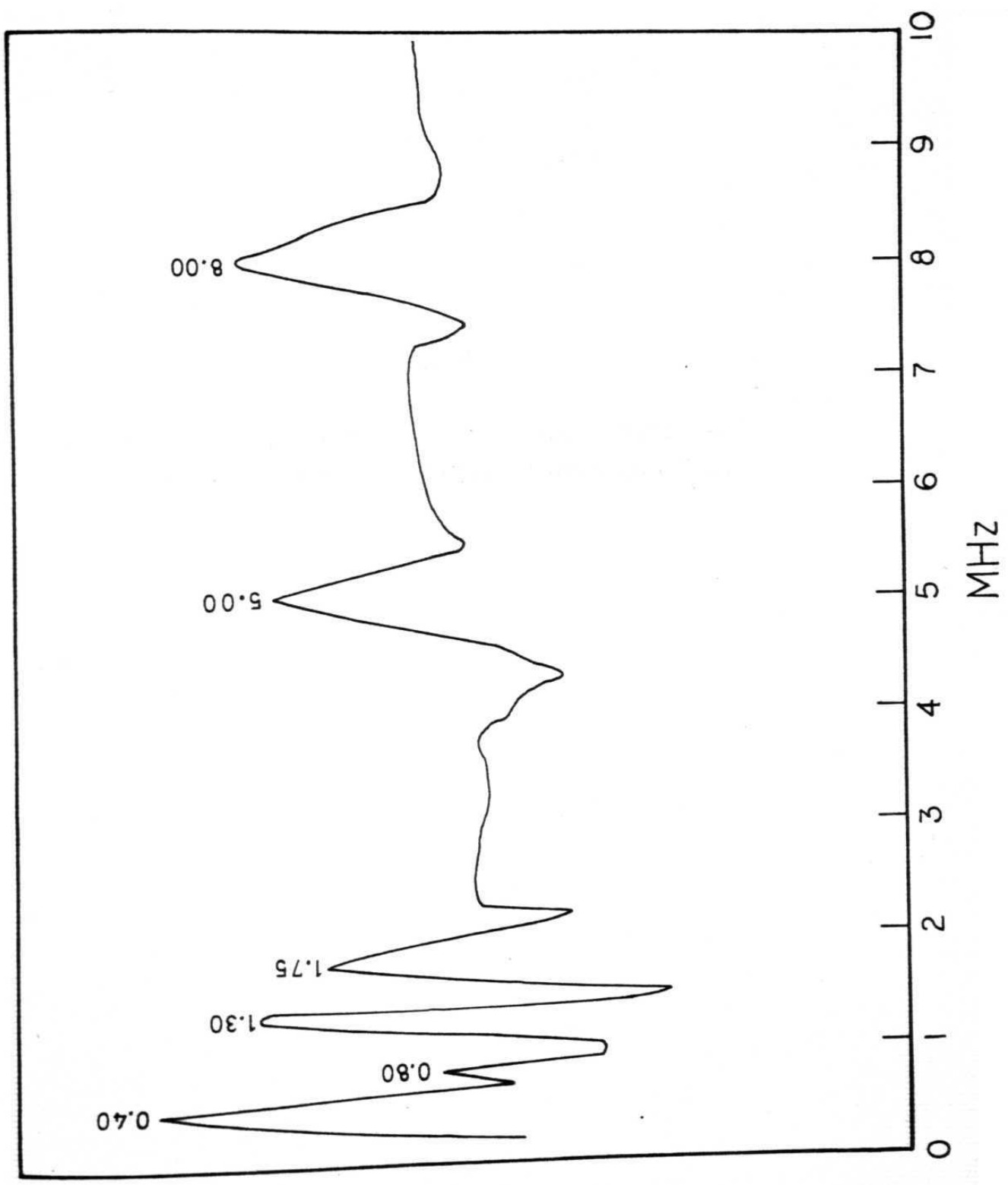for hemoglobin nitroxide shown in Fig. 7.

Fig. 9

Three pulse echo envelope for hemoglobin nitroxide +
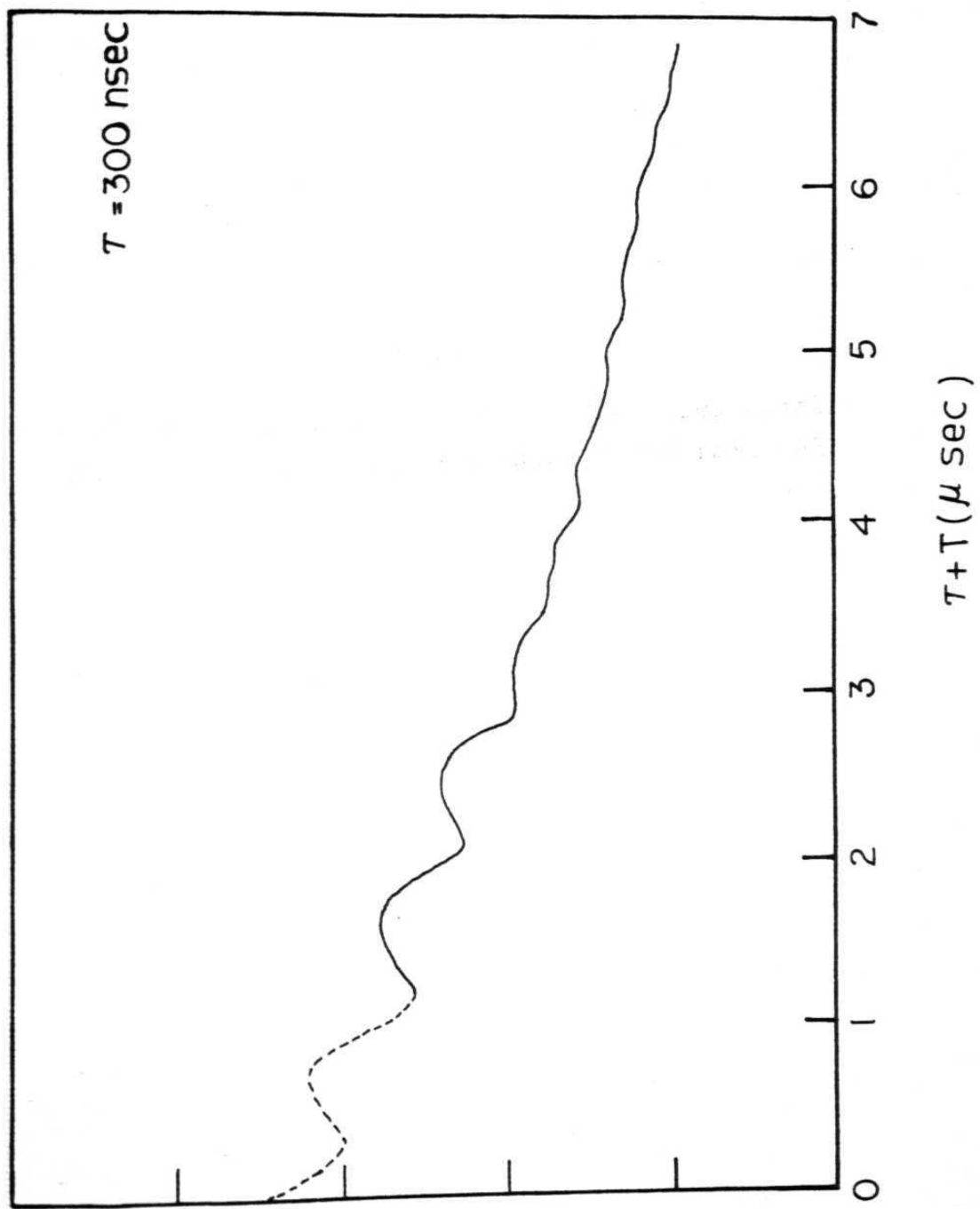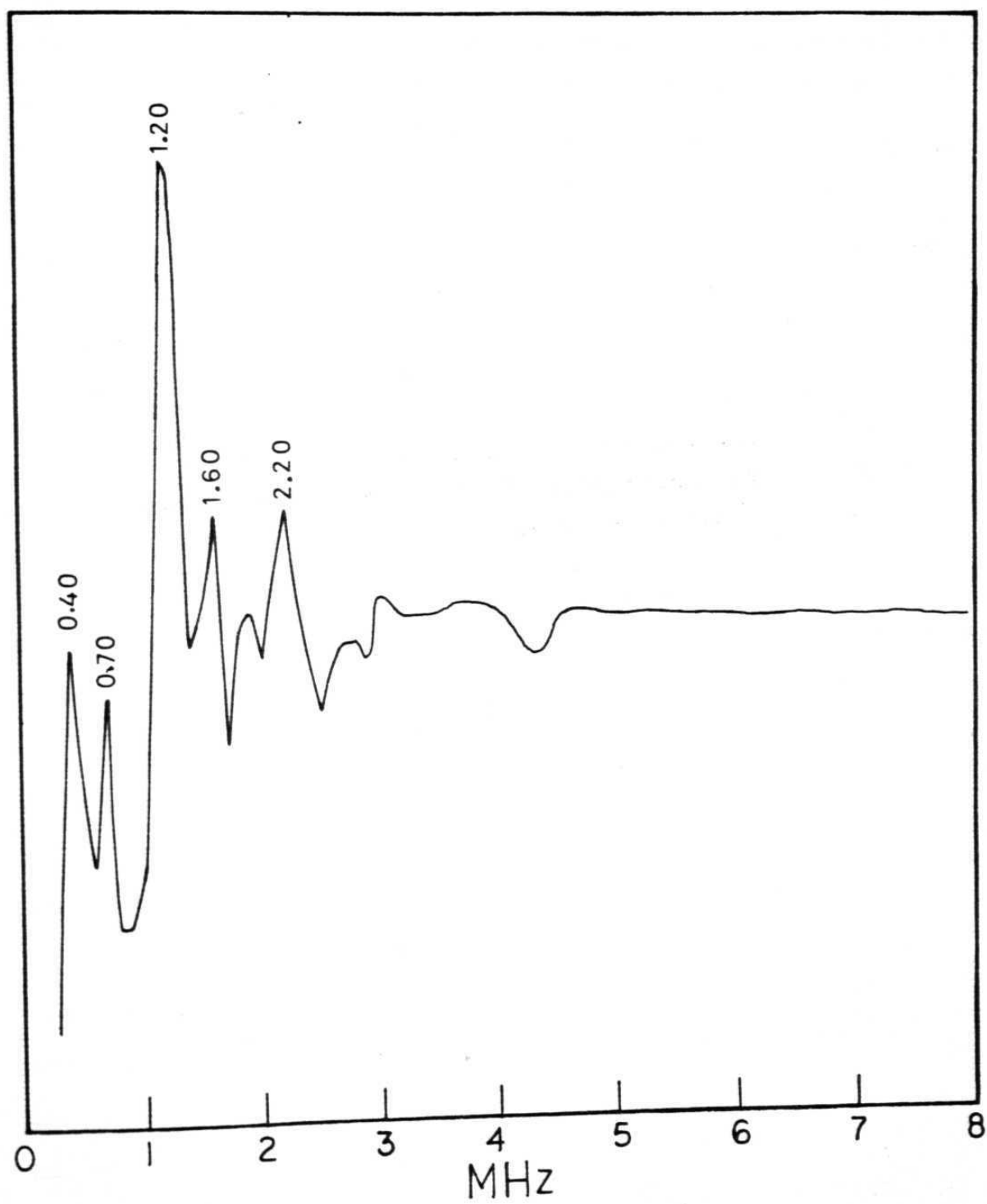Inositol hexaphosphate at pH = 6.8 and τ = 300 nsec.

Fig. 10

The Fourier cosine transform of the echo envelope
for hemoglobin nitroxide + Inositol hexaphosphate
shown in Fig. 9.

the case of myoglobin nitroxide. A comparison between these frequencies shows that they arise from the nitrogen N3 of the proximal histidine. The frequency at 5.0 MHz is due to the addition of the Zeeman and the contact coupling energies, denoted by the transition f_2 shown in **Fig. 1** of Chapter 3. The isotropic hyperfine coupling constant for the N3 nucleus calculated from the transition energies was $|a|$ = 2.5 MHz.

In Fig. 9 and 10 the modulation and the corresponding FT spectrum of HbNO+IHP at a value of τ = 300 nsec. are shown. The FT spectrum shows five frequency components at 0.40, 0.70, 1.20, 1.60 and 2.20 MHz. The origins of the 0.40, 1.20 and 1.60 MHz peaks is the same as the one described in the case of HbNO. The peak at 0.70 MHz is from the protonated nitrogen N3 of the proximal imidazole. The quadrupole frequencies from the protonated imidazole N3 have been observed by Hunt et al[24] using NQR methods and later Peisach et al[19] have found similar frequencies in the [^{14}N] imidazole-heme-NO complex. The corresponding frequency at 1.4 MHz is most probably split into 1.2 and 1.6 MHz. This can be inferred from the unusually large intensity and width of the 1.2 MHz line. The component at 2.2 MHz is a combination frequency. In a protonated imidazole complex two of the zero-field quadrupole frequencies (ν_0 and ν_-) are around 0.7 MHz and the third one is at 1.4 MHz. These results are in good agreement

with those obtained by Hunt et al[24] and Peisach et al[19].

A comparison of the frequency components from HbNO and HbNO+IHP shows that there is a change at the heme site coupled to the binding of IHP to hemoglobin. The frequency spectrum from HbNO+IHP shows additional frequency components besides those observed from HbNO complex. This indicates that some sort of structural change takes place only at some of the heme sites. From other spectroscopic studies it has been observed that only the α-subunits of hemoglobin are sensitive to conformational changes on binding by IHP to the Hb tetramer[28-30]. These results have clearly shown that such a coexistence of two types hemes exist in HbNO+IHP. However, from the present studies, it is not possible to conclude which of the subunits reflects such a conformational change in their electronic properties. Also it may be concluded from the above results that binding of IHP to HbNO causes the remote nitrogen (N3) of the proximal imidazole of His F8 to get protonated. However, this protonation seems to take place only in some of the subunits as discussed above.

From EPR spectroscopy it was suggested that the three line superhyperfine structure (SHFS) in HbNO+IHP could be due to a five-coordinated heme structure[29-30]. It was concluded that the iron-proximal histidine N1 bond possibly

breaks down as a result of the binding of IHP to Hb. Infrared and Resonance Raman studies have supported this view point[32-34]. But recent EPR studies using more sensitive detection approaches had suggested that such a bond cleavage may not occur with the binding of IHP[35-36]. Instead, the imidazole N3 of the proximal histidine gets protonated changing the geometry of the NO-complex. The change in electronic properties of HbNO+IHP reflects this. Our results clearly show that such a protonation of the remote nitrogen (N3) of the imidazole is the result and that the imidazole nitrogen gets deprotonated when IHP is released from hemoglobin. Thus our results clearly show such a conformational change on binding of IHP to hemoglobin.

These studies on Hb derivatives have clearly shown a few points which are extremely important from the view point of the physico-chemical properties of the protein. In all the four derivatives considered here the modulation arose from the remote nitrogen of the histidine. But the modulation shows variations depending on the ligand at the sixth position. For instance, $HbCN^-$ and HbN_3^- have shown significant differencies in their frequency components thus showing the ligand dependent electronic structural changes at the heme. These differences are not clear from the conventional spectroscopic techniques. Also, the influence of the conformational change in the bulk of the protein,

on the heme, has been clearly demonstrated from the differences in the frequency components in both the cases. Moreover, the protonation of the remote nitrogen (N3) of the histidine F8 has been confirmed and the deprotonation in the oxy-conformation has been established. At the same time, this protonation and deprotonation seems to occur in only some of the subunits of hemoglobin.

Table I

The optical absorption maxima with the respective millimolar extinction coefficients of some of the hemoglobin derivatives.

Derivative	Wavelength nm	Millimolar Extinction Coefficients mM
Deoxyhemoglobin	555	12.5
	430	133
	274	29.2
Oxyhemoglobin	541	13.8
	577	14.6
	415	125
	344	27
	276	34.4
Methemoglobin pH 6.4	1000	0.8
	629	4.4
	500	10.0
	405	179
Ferrihemoglobin hydroxide	820	0.7
	575	9.2
	541	11.0
	410	120
Ferrihemoglobin cyanide	541	12.5
	418	124
Ferrihemoglobin azide	575	9.9
	541	12.8
	417	134
Hemoglobin nitroxide	545	12.6
	575	13.0

References

1. J.M. Baldwin, 'Structure and Function of Hemoglobin, Prog. in Biophys. and Molec Biol. 29, 225 (1975).

2. M.F. Perutz, 'British Medical Bulletin', 15, 21 (1976).

3. K.Wuthrich, Struct. and Bonding 8, 53 (1970).

4. E. Antonini and M. Brunori, 'Hemoglobin', Ann. Rev. Biochem. 39, 977 (1970).

5. E. Antonini and M. Brunori, 'Hemoglobin and Myoglobin in Their Reactions with Ligands', North Holland, Amsterdam, 1971.

6. M. Weissbluth, 'Hemoglobin-Cooperativity and Electronic Properties', Springer-Verlag, New York, 1974.

7. G.M. Henis-Zoen, Biophys. J. 10, 196 (1970).

8. J.S. Griffith, Mol. Phys. 21, 135 (1971).

9. J. Peisach, W.E. Blumberg, B.A. Wit enberg, J.G. Wittenberg and L. Kampa, Proc. Nat. Acad. Sci. (U.S.) 63, 934 (1969).

10. J. Peisach, W.E. Blumberg, S. Ogawa, E.A. Rachmitewitz, R. Oltzik, J. Biol. Chem. 246, 3342 (1971).

11. G. Feher, R.A. Isaacson, C.P. Scholes and R.L. Nagel, Ann. N.Y. Acad. Sci. 222, 86 (1973).

12. C.P. Scholes, R.A. Isaacson and G. Feher, Biochim. Biophys. Acta 263, 448 (1972).

13. C.P. Scholes and H.L. Van Camp, Biochim. Biophys. Acta 434, 290 (1972).

14. C.P. Scholes in 'Multiple Electron Resonance Spectroscopy', Ed. M.M. Dorio. and J.H. Freed, Ch. 8, p297 Plenum Press, N7, 1979.

15. H.L. Van Camp, C.P. Scholes and C.F. Mulks, J. Amer. Chem. Soc. 98, 4094 (1976).

16. J.S. Morrow and F.R.N. Gurd, C.R.C. Reviews in Biochem. 3, 401, 1978

17. K. Wuthrich, 'NMR in Biological Research:Peptides and Proteins, 'North Holland Publ. Co., Amsterdam, 1976.

18. J.M. Salhany, S. Ogawa and R.G. Shulman, Biochemistry, 14 2180 (1975).

19. J. Peisach, W.B. Mims and J.L. Davis, J. Biol. Chem. 254, 12379 (1979).

20. D.L. Drabkin, J. Biol. Chem. 164, 703 (1946).

21. M.F. Perutz, J. Cryst. Growth 2, 54 (1968).

22. R. Benesch, R.E. Benesch and C.I. Yu, Proc. Nat. Acad. Sci. (U.S.) 59, 526 (1969).

23. W. Helkmann and C. Bauer, Analyt. Biochem. 75, 382 (1976).

24. M.J. Hunt, A.L. Mackay and D.T. Edmonds, Chem. Phys. Lett. 34, 473 (1975).

25. R.P.J. Merks and R. de Beer, J. Phys. Chem. 83, 3319 (1979).

26. C.H. Ashby, C.P. Cheng and T.L. Brown, J. Amer. Chem. Soc. 100, 6057 (1978).

27. K. Nagai, H. Hoi, S. Yoshida, H. Sakamota and H. Morimoto, Biochim. Biophys. Acta, 532, 17 (1978).

28. Y. Henry, R. Banerjee, J. Mol. Biol. 73, 469 (1973).

29. F. Taketa, W.E. Antholine and J.Y. Chem. J. Biol. Chem. 253, 5448 (1978).

30. H. Kon, Biochim. Biophys. Acta. 379, 103 (1975).

31. A. Szabo and M.F. Perutz, Biochemistry 15, 4427 (1976).

32. J.C. Maxwell and W.S. Caughey, Biochemistry, 15, 388 (1976).

33. M.F. Perutz, J.V. Kilmartin, K. Nagai, A. Szabo and S.R. Simon, Biochemistry 15, 378 (1976).

34. J.D. Stong, J.M. Bunke, P. Daly, P. Wright and T.G. Spiro, J. Amer. Chem. Soc. 102, 5815 (1980).

35. M. Chevion, J.M. Salhany, J. Peisach, C.L. Castillo and W.E. Blumberg, Israel J. Chem. 15, 311 (1976-77).

36. R. Hille, J.S. Olson and G. Palmer, J. Biol. Chem. 254, 12110 (1979).

CHAPTER VI

CONCLUSIONS

In this thesis the FT ESEEM technique has been applied to analyse the electron spin echo envelope modulation spectra obtained from single crystals, glassy and polycrystalline materials, and randomly oriented biological macromolecules. The systems chosen have relatively short phase memory times and many of them exhibited complex modulation patterns involving deuterons, nitrogens and chlorides.

Firstly, the single crystal modulations have been studied. The frequency components, obtained upon Fourier transformation of the time domain data, contained the ENDOR frequencies of chlorides as well as the zero-field quadrupole frequencies of nuclei with $I = 1$. The zero-field quadrupole frequencies arise because of the cancellation of the fields due to nuclear Zeeman and contact couplings. The coupling parameters derived from these frequency components differed with the crystal studied, viz. NH_4Cl, NH_4Br and ND_4Cl. Also, these parameters are different in the two centres studied in NH_4Cl. These differences reflect the changes in the local electronic structure. The nuclei which are immediately liganded to Cu^{2+} did not contribute to the modulation. The modulation arises mostly from nuclei which are in the second coordination sphere. This means that the FT ESEEM technique is very sensitive in detecting small changes in the local electronic structure. In the present case the distances of the nuclei which contributed to the modulation are $\sim 4A^{o}$ and slightly more in some cases.

Next the FT technique has been applied to glassy and polycrystalline materials. These materials have previously been studied in the time domain by the simulation of the modulation pattern. The modulations are relatively simple and only the two-pulse data has been studied. It was possible to determine very small quadrupole couplings to the deuterium nuclei by the FT analysis. This information could not be obtained from the time domain analysis. The quadrupole constant derived from the frequency components in the case of A_g^o in Ice (Site II) is in excellent agreement with the value reported from NQR studies in Ice.

Finally, the FT technique has been applied to study the ESEEM data from different derivatives of low-spin hemoglobin. These studies have shown some interesting points regarding the structure and conformation of the protein. In almost all cases modulation from the distant nitrogen (N3 of His F8) of the proximal imidazole was identified. The frequencies as well as the coupling constants for this nitrogen differed from one derivative to the other. This shows that the finer structural para-meters vary around the heme depending upon the ligand in the sixth position, even though the spin of iron is always 1/2. Besides, the influence of the protein structure on the electronic properties of the heme has been clearly observed from the FT ESEEM studies of HbNO and HbNO+IHP.

The protonation of the distal nitrogen (N3 of His F8) of the proximal imidazole in some of the Hb subunits in HbNO+IHP was established. This confirms the previous EPR studies which pointed out to such a protonation which alters the heme electronic structure drastically. Thus the influence of conformational change in the protein at the heme could be directly observed.

The complexes studied have varying natures. However, from the FT ESEEM technique almost similar information has been obtained irrespective of the nature of the complex. In single crystals the base line is more stable because the decay function is more near to the true decay. The effects of the window function and the extrapolation to time $T + \tau = 0$ have been studied in most of the cases. The frequency components obtained on Fourier transformation after multiplying the time domain data by a window function showed frequency shifts depending on the width of the window. This shift depends on the resolution in the frequency domain. This resolution in turn depends upon the length of time upto which the time domain data has been recorded and hence on the phase memory times. For systems with long phase memory times, the resolution in the frequency domain could become sufficiently high, so that the frequency shifts are not prominent. The extrapolated data reproduces frequencies observed in the truncated data. However, the FT data using the window showed better resolution and baseline stability.